Finite Element Simulation of Precast/Prestressed Insulated Sandwich Panels Optimized for Construction of Government Facilities

by

Joseph Morrison Nickerson

A thesis submitted to the Graduate Faculty of
Auburn University
in partial fulfillment of the
requirements for the Degree of
Master of Science in Civil Engineering

Auburn, Alabama
August 2, 2014

Keywords: insulated sandwich panel, finite element modeling,
prestressed concrete, ductility

Approved by

James S. Davidson, Professor of Civil Engineering
Justin D. Marshall, Assistant Professor of Civil Engineering
Robert W. Barnes, James J. Mallett Associate Professor of Civil Engineering

Abstract

This report discusses the development of finite element modeling methodologies for the static and dynamic response of insulated sandwich panels to uniform pressure loads. Experimental testing, which included solid panel and sandwich panel static testing, component level testing of shear tie connectors, and blast testing of sandwich panels, was used for FE model validation. The use of a beam-spring system to capture the shear transfer between concrete wythes of various shear connectors accurately was a primary focus of the modeling approach. The FE modeling approach was also used to address questions related to the design of wall panels for blast loads. The ductility of prestressed members and the performance of sandwich panels in comparison to solid panels were highlighted. The performance of load-bearing wall panel subjected to blast loads in comparison to non-load-bearing wall panels was investigated, and recommendations on incorporating axial loads into single-degree-of-freedom analysis tools were made.

Table of Contents

List of Tables

List of Figures

Chapter 1

Introduction

1.1 Background

Since the threat of terrorist attacks on our country has increased in the recent years, research on the evaluation of these threats and design of structures to resist them has likewise increased. Blast design has been performed for many years in the chemical industry due to the possibility of accidental explosions. Most government and Department of Defense buildings are now being required to meet blast design criteria as well.

Design of structures to resist blast loads is very different than designing for typical loads, i.e. wind, gravity, etc. Blasts create very large overpressures that may only last milliseconds These impulse loads can induce significant accelerations and displacements in structures. Structural components subjected to blast impulses are typically designed to be heavily damaged in order to dissipate the energy from a blast wave while protecting life safety.

The precast/prestressed sandwich panel is a modern type of wall construction consisting of a layer of foam insulation sandwiched between two concrete wythes. Shear connectors are used to tie the concrete wythes together, and non-metallic, composite materials are becoming more and more common in these connectors to prevent thermal bridging between the concrete wythes. This type of wall construction is becoming more popular today in exterior cladding of buildings due to the energy efficient nature of their design.

1.2 Objectives

The primary objective of this project was to develop a finite element (FE) modeling approach for simulating the large displacement response of precast/prestressed sandwich wall panels to blast loads. Other goals of the research included using the developed FE modeling approach to address the following questions related to blast design:

- Are response limits for prestressed members used in blast design too conservative?
- Can sandwich panels be used in blast design?
- How can the design of sandwich panels be enhanced for blast loads?
- Can debonding sections of reinforcement increase the ductility of wall panels?
- How do axial loads affect the response of load-bearing wall panels subjected to blasts?
- How should the effects of axial load be incorporated into current SDOF analysis tools used in blast design?
- How do lateral loads affect the axial capacity of wall panels?

1.3 Scope and Methodology

In order to complete the primary objective of the project, the results of experimental testing, which included static flexural testing of solid panels and sandwich panels, direct shear tests of various shear tie connectors, and dynamic blast testing of sandwich panels, were used to validate the accuracy of FE models. The numerical investigations of the large displacement, static models were executed using a general-purpose FEA software package, Abaqus/CAE. The modeling techniques developed and validated with Abaqus/CAE were then implemented into dynamic, nonlinear models using the explicit FEA software package, LS-DYNA.

Once a FE modeling methodology was validated, the results of static and dynamic FE models were used to make observations about the blast performance of sandwich panels.

Additionally, FE models of solid panels and sandwich panels beyond the scope of the testing were developed in order to make further investigations related to the blast design of sandwich panels, including a parameter study on the properties of shear ties. Although none of the testing included load-bearing panels, static and dynamic analyses of panels subjected to combined lateral and axial loads were also completed in order to investigate the effect of axial load on the lateral response of panels subjected to blast loads and evaluate current blast criteria and analysis methods for load-bearing panels.

The scope of the testing and FE modeling was limited to simply supported panels with no fenestrations. Although a variety of sandwich panel configurations were tested and modeled, the configurations were limited to panels with two inches of insulation, and most of the configurations consisted of panels with three inch concrete wythes, i.e. a 3-2-3 layout.

1.4 Report Organization

This report is organized in six chapters. Chapter 1 lists the objectives, scope and methodology, and report organization. Chapter 2 provides a literature review of issues relating to designing for blast loads and previous sandwich panel research. Chapter 3 discusses the FE modeling methodology and validation. Chapter 4 discusses the ductility of precast, prestressed concrete panels and their applicability in blast design. Chapter 5 discusses the effect of axial load on the flexural response on wall panels. Chapter 6 summarizes the project and provides conclusions and recommendations for future research.

Chapter 2

Literature Review

2.1 Overview

Ensuring structural integrity of a building during a blast threat has been a recognized concern of military agencies for many years, initially in response to bomb threats during World War II. These concerns continued during the Cold War, but more recently, due to the World Trade Center and Oklahoma City bombings in 1993 and 1995, the focus of designing buildings for blast loads has shifted to localized terrorist threats (NRC 1995).

The current philosophies on designing exterior cladding to resist impulse loads generated from far-off blast threats were reviewed. Previous research on the design, behavior, and numerical modeling of insulated sandwich panels was also investigated.

2.2 Designing Concrete Components for Blast

Designing building components to resist the effects of blast is becoming more and more common. Many government and department of defense buildings now require some level of blast-resistance design. Methods for designing for blast loads have been developed for most common construction types. The Department of Defense United Facilities Criteria document 3-340-02, *Structures to Resist the Effects of Accidental Explosions,* provides a comprehensive overview of calculating blast loads and structural component response (DOD 2008). The American Society of Civil Engineers' Task Committee on Blast-Resistant Design has also published a guide, *Design of Blast Resistant Buildings in Petrochemical Facilities* (ASCE 1997).

Designing for blast differs greatly from wind, gravity, etc. First, the design philosophy in blast is to dissipate the energy imparted by the blast wave, while components are typically designed to meet strength demands for other load types. The area under the pressure-time curve, or the impulse, is thought of as the energy imparted by the blast wave. The area under the component's resistance-deflection curve is the strain energy that the component absorbs. Unlike design for typical loads, components subjected to blast are designed to be significantly damaged. The primary goal in blast design is occupant safety; however, as long as the component does not completely fail, the more damage and deformation the component undergoes the more energy that is dissipated. Therefore, the amount of plastic deformation capacity of a component is very important in blast design. A ductile flexural response is desired, so other design requirements, such as shear and connection capacity, are commonly designed to exceed the ultimate flexural resistance. Reinforced concrete components are generally considered to have a ductile flexural response as long as they are under-reinforced and another brittle failure mechanism does not control, e.g. shear or bond failure. Prestressed concrete components are generally not considered to be ductile in flexure because of the limited strain capacity of prestressing strands compared to conventional reinforcing steel. While the concrete is expected to crush at large deflections in reinforced concrete components, prestressed concrete components are expected to prematurely fail because of strand fracture. Thus, they need a higher flexural resistance in order to absorb the same amount of strain energy as reinforced concrete components (Alaoui and Oswald 2007).

Another big difference in blast design is that it is based on deflection limits instead of strength or stress limits. These limits are typically given in terms of support rotation or ductility ratio, and limits are specified for different construction types based on results of blast testing (Alaoui and Oswald 2007). Exact limits vary depending on the design guide used, but a

comparison of the limits for reinforced and prestressed concrete and their significance will be discussed further in Chapter 5.

There are various methods for determining the dynamic response of a structural component to blast loads. Complex finite element analysis (FEA) software is widely available if an extensive analysis is required; however, doing a FEA generally requires in depth knowledge of the software and can be time consuming. Therefore, a single-degree-of-freedom (SDOF) analysis is a more common tool used for blast design. A SDOF analysis idealizes a component as a spring-mass system with the deflection of the mass equaling the maximum deflection of the component. This method is commonly integrated into spreadsheets that are convenient for practicing engineers (Alaoui and Oswald 2007).

2.2.1 Blast Loads

Blast waves can have several sources, including accidental industrial explosion of petroleum facilities, chemical plants or storage area as well as terrorist attacks. Blast waves propagate from their source in a hemispheric fashion before impacting a building surface. Upon impacting a structure, the pressure instantaneously rises and then decays with time as the wave is reflected off the structure's surface. The pressure-time history of a blast wave impacting a structure includes an initial positive phase and a negative phase, i.e. suction, as the wave is reflected (Brun et al. 2012). Unlike other dynamic loads, blast loads typically only last milliseconds. Figure 2-1 shows a typical pressure-time history for a blast wave.

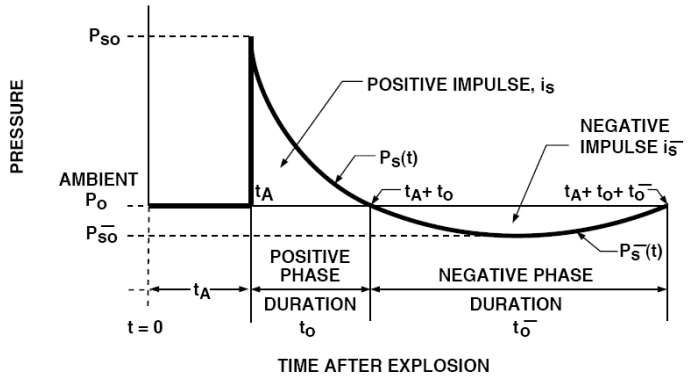

Figure 2-1: Typical Pressure-Time History of an Airblast in Free Air (USACE 2008a)

Extensive research has been completed to define the pressure-time history created for a given blast event based on the stand-off distance from the component and the equivalent TNT charge weight of the explosion. However, for simplicity of analysis and design blast loads are typically estimated using a right triangular pressure-time history, as seen in Figure 2-2. The most important parameters of a blast load are the peak pressure and the impulse. Right triangular loads are developed by preserving the maximum peak pressure and the total impulse of the positive load phase from the actual blast load predicted by analytical models or measured during testing. This simplification is generally considered conservative since it disregards the negative suction phase of the load (Brun et al. 2012; Alaoui and Oswald 2007).

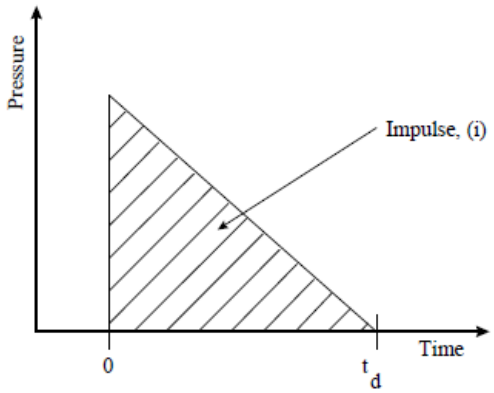

Figure 2-2: Simplified Right Triangular Blast Pressure History for Positive Phase Blast Load (USACE 2008a)

2.3 Precast/Prestressed Sandwich Wall Panels

Precast sandwich panels are composed of a layer, or wythe, of rigid insulation sandwiched between two concrete wythes, as seen in Figure 2-3. Some form of steel or composite shear connector is generally used to hold the system together. Often, the concrete wythes are prestressed to prevent cracking under shipping and handling and service loads. They are fabricated in a precast concrete plant, shipped the project site, and erected with cranes. They are primarily used as exterior cladding for a building and can be designed as non-load-bearing or load-bearing wall panels. Sandwich panels have gained in popularity in the past decades because of their thermal efficiency (PCI Committee 2011). Other benefits of this system include speed of erection, the quality control that comes from manufacturing in a precast plant, and the design flexibility of architectural finishes that can be applied to the exterior face (Losch 2005).

Figure 2-3: Precast/Prestressed Sandwich Wall Panels

The flexural design of composite sandwich panels is similar to solid panels. The main difference is that additional calculations to ensure adequate shear transfer between the wythes must be completed. Also, the thickness of the concrete wythes and the lack of concrete in between the wythes must be considered when calculating section properties (PCI Committee 2011).

2.3.1 Shear Transfer in Sandwich Panels

Sandwich panels can be designed as composite, non-composite, or partially composite panels. In a composite panel, the concrete wythes act as one unit to resist the applied loads. In a non-composite panel, the concrete wythes act independently, and a partially composite panel behaves somewhere in between composite and non-composite. The degree of composite action is dependent upon the amount of shear transfer that is provided between the concrete wythes. Shear connectors are used to transfer the shear forces that develop between the concrete wythes during flexural bending (Losch 2005). Traditionally, solid zones of concrete or bent steel reinforcing bars have been used to provide the shear transfer needed for composite action. However, these traditional connectors have the negative effect of providing a thermal bridge between the concrete wythes (Frankl et al. 2011).

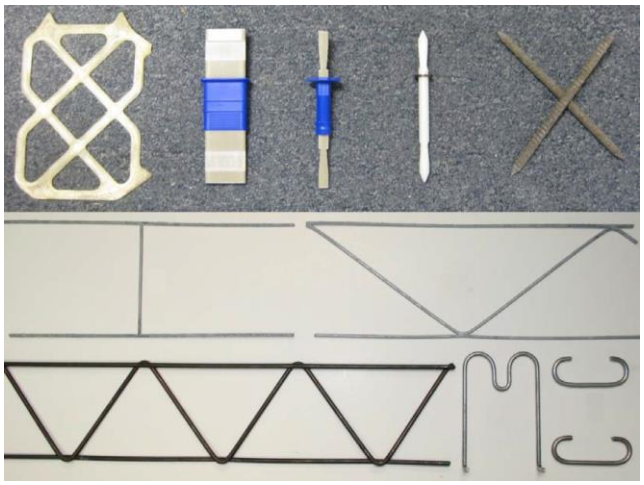

Figure 2-4: Various Sandwich Panel Shear Tie Connectors (adapted from Naito et al. 2009)

Mechanically, composite action can be described in terms of the distribution of strain through the cross section. In fully composite action, there is a continuous distribution of strain through the whole cross section and only one neutral axis. In non-composite action, each concrete wythe has its own strain distribution and neutral axis.

Traditionally, there are two methods for evaluating the interface shear force required for composite action. In the first method, the horizontal shear demand is calculated along the length of the panel based on the flexural shear force, V , and section properties.

$$q = \frac{VQ}{I_g} \tag{2-1}$$

where

$q =$ shear flow

$Q =$ first moment of the concrete wythe area about the neutral axis

$I_g =$ gross moment of inertia

This method results in a linear distribution of shear demand along the length of the beam for a simply supported member subjected to uniform transverse load; however, this method is based on the assumptions of elastic material behavior and plane sections remain plane, which are violated when cracking or yielding occurs (Nijhawan 1998).

Another method for calculating the horizontal shear demand is based on the ultimate moment capacity of the member. In this method the shear demand for each half-span of the panel is calculated as the lesser of the maximum tensile or compressive force in the flexural moment couple. The calculation of the maximum compressive force can be simplified as the unconfined compressive strength times the area of the entire concrete wythe in compression. For all practical designs, the maximum tensile force from the reinforcement will be less than the maximum

compressive capacity, and enough shear connectors must be provided in each half-span of the panel to transfer this force between the wythes for the panel to act compositely (PCI Committee 2011). This method is recommended in the PCI Design Handbook, Section 4.3.5 (PCI 2004). This approach assumes that the shear transfer mechanism can carry this shear force uniformly over the length of the panel. This assumption may be accurate for steel connectors that can yield; however, a calculation of the shear demand proportional to the flexural shear force along the length of the panel may be more accurate for brittle shear connectors made of composite materials (Salmon et al. 1997; Bush and Stine 1994).

2.3.2 Methods for Evaluating Composite Action

In design, sandwich panels are usually considered composite if enough shear transfer capacity is provided to allow crushing of the concrete or yielding of the reinforcement without failure of the shear connectors (Benayoune et al. 2008). However, in reality, most sandwich panels are neither fully composite nor non-composite (Bush and Stine 1994). Although evaluating the composite action provided by shear tie connectors is crucial to the flexural design of sandwich panels, there is not one accepted approach in the literature for calculating the degree of composite action. It is generally approached in one of two ways: either the stiffness or strength of the panel.

Using the stiffness of the panel to evaluate composite action is common in sandwich panel research, because serviceability and deflection requirements commonly control design of prestressed/precast panels; therefore, the uncracked, elastic response of the panels is of interest. Frankl et al. (2011) used a comparison of measured lateral displacements from sandwich panel tests to theoretical composite and non-composite displacements to evaluate the composite action of panels reinforced with carbon fiber reinforced polymer (CFRP) shear grid. Benayoune et al.

(2008) used the ratio of an effective moment of inertia, calculated based on measured strain values at the top and bottom face, to theoretical gross moment of inertia of a composite panel.

These definitions can be useful when evaluating the elastic performance of sandwich panels, but once cracking of the concrete occurs and nonlinear behavior begins, these approaches are not applicable. Thus, using the ultimate strength of a sandwich panel is also used to evaluate the degree of composite action. Benayoune et al. (2008) also proposed the use of the ratio of experimental or numerical ultimate strength to the theoretical calculated composite strength as a measure of the degree of composite action.

Hassan and Rizkalla (2010) proposed an analytical approach for calculating the degree of composite action of a sandwich panel, based on the interface shear force required to resist the applied load. Similar to the method proposed in the PCI Design Handbook, they defined the transferred interface shear force as equal to the sum of the internal forces on the inner or outer wythe at midspan. They used this definition of the shear force to develop analytical equations for the degree of composite action and moment capacity based on equilibrium, moment-curvature relationships, and an assumption of uniform curvature over the cross section.

2.4 Numerical Modeling of Sandwich Panels

Finite element modeling has commonly been included in past research of sandwich panel systems. Pessiki and Mlynarczyk (2003) modeled sandwich panels with solid concrete zones and discrete steel connectors, but the analyses were only linear elastic. Hassan and Rizkalla (2010) modeled sandwich panels reinforced with CFRP shear grid using solid elements for the three wythes and truss elements for the shear grid; however, the analyses were also limited to the linear elastic range. Therefore, the input was limited to a modulus of elasticity, and comprehensive material properties of the CFRP material were not needed. Benayoune et al.

(2006) adopted a 2-D FEM approach with solid and truss elements to model eccentrically loaded and laterally loaded one-way precast sandwich panels. Benayoune et al. (2008) used a 3-D FEM approach with shell and beam elements to model laterally loaded two-way precast sandwich panels. His approach included material and geometric nonlinearities; however, the only connectors modeled were steel truss connectors. This approach was viable since assuming only axial forces in the truss elements is reasonable, and the material properties of steel needed for the connector material model are readily available.

Other research on sandwich panels presented by Salmon et al. (1997), Bush and Wu (1998), Kabir (2005), and Gara et al. (2012) also included the use of finite element modeling, but the details of these analyses will not be described here. In general, solid elements were used to model the concrete and insulation wythes. Most shear connectors were modeled explicitly using truss or beam elements and material properties. Many analyses, however, were limited to the linear, elastic range. Some research programs did include large displacement, nonlinear FE analyses, but these analyses were limited to panels with steel shear connectors. No nonlinear analyses of panels with thermally efficient shear connectors were found in the literature.

2.5 Blast Testing of Sandwich Panels

Although much static testing of concrete sandwich wall panels has been completed, dynamic testing of sandwich panels, especially under blast loads, was of interest to this study. Unfortunately, such testing is quite limited. Yongxiang et al. (2009) tested the performance of concrete sandwich panels to surface contact explosions; however, close-in detonations were outside of the scope of this study. Two series of full-scale blast testing of concrete sandwich panels conducted by the AFRL were the first of their kind. Previously, sandwich panel research had not only been limited to static testing but also limited to small displacement tests. The test

series consisted of non-load-bearing, single and multi-story sandwich panels subjected to various blasts at significant stand-off distances. The testing demonstrated that the sandwich panels provided adequate resistance to the blast demands (Naito et al. 2008; Naito et al. 2011b). These tests and a comparison of FE models with test results will be further discussed in Chapters 3 and 4.

Chapter 3

Modeling Methodology and Validation

3.1 Overview

The primary challenges associated with FE modeling of foam-insulated concrete sandwich panels include accurately describing and incorporating the fracture and damage behavior of reinforced concrete, integrating foam constitutive models, accurately describing the transfer of shear between concrete wythes, incorporating strain rate effects on material behavior, and simulating initial conditions associated with the prestressed reinforcement strands. Validation of input parameters was accomplished in four parts: (1) simple solid concrete panels (prestressed and conventionally reinforced) subjected to concentrated load at midspan and uniform loading, (2) static testing of shear connectors, (3) static testing of sandwich panels (prestressed and conventionally reinforced) subjected to uniform loading, and (4) full-scale dynamic tests of sandwich panels (prestressed and conventionally reinforced). Component and material level test results were used to define appropriate constitutive model input. Direct shear tests were used to evaluate the shear resistance input required to simulate the various ties used in the full-scale sandwich panel specimens.

Numerical investigations of static models were executed by a general-purpose FE analysis package, Abaqus/CAE. The modeling techniques developed and validated using Abaqus/CAE were then implemented in dynamic models using LS-DYNA.

3.2 Solid Reinforced Concrete Flexure Tests

Two series of solid reinforced concrete panels that were tested statically in flexure at Lehigh University were used to validate the material model for concrete used in the FE analyses. Conventionally reinforced concrete specimens provide good data to compare with FE models, because, unlike sandwich panels, the concrete and rebar properties are the main variables that govern the behavior of these systems. These tests were used to establish input parameters for the concrete material model before other variables, e.g. wythe configuration, shear ties, etc., were introduced into the FE models.

The first test series consisted of small, singly reinforced panels that were monotonically loaded via a displacement controlled line load applied at center span. The panels were simply supported with a roller free to move at one end and a clamped roller at the other. Typical panel details are illustrated in Figure 3-1. Material strengths of the panels were determined by evaluating available concrete and reinforcement samples. Tensile testing of steel samples was conducted in accordance with ASTM E8-04. The elastic modulus, yield stress, ultimate stress, fracture strain, and a full stress-strain curve were determined through a series of tensile tests on reinforcement. Concrete compressive strength was evaluated in accordance with ASTM C39 and C469.

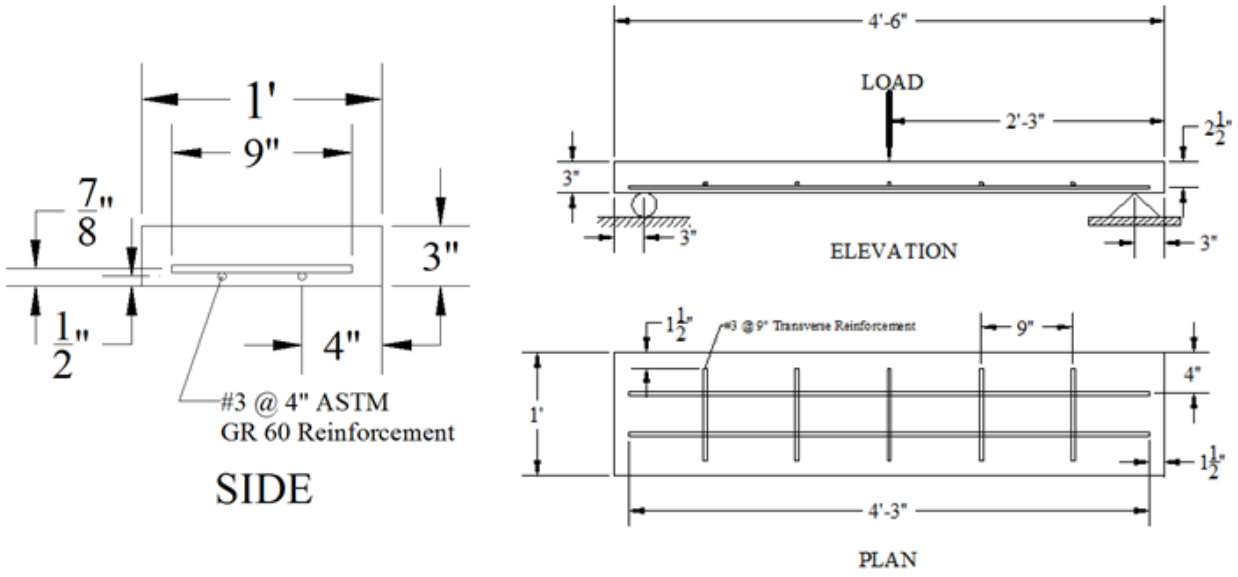

Figure 3-1: Small Solid Panel Details

The second test series consisted of full-scale, doubly-reinforced wall panels. Conventionally reinforced and prestressed panels were tested. To simulate a uniform pressure loading, a pressure bladder was custom fabricated to apply load to an approximately 120 in. by 32 in. contact area. The bladder was filled with water rather than air, as air is a compressible material that will begin to store energy when compressed by the panel. Typical panel details and loading setup are illustrated in Figure 3-2. Five 4x8 cylinders were tested in accordance with ASTM C39 at the start of testing to determine the compressive strength of the concrete. This test series was used to validate the material input parameters determined from the first test series, validate an approach for incorporating the effect of prestressing reinforcement, and verify the effectiveness of a nonlinear incremental solution method.

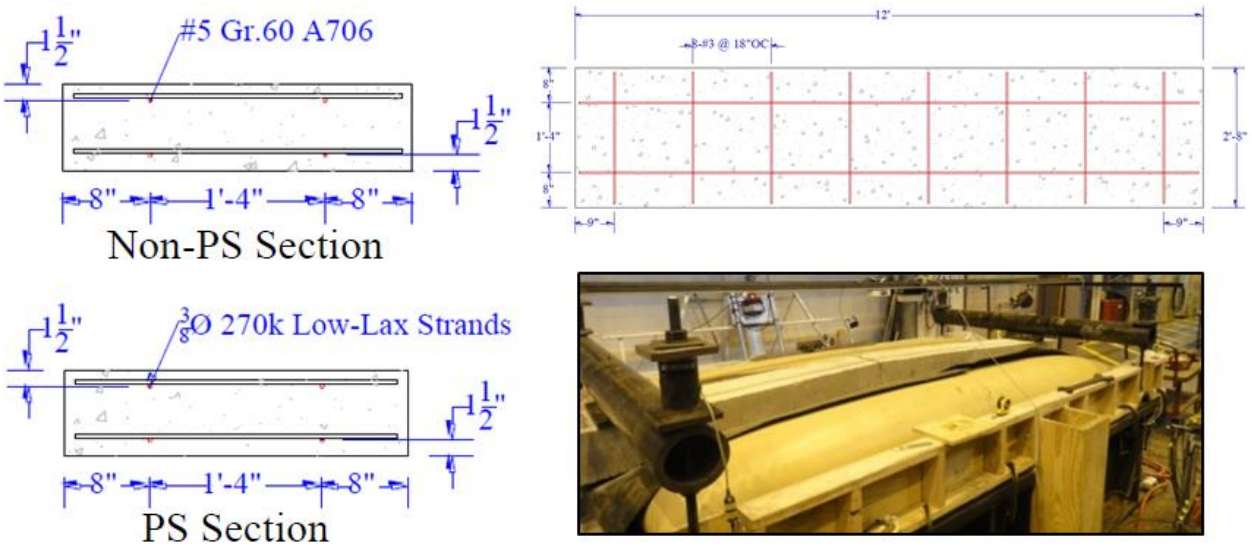

Figure 3-2: Large Solid Panel Details and Test Setup

3.2.1 Material Model for Concrete in Abaqus/CAE

Concrete is comprised of a wide range of materials, whose properties are quantitatively and qualitatively different. It is necessary to identify a large number of parameters if a structural, heterogeneous material such as concrete is taken into account. The Abaqus/CAE Concrete Damage Plasticity (CDP) constitutive model used in this study is based on the assumption of scalar (isotropic) damage and is designed for applications where the concrete is subjected to arbitrary loading conditions, including cyclic loading. The model takes into consideration the degradation of the elastic stiffness induced by plastic straining both in tension and compression. The model assumes that the primary failure mechanisms are tensile cracking and compressive crushing and that these responses are characterized by damaged plasticity, as shown in Figure 3-3 (SIMULIA 2010b).

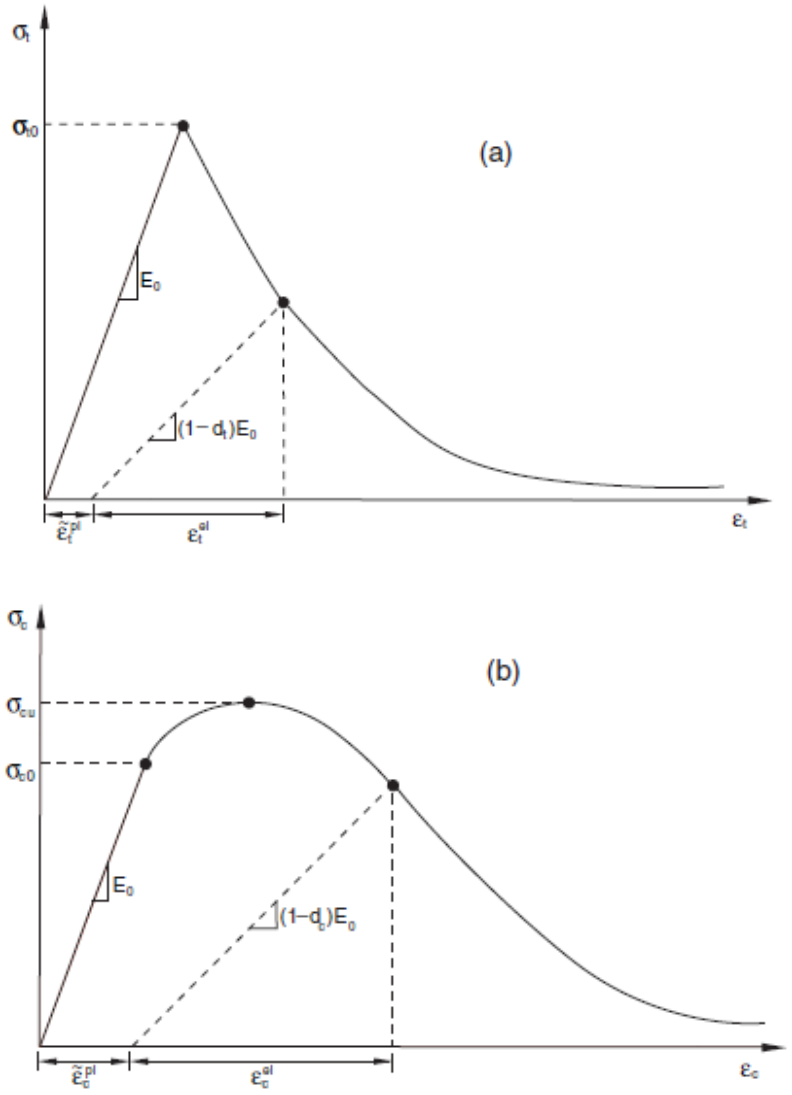

Figure 3-3: Response of Concrete to Uniaxial Loading in (a) Tension and (b) Compression (SIMULIA 2010b)

3.2.1.1 Viscoplastic Regularization

Material models exhibiting softening behavior and stiffness degradation often lead to severe convergence difficulties in implicit analysis programs, such as Abaqus/CAE. A common technique to overcome some of these convergence difficulties is the use of a viscoplastic regularization of the constitutive equations, which causes the consistent tangent stiffness of the softening material to become positive for sufficiently small time increments.

The concrete damaged plasticity model can be regularized in Abaqus/CAE using viscoplasticity by permitting stresses to be outside of the yield surface. A generalization of the Duvaut-Lions regularization, according to which the viscoplastic strain rate tensor, $\dot{\varepsilon}_v^{pl}$, is defined as

$$\dot{\varepsilon}_v^{pl} = \frac{1}{\mu}(\varepsilon^{pl} - \varepsilon_v^{pl}) \tag{3-1}$$

Here μ is the viscosity parameter representing the relaxation time of the viscoplastic system, and ε^{pl} is the plastic strain evaluated in the inviscid backbone model.

Similarly, a viscous stiffness degradation variable, $\dot{d}_v$, for the viscoplastic system is defined as

$$\dot{d}_v = \frac{1}{\mu}(\mathrm{d} - d_v) \tag{3-2}$$

where *d* is the degradation variable evaluated in the inviscid backbone model. The stress-strain relation of the viscoplastic model is given as

$$\sigma = (1 - d_v)\,\mathrm{D}_0^{el} : (\varepsilon - \varepsilon_v^{pl}) \tag{3-3}$$

Using the viscoplastic regularization with a small value for the viscosity parameter (small compared to the characteristic time increment) usually helps improve the rate of convergence of the model in the softening regime, without compromising results. The basic idea is that the solution of the viscoplastic system relaxes to that of the inviscid case as $t/\mu \to \infty$, where *t* represents time. The value of the viscosity parameter can be specified as part of the concrete damaged plasticity material behavior definition. If the viscosity parameter is different from zero, output results of the plastic strain and stiffness degradation refer to the viscoplastic values, ε_v^{pl} and d_v (SIMULIA 2010e). In Abaqus/CAE the default value of the viscosity

parameter is zero, so that no viscoplastic regularization is performed, but a value of $1e^{-5}$ was used in the models in order to improved convergence.

3.2.1.2 Material Parameters of Concrete Damaged Plasticity Model

The material parameters of the concrete damage plasticity model are presented in Table 3-1. For the identification of the constitutive parameters of the CDP model, the following laboratory tests are necessary: 1) uniaxial compression, 2) uniaxial tension, 3) biaxial failure in plane state of stress, 4) triaxial test of concrete (superposition of the hydrostatic state of stress and the uniaxial compression stress). These tests are necessary to identify the parameters, which determine the shape of the flow potential surface in the deviatoric and meridian plane and the evolution rule of the material parameters (the hardening and the softening rule in tension and compression) (Jankowiak and Lodygowski 2005). Since data from uniaxial compression tests of concrete cylinders were the only test data available for identification of CDP parameters, default values suggested by Abaqus/CAE literature were used with the exception of the viscosity parameter, where a value of $1e^{-5}$ was used to improve convergence of the models.

Table 3-1: Material Parameters of Concrete Damaged Plasticity Model

Concrete		Parameters of CDP model	
E(psi)	3.6E+6	ψ , dilation angle	15°
ν	0.18	ε , flow potential eccentricity	0.1
Density (pcf)	150	$\sigma_{b0} / \sigma_{c0}$ *	1.16
Compressive strength (psi)	5,000-8,000	K_c **	0.667
Tensile strength (psi)	300-500	μ , Viscosity parameter	0.00001
Concrete Compression Hardening		Concrete Tension Stiffening	
Yield stress (psi)	Crushing strain	Remaining stress after cracking (psi)	Cracking strain
4336	0.0	400	0.0
5319	0.000575	328	0.0001
5782	0.001025	251	0.0003
6000	0.001325	216	0.0004
5608	0.001825	180	0.0005
4278	0.002725	121	0.0008
2428	0.004825	81	0.001
115	0.009825	4	0.002

*The ratio of initial equibiaxial compressive yield stress to initial uniaxial compressive yield stress.

**The ratio of the second stress invariant on the tensile meridian, *q*(TM), to that on the compressive meridian, *q*(CM).

3.2.2 Reinforcement (Reinforcing Bars and Prestressing Strands)

Reinforcing bars and prestressing strands were modeled using a plasticity material model and truss elements, which were superposed on a mesh of solid elements used to model the concrete. In this approach the concrete behavior is considered independently of the rebar, while the coincident rebar and concrete nodes were merged in order to simulate the bond between

concrete and rebar. The rebar strength parameters were based upon laboratory testing of reinforcement samples used in construction. The prestressing strand strength parameters were based upon typical stress-strain curves for prestressing strands adapted from equations given in the PCI Design Handbook (PCI 2004), since data from test samples was not available. Nonlinear stress-strain curves including strain hardening were used for both types of reinforcement. Table 3-2 summarizes material parameters for the reinforcing bars (Figure 3-4) and the prestressing strands (Figure 3-5).

Table 3-2: Material Strengths for Reinforcement

	Modulus of elasticity (psi)	Poisson's ratio	Density (pcf)	Yield strength (psi)
Rebar	2.9E+7	0.3	490	70,350*
Strand	2.9E+7	0.3	490	245,000**

*See Figure 3-4. **See Figure 3-5.

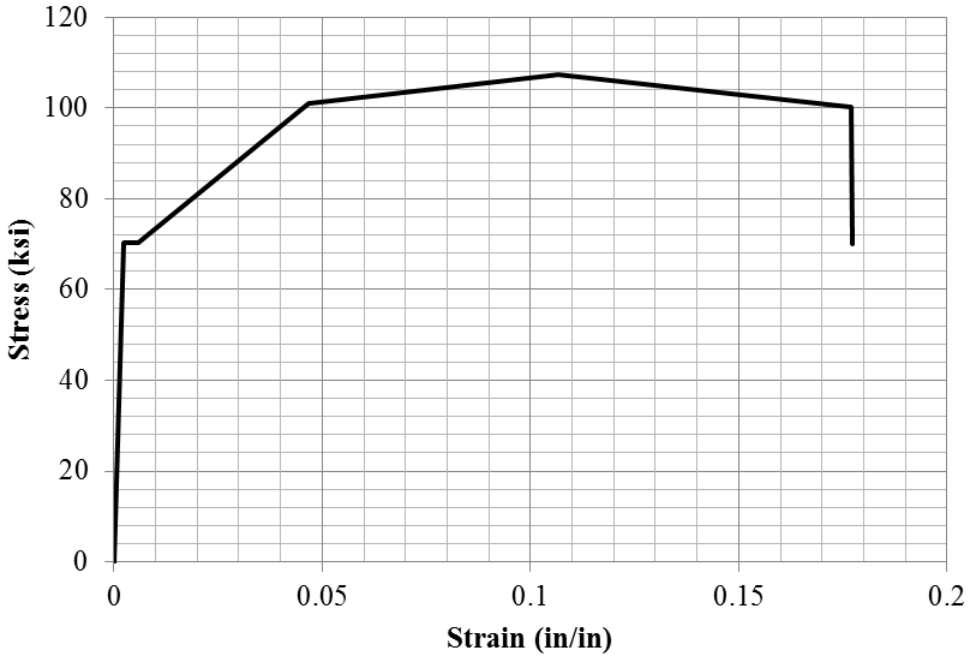

Figure 3-4: Stress-Strain Relationship of Reinforcing Bars Used in FE Analyses

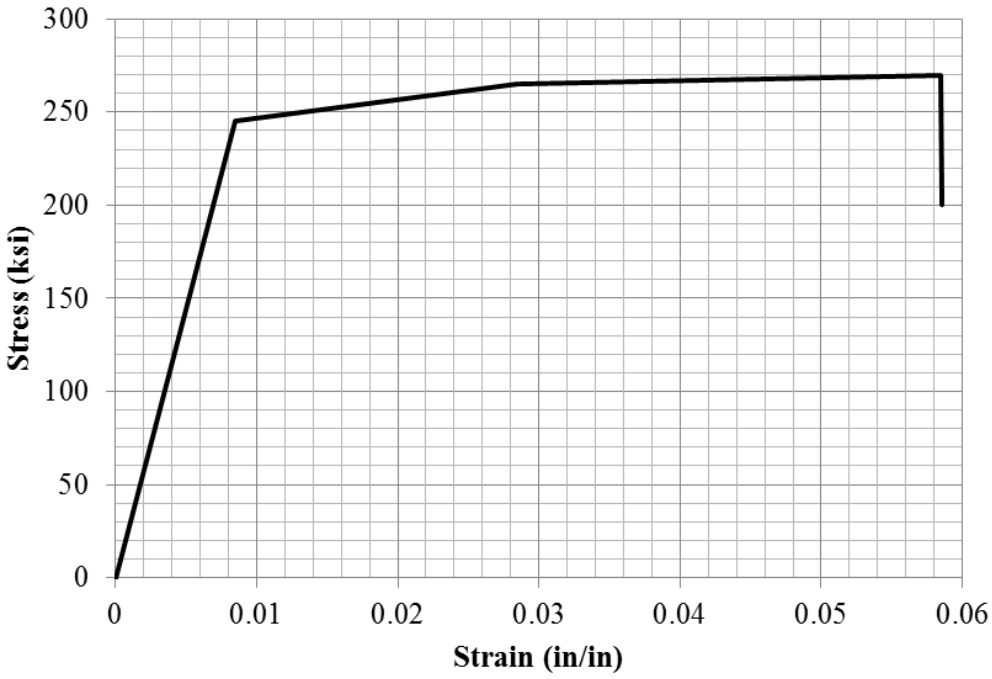

Figure 3-5: Stress-Strain Relationship of Prestressing Strand Used in FE Analyses (adapted from PCI 2004)

3.2.3 Geometry, Elements, Loading, and Boundary Conditions

The concrete and reinforcements were modeled using solid elements (C3D8R; 8-node quadratic brick) and truss elements (T3D2; 2-node truss), respectively. The solid and truss elements were modeled with a coincident mesh resolution and their nodes were merged to simulate a fully-bonded interface between the concrete and reinforcement. Nodal translational degrees of freedom were restrained to simulate a simply supported condition. In the FE models of the small concrete panels, nodal displacements were enforced at midspan to simulate the loading, and a general solver was used since the loading was displacement controlled. In the FE models of the large panels, a uniform pressure was applied across the 10 foot clear span, and an arc length solver was used since the loading was force controlled.

3.2.4 Nonlinear Incremental Analysis

Geometrically nonlinear static problems sometimes involve buckling or collapse behavior, where the load-displacement response shows a negative stiffness and the structure must release strain energy to remain in equilibrium. This study used Riks method to predict geometrical nonlinearity and material nonlinearity of reinforced concrete structures. The Riks method uses the load magnitude as an additional unknown; it solves simultaneously for loads and displacements. Therefore, another quantity must be used to measure the progress of the solution; Abaqus/CAE uses the "arc length," along the static equilibrium path in load-displacement space. This approach provided solutions regardless of whether the response is stable or unstable (SIMULIA 2010a).

3.2.5 Simulation of Prestressing Effects in Abaqus/CAE

Initial conditions can be used to model prestressing effects in reinforcement of prestressed solid and insulated panels. The structure must be brought to a state of equilibrium before it is actively loaded by means of an initial static analysis step with no external loads applied. If prestress is defined in the reinforcement and unless the prestress is held fixed, it will be allowed to change during an equilibrating static analysis step; this is a result of the straining of the structure as the self-equilibrating stress state establishes itself. An example is the pretension type of concrete prestressing in which reinforcing tendons are initially stretched to a desired tension before being embedded in concrete. After the concrete cures and bonds to the reinforcement, release of the initial prestressing strand tension transfers load to the concrete, introducing compressive stresses in the concrete. The resulting deformation in the concrete reduces the stress in the strand. A keyword in Abaqus/CAE, Initial Conditions, was used to define an initial prestress for reinforcement (SIMULIA 2010d).

3.2.6 Solid RC Test Results and FE Comparison

As seen in Figure 3-6, all of the FE models show good comparison to the test results of the solid specimens. The FE models for the large panels had a slightly higher strength than the tests, which is likely due to slight differences between actual material properties of concrete and steel and FE input parameters or variability in the constructed specimen from the design layout. All of the FE models did capture the correct failure mechanisms, concrete crushing for the non-PS specimens and prestressing strand fracture for the PS specimen. The FE model of the large PS specimen failed at a slightly larger deflection than the tested specimen. This difference occurred because a typical stress-strain curve for seven-wire low-relaxation prestressing strands, which likely had an ultimate strain that differed from the actual material used, was chosen to model the strands since no test data from samples was available. Although the ultimate strain used in the model was based on a recommendation in the PCI Design Handbook (PCI 2004), the minimum ultimate strain specified in ASTM A416, the ASTM specification that governs the required material properties of seven-wire steel strands, is only 3.5 percent. Therefore, the ultimate strain used in the model was likely larger than the actual ultimate strain of the strands used in the tests, and since the strain capacity of the prestressing strands controlled the ductility of the panels, the FE model and test failed at different deflections.

The results in Figure 3-6 are presented in terms of force (or pressure) versus rotation. Rotation refers to the approximate support rotation of the panels. Although deflection is more common means of reporting the flexural response of beams tests, rotation was used in many of the test vs. FE comparison figures, because rotation is commonly used as a response limit in blast design. This concept will be further discussed in Chapter 4. In essence, support rotation relates the midspan deflection of the panel to the span length. The midspan deflection was measured in

the tests and FE models, and the support rotation, θ, was calculated using Equation 3-4. This equation assumes all of the panel curvature is concentrated in a single hinge at midspan. Although this is an inaccurate representation of the deflected shape of a panel prior to yield, it was considered a reasonably accurate assumption for the post-yield behavior of the panels and used to calculate rotation throughout the entire response history for simplification purposes.

$$\theta = \arctan\left(\frac{\Delta}{L/2}\right) \tag{3-4}$$

where

Δ = midspan deflection

L = clear span length

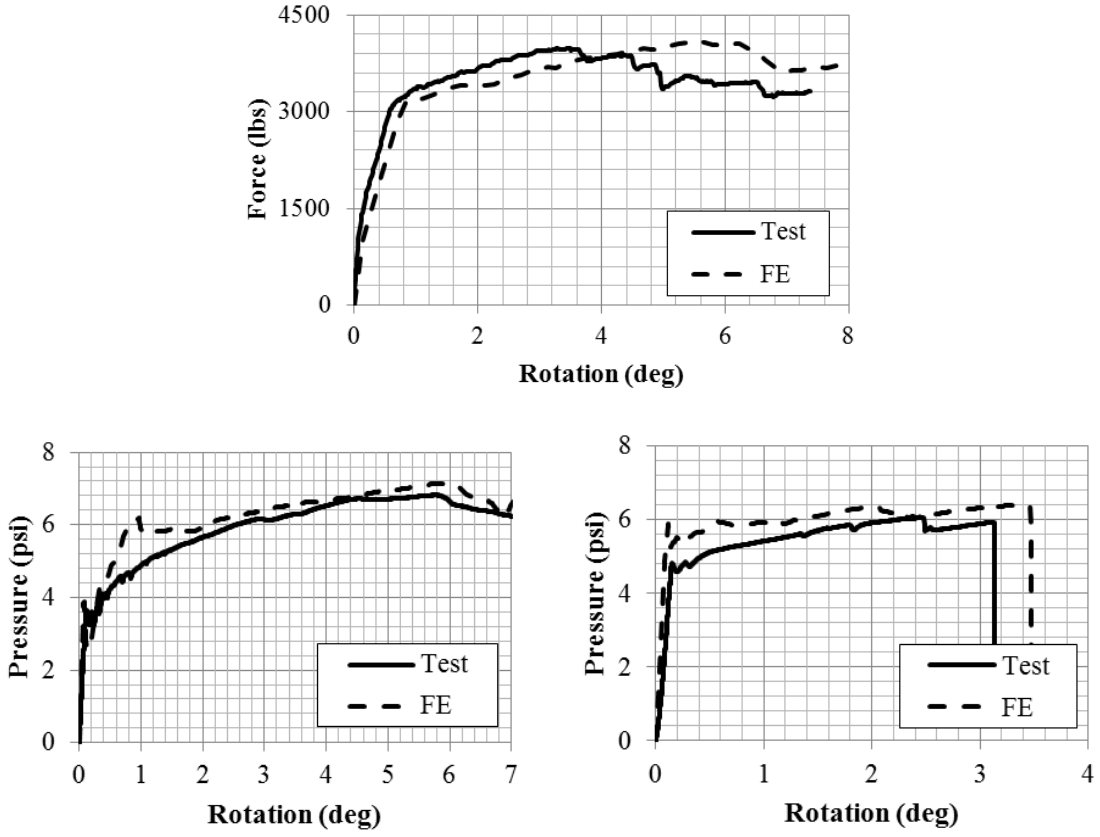

Figure 3-6: Comparison of Solid RC Test and FE Results - Small Non-PS (top), Large Non-PS (left), Large PS (right)

3.3 Insulated Sandwich Panel Flexural Tests

The construction of sandwich panels introduces several more variables that must be considered in order to model these systems accurately. These variables include the configuration of concrete and foam layers, the type of insulation used, and the shear tie system. Direct shear tests of various shear ties were completed to better understand shear tie behavior and provide a means for modeling (Naito et al. 2009). A series of conventionally reinforced and prestressed sandwich panels tested at the University of Missouri was used to validate the modeling approach used for sandwich panels. A load tree, as seen in Figure 3-7, was used to apply a uniform distributed load across the panels (Naito et al. 2011a).

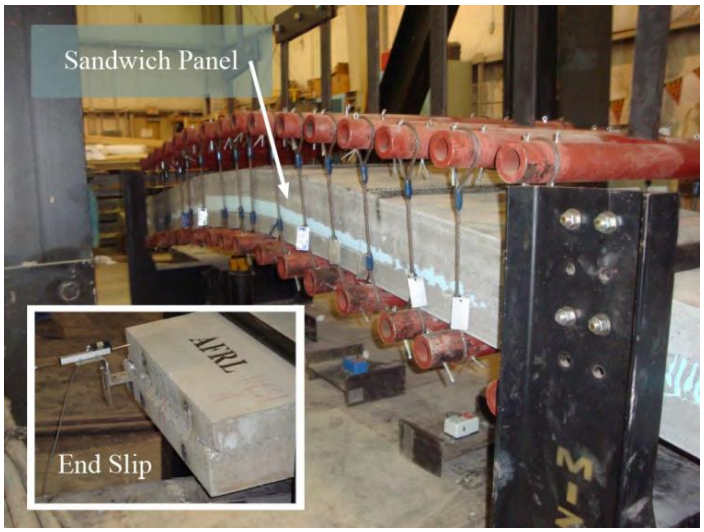

Figure 3-7: Single-span Loading Tree (Naito 2011a)

3.3.1 Shear Connectors

There are several means of transferring shear between concrete wythes in precast sandwich panels. Solid concrete regions that pass through the foam and various steel connectors have been used in the industry for quite some time for connecting concrete layers and transferring shear. Solid concrete regions provide good points for attached hardware used in handling, transportation, and construction. Steel connectors, such as C-clips and M-clips, are also

inexpensive and widely available options for connecting concrete layers. The drawback for both solid concrete regions and steel connectors is they allow for a thermal bridge through the insulation, decreasing the thermal efficiency of the panel. Energy-efficient shears ties were developed from materials such as fiberglass and carbon fiber and are currently being used in modern energy-efficient construction. Shear ties can also be categorized as non-composite or composite, depending upon the amount of composite action required for the service life of the sandwich panel being designed.

3.3.1.1 Shear Tie Test

A series of direct shear tests was conducted on various commonly used shear ties in industry today. The results from these tests were used to define the shear resistance of ties between the wythes of the sandwich panels. The testing configuration consisted of three concrete layers, two shear ties, and two layers of foam as shown in Figure 3-8. The symmetrical test configuration was chosen to minimize eccentricity. The outer two concrete wythes were fixed at the bottom, and the middle layer of concrete was pulled vertically. Total vertical load and vertical displacement were recorded. Since the system consisted of two ties, total load was divided by two to provide an accurate resistance for a single tie. Extreme differences in resistances provided by commercially available shear ties were observed, as seen in Figure 3-9 (Naito et al. 2009).

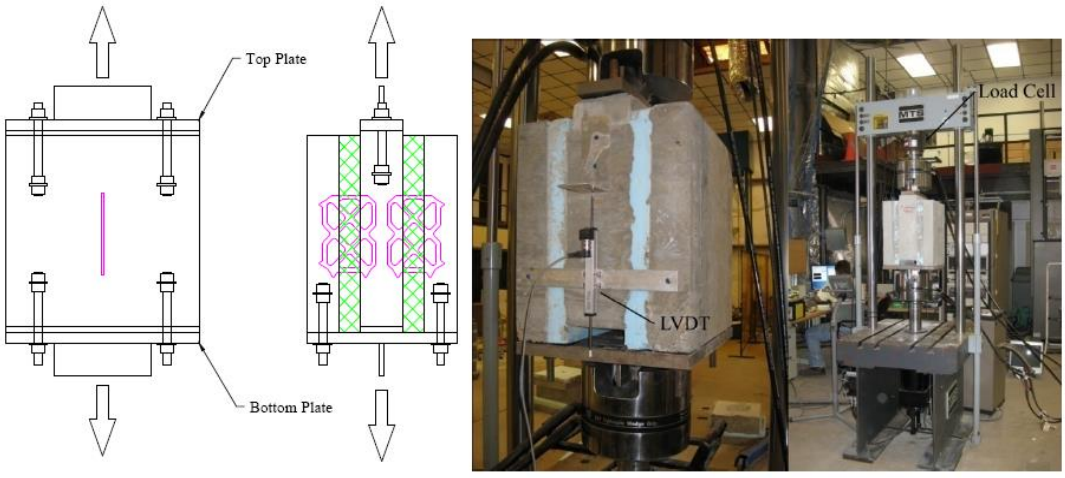

Figure 3-8 Direct Shear Test Configuration (Naito et al. 2009)

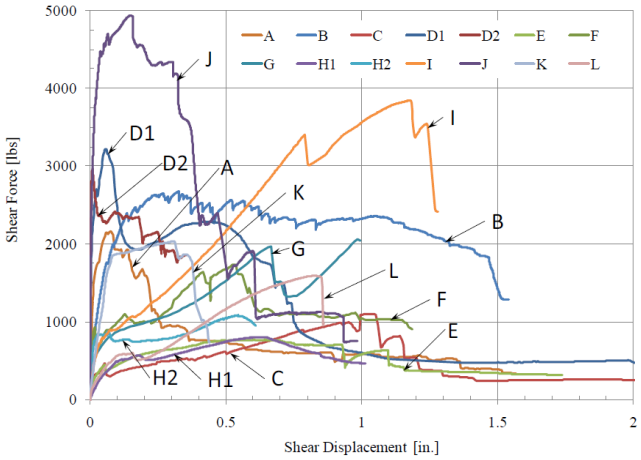

Figure 3-9: Comparison of Shear Tie Connector Performances (Naito et al. 2009)

3.3.1.2 Shear Tie Modeling Methodology

The results of the static shear tie tests were used to develop resistance curves to be used in the FE models. Originally, modeling the ties explicitly with the geometry and material properties of each tie was considered; however, due to the complexity and variety in tie geometries and the limited material property data available, the ties were modeled indirectly using the data collected from the direct shear tests. This data was used to develop shear resistance curves for each type of tie, and these resistance curves were implemented into the models using spring elements.

Two different approaches for implementing spring elements into the system were considered. The goal of the modeling approach for the shear ties was to tie the concrete wythes together and to simulate the correct shear force transferred through the ties as the concrete wythes slip apart. The two approaches used two different spring elements, which will be referred to as “global” and “local” springs. Both springs connect two nodes and apply a force based on a relative displacement between the two nodes. They will be referred to as “global springs” and “local springs,” because the relative displacement between the nodes is measured based on displacements in a specified global coordinate direction for one spring and in a local coordinate

direction for the other spring. These springs are referred to as Spring2 and SpringA elements in Abaqus/CAE (SIMULIA 2010c); however, the shear tie modeling methodology is not exclusive to Abaqus/CAE, so the general descriptive names, global and local springs, will be used.

The first approach that was attempted used global spring elements to attach the concrete nodes at the interior faces of the top and bottom concrete wythes, as seen in Figure 3-10. Individual springs were used to represent each tie in the panel and were assigned a nonlinear resistance curve that was applied in the longitudinal shear direction of the ties. For example, the sandwich panel shown in Figure 3-11 is oriented such that the longitudinal shear direction of the springs corresponds to the global Y-axis; therefore, for this particular model, the resistance curve for each spring would be applied in the global Y-axis direction. As Node 1 and Node 2 displace in the global Y-axis direction relative to each other, the spring applies a force in the Y-axis direction at each node based on the assigned resistance curve.

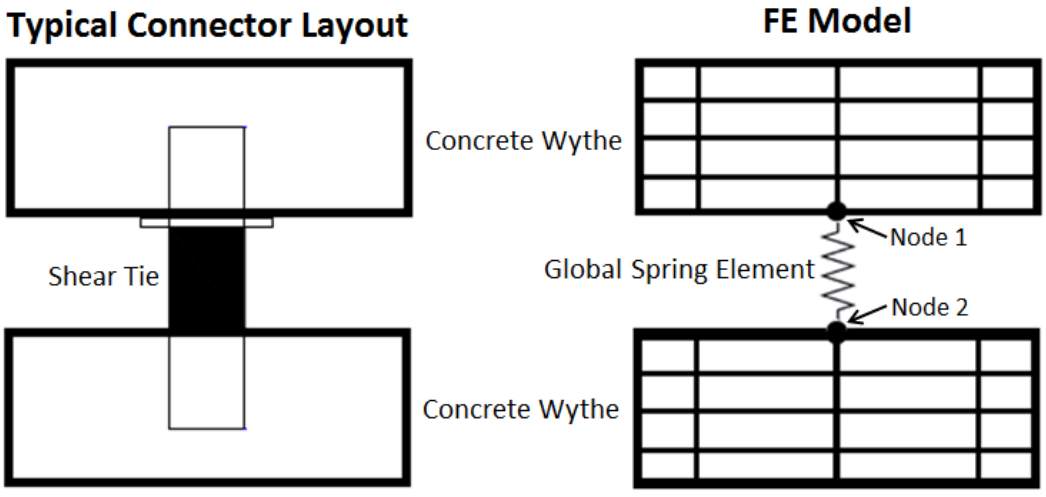

Figure 3-10: Global Spring Modeling Approach

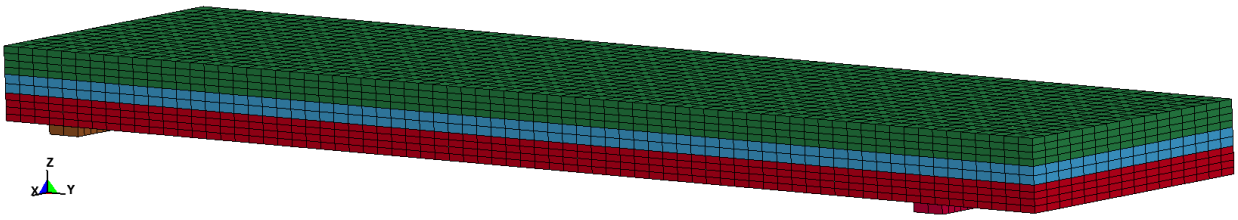

Figure 3-11: Sandwich Panel Orientation

This approach, however, was not able to capture the behavior of the ties effectively in a large displacement scenario. As the panel displaces and rotates about its supports, the orientation of the ties changes. As depicted in Figure 3-12, this change in orientation results in the relative displacement between the two nodes in the Y-axis direction to be less than the actual slip of the concrete wythes; therefore, this approach does not simulate the correct shear force transferred by the ties.

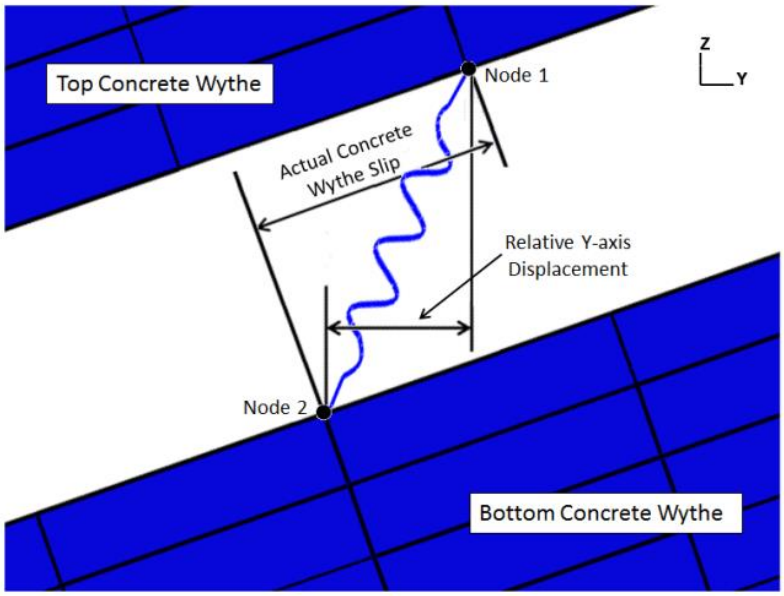

Figure 3-12: Large Displacement Behavior of Global Spring Element

Since the global springs were not able to capture the large displacement behavior of the ties accurately, another approach was developed using local spring elements. These spring elements also attach two nodes and are assigned a nonlinear resistance curve; however, instead of relating the resistance curve to the relative displacement of the nodes in a global axis direction, these springs relate the resistance curve to the absolute displacement between the nodes. The springs measure the absolute displacement between the nodes and apply a force at each node based on the resistance curve with the line-of-action of the force being the line joining

the two nodes. This allows the line of action to rotate in a large displacement analysis (SIMULIA 2010c).

In the global spring approach, the spring connected the concrete node at the interior face of the top wythe to the concrete node at the interior face of bottom concrete wythe; however, to implement these local springs, a different approach was required. In addition to the local spring element, two beams elements were used to simulate each tie with a beam-spring system. As seen in Figure 3-13, each beam element runs through the thickness of a concrete wythe into the middle of the insulation wythe. The beam nodes were merged with the concrete nodes, and the tips of the beams meet at the center of the panel thickness. The local spring element is used to connect the nodes at the tips of the beams, referred to as Node 1 and Node 2 in Figure 3-13.

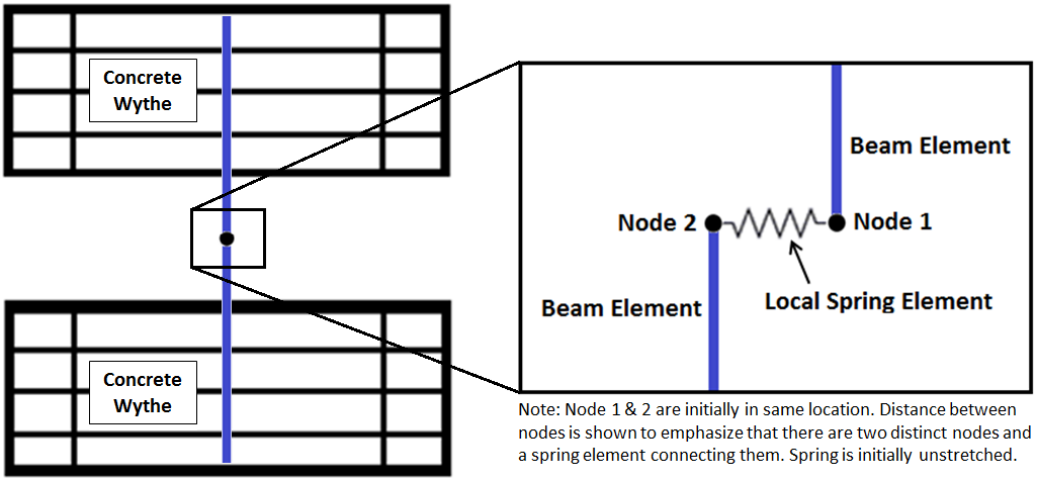

Figure 3-13: Local Spring Modeling Approach

The beams were given an artificially large stiffness to make them essentially rigid and eliminate deflections in the beams. This ensured that the orientation of the beams remained perpendicular to the face of the top and bottom concrete wythes. As seen in Figure 3-14, as the panel deflects and the concrete wythes slip apart, the nodes separate, and the spring stretches. As the spring stretches it applies a force at the tips of the beams, and the beams carry that force as a

shear force into the top and bottom concrete wythes. Figure 3-14 shows that, even as the panel rotates, the line of action of the spring is able to rotate and accurately capture the slip between the concrete wythes.

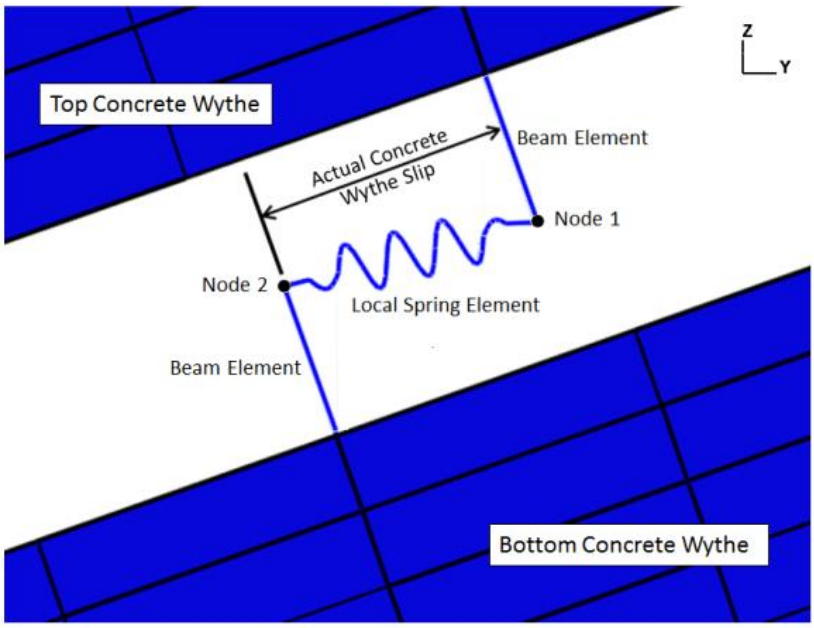

Figure 3-14: Large Displacement Behavior of Local Spring Element

The springs and part of the beam elements occupy the same space as the foam wythe but have no interaction with the elements used to simulate the foam. Multiple spring elements were used along the length of the panel to simulate each discrete tie. In panels with a distributed tie system, discrete spring elements were still used, and an equivalent resistance curve was calculated based on the spacing of the springs. Different spacing of the springs was evaluated, but there was no considerable difference in the results of these models. A spacing of 16 inches was chosen for the springs used to simulate distributed ties, because 16 inches was also a common spacing for discrete ties.

One aspect of shear ties that this approach does not consider is the axial force transferred by the ties. The modeling approach only accounts for the transferred shear force, but this discrepancy was considered acceptable because the shear behavior of the tie is its primary

function in the wall system. It was also understood that the compression of the foam would result in additional elongation of the spring not associated with shear displacement as seen in Figure 3-15. This effect was monitored and considered negligible since the elongation due to shear was much larger than the elongation due to compression.

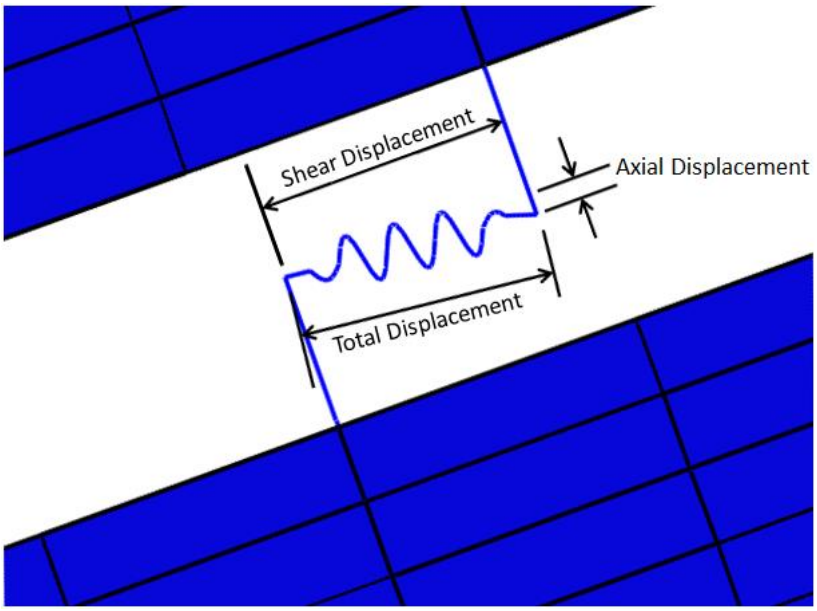

Figure 3-15: Spring Elongation due to Foam Compression

3.3.1.3 Shear Tie Resistance Curves

The results from the shear tie tests were used to develop simple resistance curves for the ties. The multipoint curves for a fiberglass composite and non-composite tie and a carbon fiber tie are shown in Figure 3-16. The curve for the carbon fiber tie shows the shear force in force per length units. This curve was used to develop the actual curves to be used for modeling by multiplying the shear force at each point by the spacing of the springs.

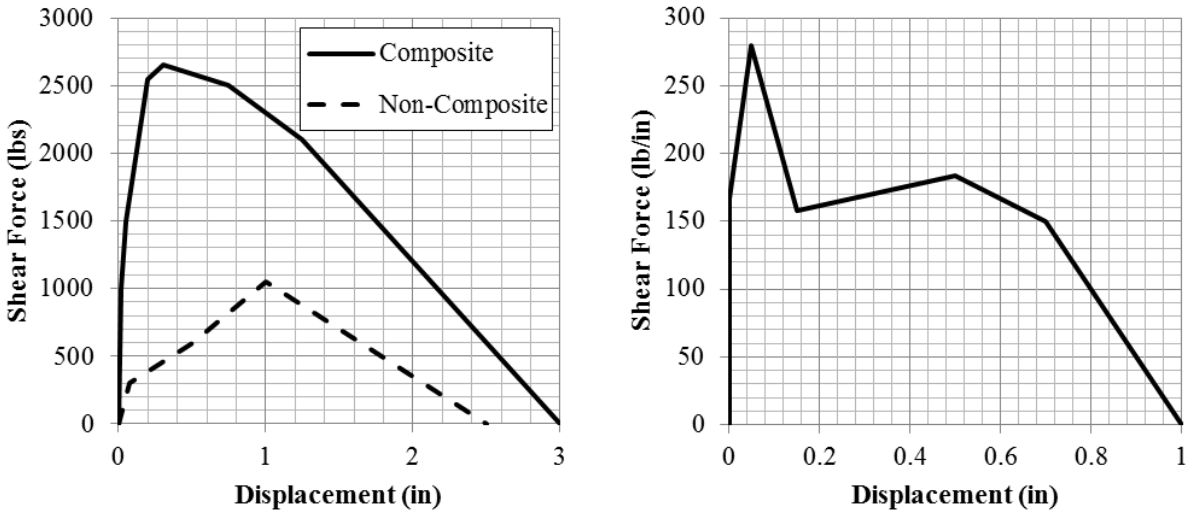

Figure 3-16: Shear Resistance Curves for Fiberglass Ties (left) and Carbon Fiber Composite Tie (right)

3.3.2 Wythe Configuration and Interface

The concrete and foam wythes were modeled as separated parts in the sandwich panel models. The top and bottom concrete wythes were connected by the beam-spring systems that were described previously. The foam was only connected to the concrete wythes by a hard contact condition. This contact condition allowed for the surfaces of the concrete to freely slip along the foam but ensured that the surfaces remained together as the panel deflected. The interface properties between the concrete and foam did not include friction since the results of the direct shear tests indirectly included the shear resistance provided by frictional forces.

3.3.3 Insulation Foam Modeling

Stress-strain data from compressive testing of XPS insulating foams, as seen in Figure 3-17, was used for the material model input for the foam elements (Jenkins 2008). Significant sandwich panel resistance differences can occur due solely to foam type, as illustrated in Figure 3-18 for XPS and polyiso. The similar shape of the resistance curves indicates that the panels formed the same failure mechanism, but the use of polyiso versus XPS caused a significant drop

in resistance throughout loading (Newberry 2011). Hassan and Rizkalla (2010) also noticed a significant difference in the peak flexural resistance of sandwich panels insulated with XPS and EPS foams and attributed this difference to the shear transfer by the bond between the concrete and foam. He proposed different shear flow capacities for CFRP shear grid with XPS and EPS foam. The difference in shear transfer from different foams was likely the cause for the difference in panel performance of the XPS and polyiso panels as well. Although different foams led to different resistances in sandwich panel testing, it was concluded that the use of one foam material model was acceptable, since the shear resistance of the foams was captured in the spring resistance curves, not the foam-concrete interface, and the bending stresses in the foam are likely negligible.

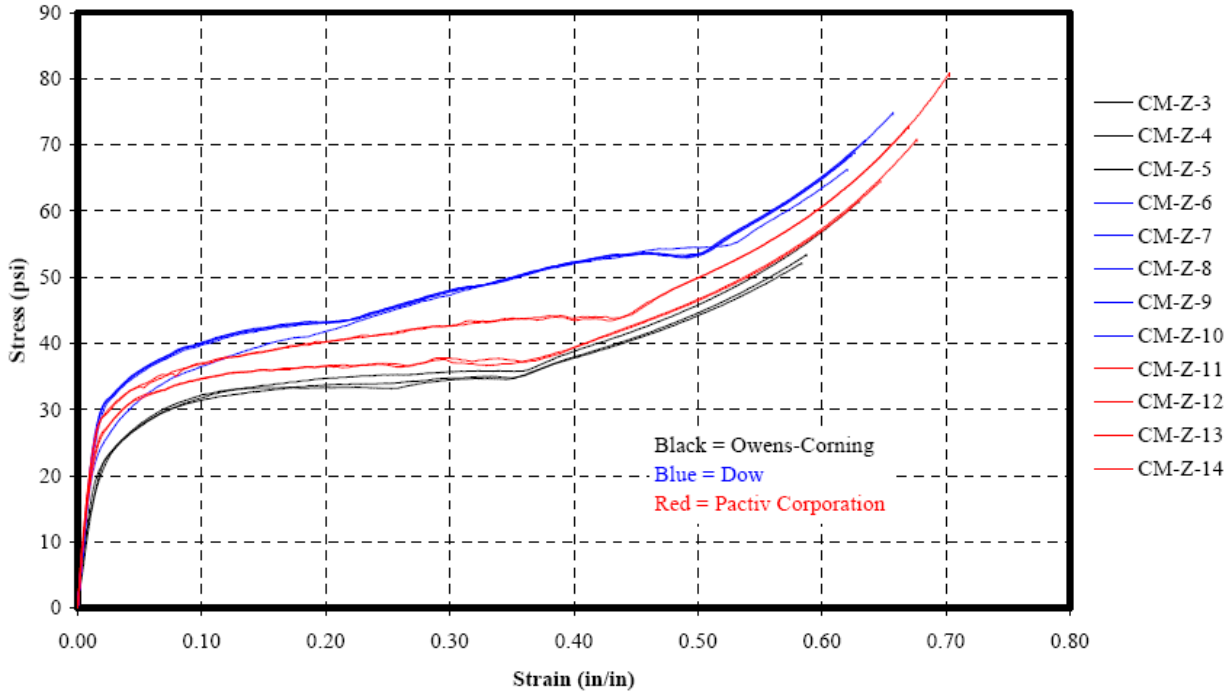

Figure 3-17: Comparison of Stress-Strain Response of Various XPS Products (Jenkins 2008)

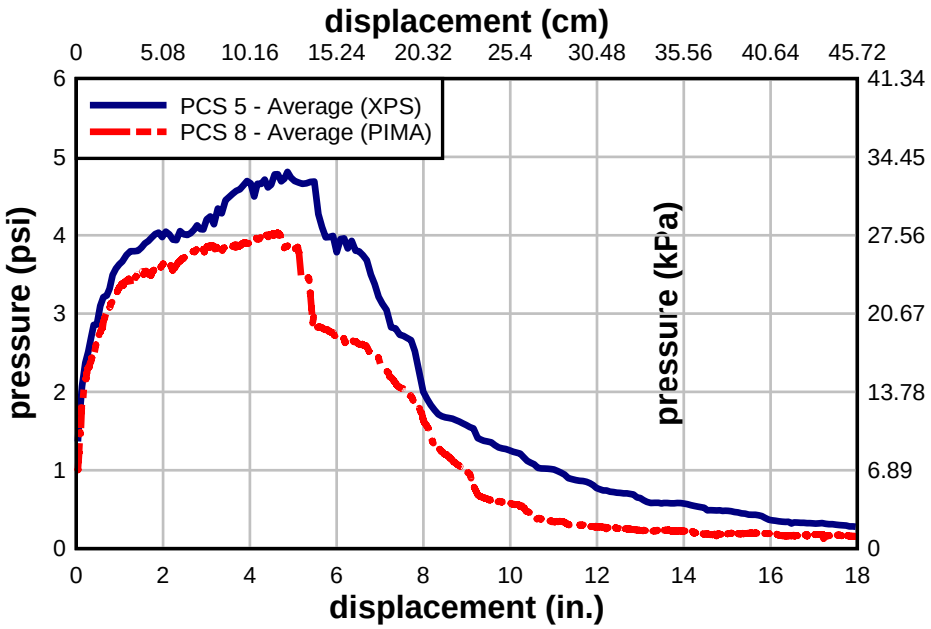

Figure 3-18: Comparison of Similar Panel Resistances with Different Foam Insulations (Newberry 2011)

Additional compression testing of EPS, XPS, and polyiso sample foam cylinders, shown in Figures 3-20, 3-21, and 3-22, was conducted by AFRL to compare the stress-strain behavior of the different foam materials (Newberry 2011). The graphs show that the foam materials have significant strain capacity and theoretically could absorb large amounts of energy if fully compressed. Statically, this capacity is insignificant since the bending stresses of the foam contribute very little to the overall resistance. It is possible that large compressive stresses could develop in the foam insulation during early stages of a dynamic blast load before panel flexure becomes the primary response. This form of energy dissipation is limited, however, by the presence of rigid shear ties, which transfer axial forces between the exterior and interior wythes.

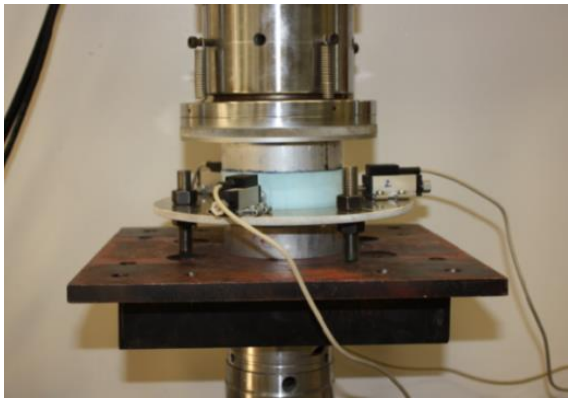

Figure 3-19: Test Setup for Compression Testing of Foam Cylinder Samples (Newberry 2011)

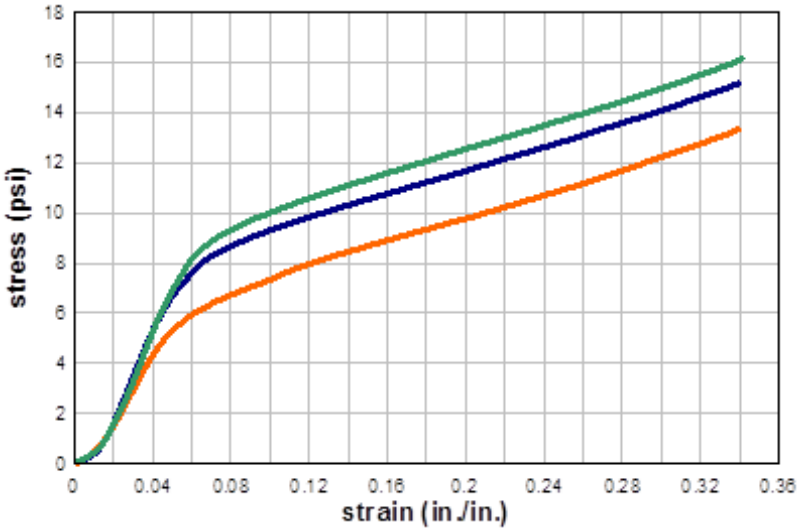

Figure 3-20: Stress-Strain Curve of EPS Foam Samples (Newberry 2011)

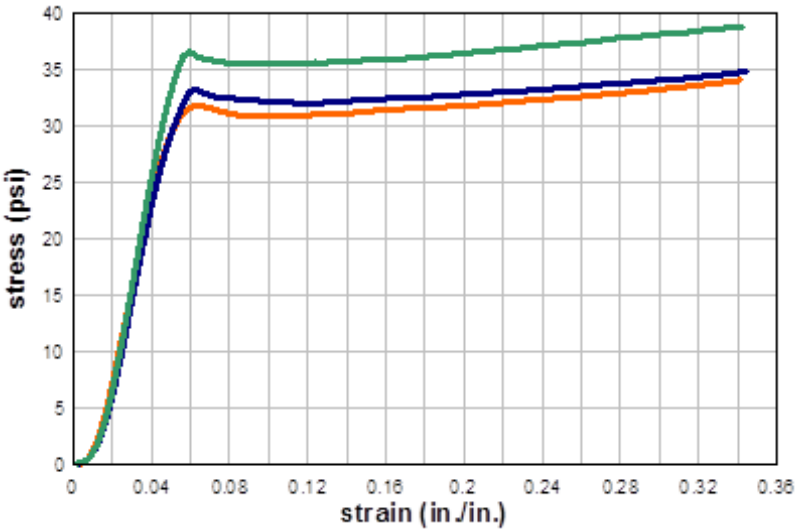

Figure 3-21: Stress-Strain Curve of Polyiso Foam Samples (Newberry 2011)

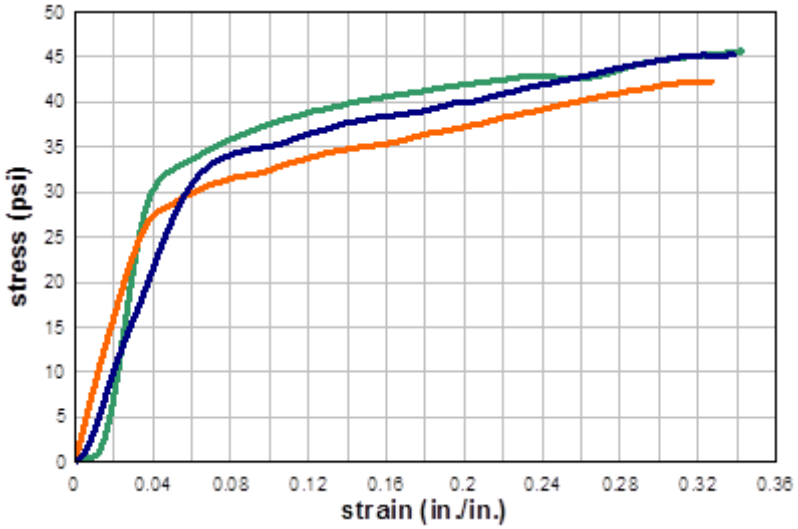

Figure 3-22: Stress-Strain Curve of XPS Foam Samples (Newberry 2011)

3.3.3.1 Material Model and Parameters for Insulation

The Crushable Foam material card in Abaqus/CAE was used to model the compressive stress-strain properties of the foam material. The specific input is shown in Table 3-3.

Table 3-3: Crushable Foam Material Card Input

Crushable Foam		Crushable Foam Hardening	
E (psi)	1370	Yield Stress (psi)	Uniaxial Plastic Strain
ν	0.1	32	0
		33	0.0063
Density (pcf)	3.5	38	0.0593
		40.7	0.1083
Compression Yield Stress Ratio	1	43.8	0.2223
		48.2	0.3363
Hydrostatic Yield Stress Ratio	0.1	53.38	0.5493
		56.4	0.7237
		67.47	0.9676

3.3.4 Static Sandwich Panel Test Results and FE Comparison

The sandwich panel testing conducted at the University of Missouri was used to validate the FE results (Naito et al. 2011a). The pressure vs. rotation results of three specimens in particular, described in Table 3-4, were selected to compare to FE results. These three specimens had a variety of different parameters, including reinforcement (non-PS and PS), wythe configuration, and shear ties. Figure 3-23 illustrates the initial comparison between the results of the testing and FE models.

Table 3-4: Static Sandwich Panel Validation Matrix

Specimen	Reinforcement Type	Wythe Conf.	Insulation	Panel Reinforcement (Longitudinal/Transverse)	Shear Ties
TS1	conventionally reinforced	323	XPS	# 3 /#3	fiberglass composite
TS2	conventionally reinforced	623	XPS	# 3 / WWR	fiberglass non-composite
PCS2	prestressed	323	EPS	3/8 strand / WWR	carbon-fiber composite

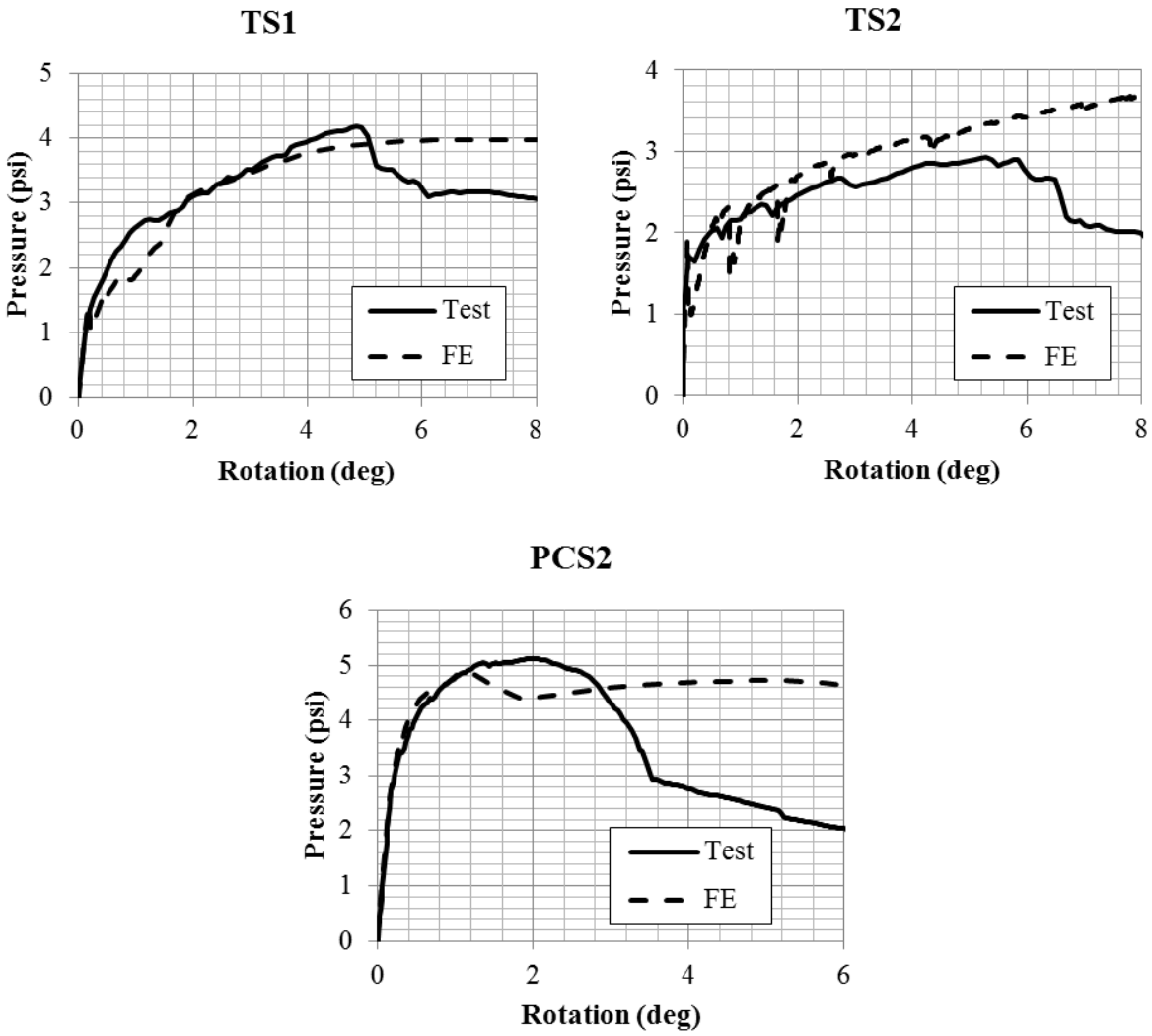

Figure 3-23: Initial Comparison of Sandwich Panel Testing vs. FE Model Results

Each of the models compared fairly well with testing in the early stages of loading. The initial stiffness and load-deformation path up until the peak strength compared well with the test results; however, after the models reached their peak strengths, they continued to deform almost plastically out to large rotations, while the test results showed a softening behavior in the panel resistances. This comparison demonstrated that the data produced from the direct shear test of the ties accurately describes the initial shear stiffness and peak shear strength of the tested ties. However, this initial approach for implementing the shear tie resistance into the model did not

capture the failure of the ties and its effect on the global behavior of the panels. There are a couple reasons for this discrepancy. First, it was observed in several tests that the shear ties began to fail on one end of the panel, unzipping toward the middle, causing unsymmetrical forces in the panels; however, numerically the FE models are perfectly symmetric with no imperfections. In the models the ties on both ends of the panel fail simultaneously resulting in a symmetric failure mechanism. This failure mechanism can cause a difference in the response of the FE model from the test panel, whose unsymmetrical failure mechanism was initiated by a slight geometric or constitutive imperfection. Also, as described earlier the resistance curves used for the ties were determined from direct shear tests. Although the main response of the ties during loading of the sandwich panels is in shear, the ties also experience axial and flexural stresses in addition to shear stresses. Based on the difference in FE and test results, it was determined that while the direct shear test did capture the stiffness and strength of the ties, it did not accurately capture the failure of the ties under the state of stress that the ties experience in a sandwich panel system.

3.3.4.1 Calibration of Shear Tie Resistance Curves

In order to account for this effect in the resistance curves, the elongation of the ties was monitored in relationship to the displacement of the panels. For each of the panels the elongation of the spring closest to the support was noted at the point where the panel begins to soften, and in the resistance curve the shear strength was rapidly brought to zero at the shear displacement equal to that amount of elongation. The final shear resistance curves used for the springs and the resulting FE vs. test comparison are shown in Figures 3-24 and 3-25.

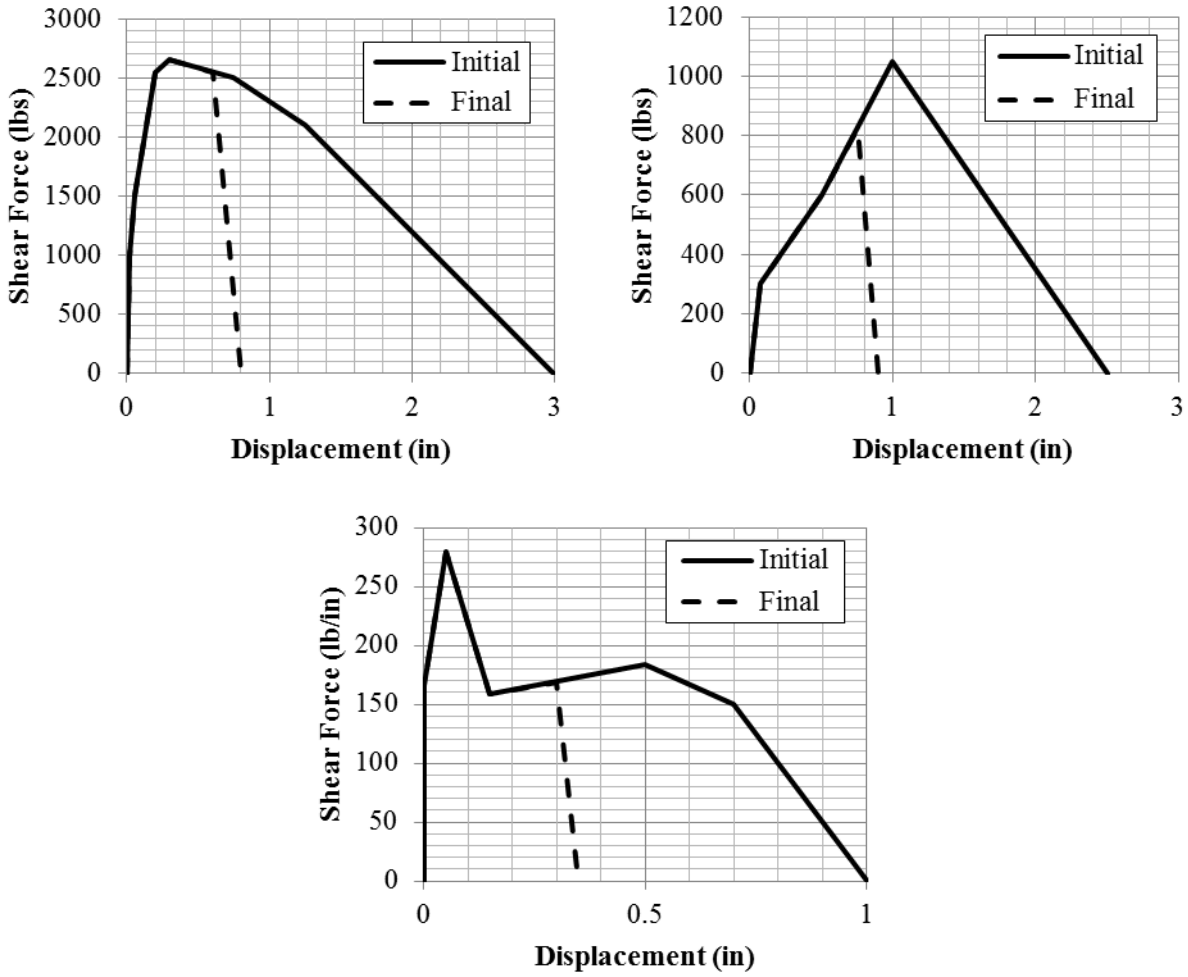

Figure 3-24: Final Shear Resistance Curves for Fiberglass Composite Tie (left), Fiberglass Non-Composite Tie (right), and Carbon Fiber Composite Tie (bottom)

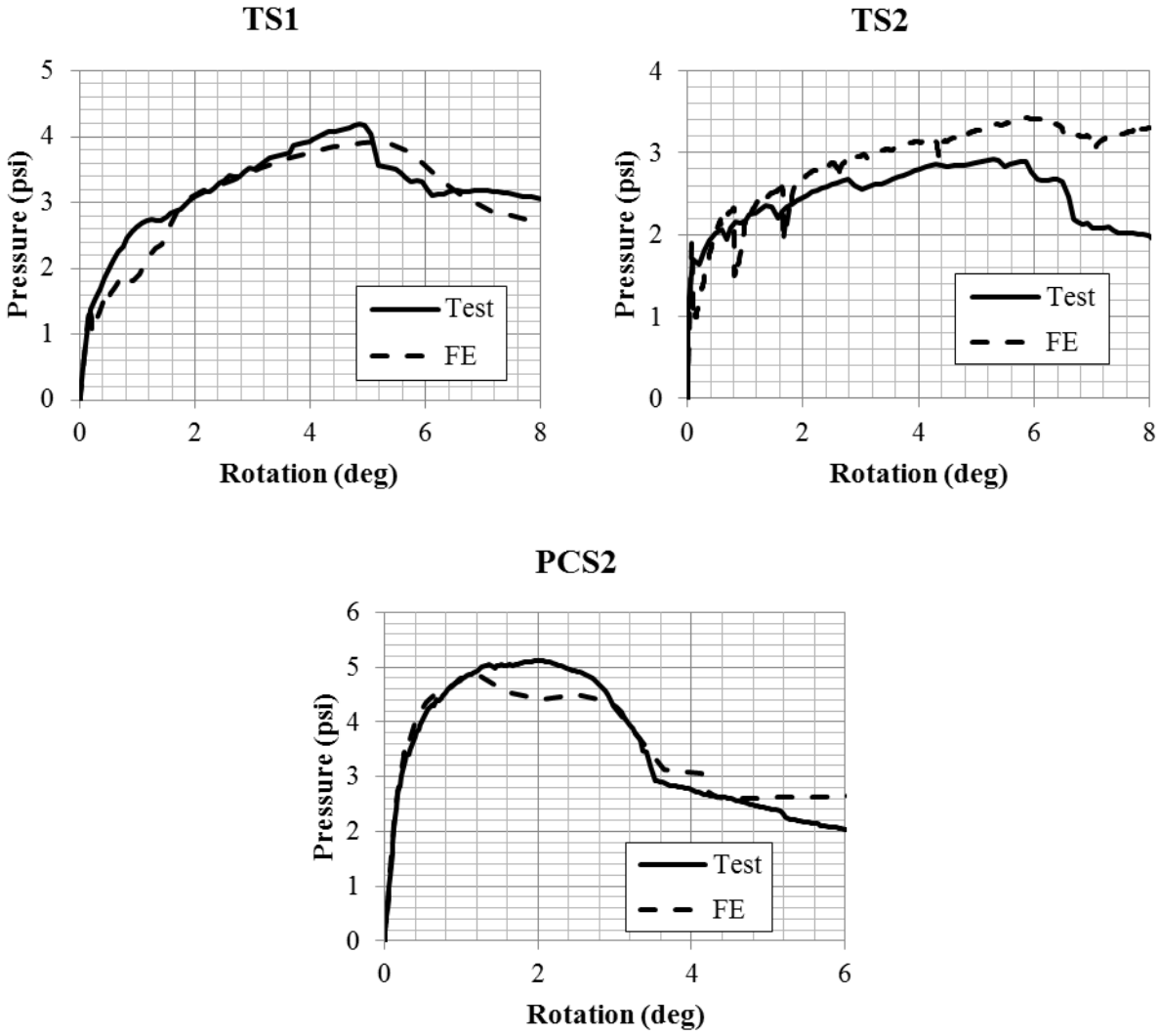

Figure 3-25: Final Comparison of Sandwich Panel Testing vs. FE Model Results

3.4 Dynamic Testing and Modeling of Sandwich Panels

All of the analyses discussed so far have been static analyses of non-PS and PS concrete members. As stated before, the purpose of these static analyses was to validate a FE modeling methodology for prestressed, insulated panels that could be used to study these systems under blast loads. The final step in the process was to implement the methodology developed with the static analyses in a dynamic FEA. LS-DYNA was used to conduct all the dynamic analyses in

this study. Results from full-scale dynamic experiments were used for the final comparison and validation of FE models.

Modeling these systems dynamically adds complexity to the analysis. The solution approach switches from just solving a set of equilibrium equations to solving the time-dependent equation of motion. Although much of the modeling methodology is the same, a few new modeling parameters arise due to the time-dependent nature of the analysis.

3.4.1 Full-Scale Dynamic Testing

Full-scale dynamic testing conducted by the Airbase Technologies Division of the Air Force Research Laboratory at Tyndall Air Force Base, Florida was used to validate the modeling methodology for sandwich panels in LS-DYNA. Two series of testing were conducted but only the second series, Dynamic Series II, was used for comparison in this study (Naito et al. 2011b). The test series included eight panels per test (four single span panels and four multi-span panels). This series was chosen because it included single span panels with a clear span close to ten feet, and the FE simulation was focused upon two of the four single span panels, a conventionally reinforced and a prestressed panel. The test series included two experiments, a small pre-detonation blast and a large primary detonation. The small pre-detonation blast was designed to induce elastic deformations in the structure, so the FE models could be compared to test results without damaging the panels. The primary detonation was designed to push the panels close to their ultimate strength and induce large deformations. The panels were all precast 3-2-3 insulated sandwich panels, including both conventionally reinforced and prestressed and fiberglass and carbon-fiber composite shear ties. The details of the panels used in this study are included in Table 3-5. The reflected pressures and dynamic deflections were recorded at midspan for each detonation. An average of the recorded pressures was used to create a load curve to be used in

the FE models for each detonation. Figure 3-26 shows the reaction structure for the single span panels.

Table 3-5: Full-Scale Dynamic Test Panel Details

Specimen No.	Wythe Configuration	Tie Type	Insulation Type	Reinforcement Type
SS1	3-2-3	carbon-fiber composite	EPS	prestressed
SS3	3-2-3	fiberglass composite	XPS	conventionally reinforced

Figure 3-26: Single Span Reaction Structure for Full-Scale Dynamic Tests (Naito et al. 2011b)

3.4.2 Material Model for Concrete in LS-DYNA

There are many material models available in LS-DYNA that can be used to model concrete, but the Concrete Damage Release III model (MAT_72R3) was chosen for this study. MAT_72R3 is a plasticity-based model which uses three independent shear failure surfaces that change shape based on the confinement pressure. The model works in parallel with the Tabulated Compaction Equation-of-State, which defines the pressure-volumetric strain response of the

model. The advantage of this model is that all of the necessary input parameters can be automatically generated based on the unconfined compressive strength. Since the unconfined compressive strength can be easily derived from simple experiments, the present concrete model is very useful, particularly when the known concrete properties are limited as is common in design (Malvar et al. 1997; LSTC 2009; El-Dakhakhni et al. 2010). Another advantage of the MAT_72_R3 model is that it has an input option for a curve defining strain rate effects.

3.4.3 Simulation of Prestressing Effects in LS-DYNA

In LS-DYNA an initial prestress condition can be applied using the CONTROL_ DYNAMIC_RELAXATION keyword. When the dynamic relaxation feature is activated, a damped explicit analysis is performed, where the initial condition is ramped up and held until a quasi-static equilibrium condition is reached by means of scaling nodal velocities by a factor (DRFCTR) each time step. When the ratio of current distortional kinetic energy to peak distortional kinetic energy falls below the convergence tolerance (DRTOL), the dynamic relaxation analysis stops and the current state becomes the initial state of the subsequent transient analysis. Once the preload state is achieved, the time resets to zero and the normal phase of the analysis automatically begins from the preload state (LSTC 2009). The prestressed condition was activated in the models by selecting ELFORM=3 (truss element) in the beam section card and specifying values for RAMPT (ramp time for stress initialization by dynamic relaxation) and STRESS (initial stress value). The dynamic relaxation feature can also be activated as an implicit analysis, which would be similar to the stress initialization process in Abaqus/CAE; however, the explicit dynamic relaxation feature was used in this study.

3.4.4 Dynamic Increase Factors

When structures are subjected to blast effects, the resulting accelerations of structural mass can lead to high strain rates in the members. These high strain rates lead to an apparent increase in strength of concrete and steel materials. To accurately capture the behavior of a structural member to blast effects in a dynamic analysis, the increase in material strength needs to be accounted for. This increase in strength is commonly accounted for using a dynamic increase factor (DIF), or the ratio of dynamic strength to static strength.

A curve defining the DIF as a function of strain rate was used to enhance the strength of concrete in tension and compression. The curve was a bilinear curve (in log-log plot) based on the CEB formulation with slight modifications to the tensile strain rate definition (Malvar et al. 1998). The strength enhancement is also defined as a function of the unconfined compressive strength; therefore, different curves were used for models with different unconfined compressive strengths. Sample input values used in LS-DYNA for a model with an unconfined compressive strength specified as 5,000 psi are shown in Table 3-6, and a sample rate effect curve is shown in Figure 3-27.

Table 3-6: LS-DYNA Rate Effect Input Values ($f_c^{'}$ =5,000 psi)

Strain Rate (1/s)	DIF
-3.E+02	9.69
-1.E+02	6.72
-3.E+01	4.50
-1.E+01	3.12
-3.E+00	2.09
-1.E+00	1.45
-1.E-01	1.36
-1.E-02	1.28
-1.E-03	1.20
-1.E-04	1.13
-1.E-05	1.06
-1.E-06	1.00
0.E+00	1.00
3.E-05	1.00
1.E-04	1.03
1.E-03	1.08
1.E-02	1.14
1.E-01	1.20
1.E+00	1.26
3.E+00	1.29
1.E+01	1.33
3.E+01	1.36
1.E+02	2.03
3.E+02	2.93

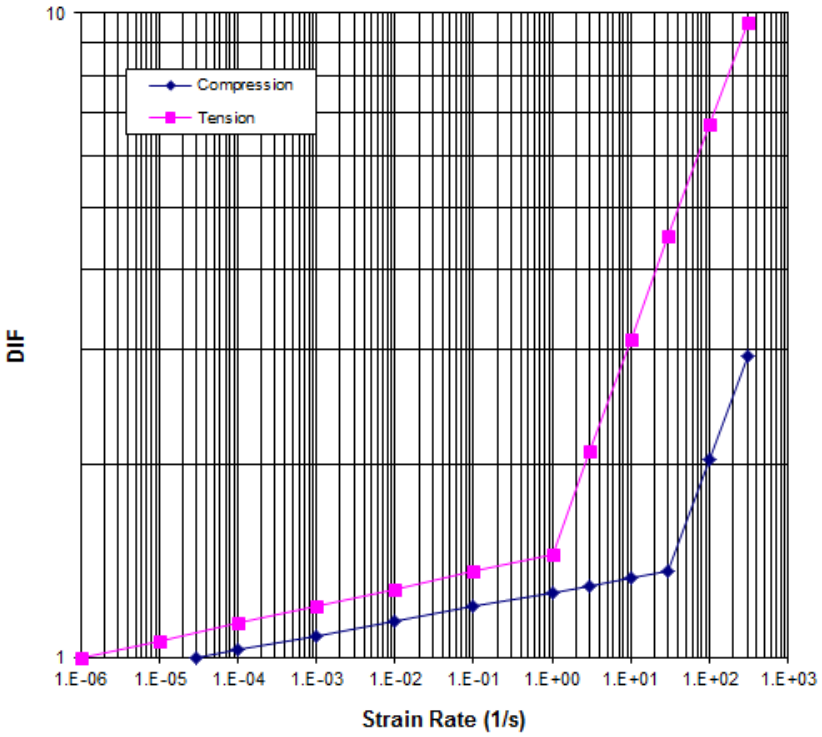

Figure 3-27: Rate Effect Curve for Concrete ($f_c^{'}$ =5,000 psi)

3.4.5 Loading, Boundary Conditions, and Solution Method

With the exception of axial loads, all of the loadings applied to the systems were meant to simulate the pressure from a blast wave. Unlike the static analyses, these pressures were not ramped up throughout the analysis but applied instantaneously and varying with time. The LOAD_SEGMENT_SET keyword was used. This card uses the pressure defined in a time history curve and a set of surfaces specified by the user to apply the load.

In the previous analyses the boundary conditions were accounted for by restraints applied to certain nodes. Although LS-DYNA has the capacity to apply boundary conditions in this manner, the boundary conditions were accounted for using a contact condition between the panels and additional supports. Supports were created using solid elements and rigid properties. The supports spanned along the width of the panels and were positioned in order to give a ten foot clear span. Boundary conditions were applied in this manner because members experiencing blast loadings will not only deflect in the direction corresponding to the overpressure but also rebound and deflect in the other direction. By applying the boundary as a contact condition, the panel is able to react with the support as it deflects in the blast wave direction but be free from the support as it rebounds.

Given that the systems being analyzed are highly nonlinear, a numerical solution is required to solve for the time dependent deformations of the systems. LS-DYNA uses the explicit central difference scheme to integrate the equations of motion. During the solution the time step is updated by looping through all the elements and using the minimum calculated critical time step of all the elements. Additionally, a scale factor is applied to the minimum value for stability reasons. The default scale factor, 0.90, was used in all of the following analyses (LSTC 2006).

3.4.6 Dynamic Test Results and FE Comparison

The comparison of the full-scale test and FE model results are presented in Figures 3-28 and 3-29. Figure 3-28 shows the comparison of the two panels during the pre-detonation blast. Deflections through multiple oscillations of the test panels' motion were recorded; however, the rebound connections were not included in the FE models, so only the comparison of the inbound deflections are shown in the figure. Figure 3-29 shows the comparison of the panels during the primary detonation blast. This blast caused much more damage, causing the rebound response to be less significant. Again, only the inbound deflection comparison is shown in the figure.

The FE models compared well with the test results in the pre-detonation cases. The apparent stiffnesses of the test and FE results matched very well. This test serves as a good comparison for the lateral stiffness of the panels, because the panels are experiencing minimal to no damage; thus, the stiffness should be unaffected. The peak deflections from the FE model were also within 20% of the test peak deflections. This comparison demonstrates that the shear tie modeling methodology simulates the shear transfer from the connectors accurately in the elastic range.

The FE models also compared fairly well with the test results in the primary detonation cases. The apparent stiffnesses of FE models were slightly less than the test stiffnesses. The peak deflections from the FE model were also within 20% of the test peak deflections. This indicates that the panels are experiencing similar amounts of damage and beginning to develop the same failure mechanisms. These comparisons were used to validate the use of this modeling methodology for insulated prestressed sandwich panels in further applications and studies.

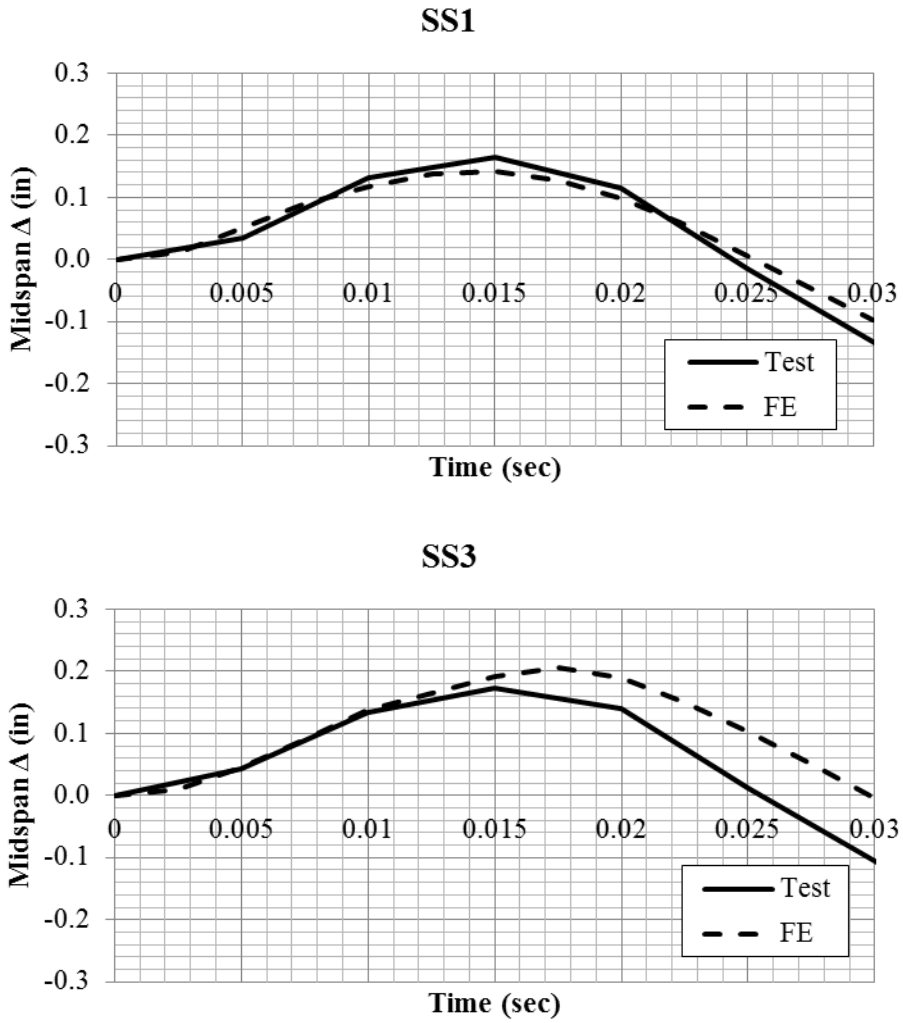

Figure 3-28: Test and FE Comparison of Pre-Detonation Blast Response

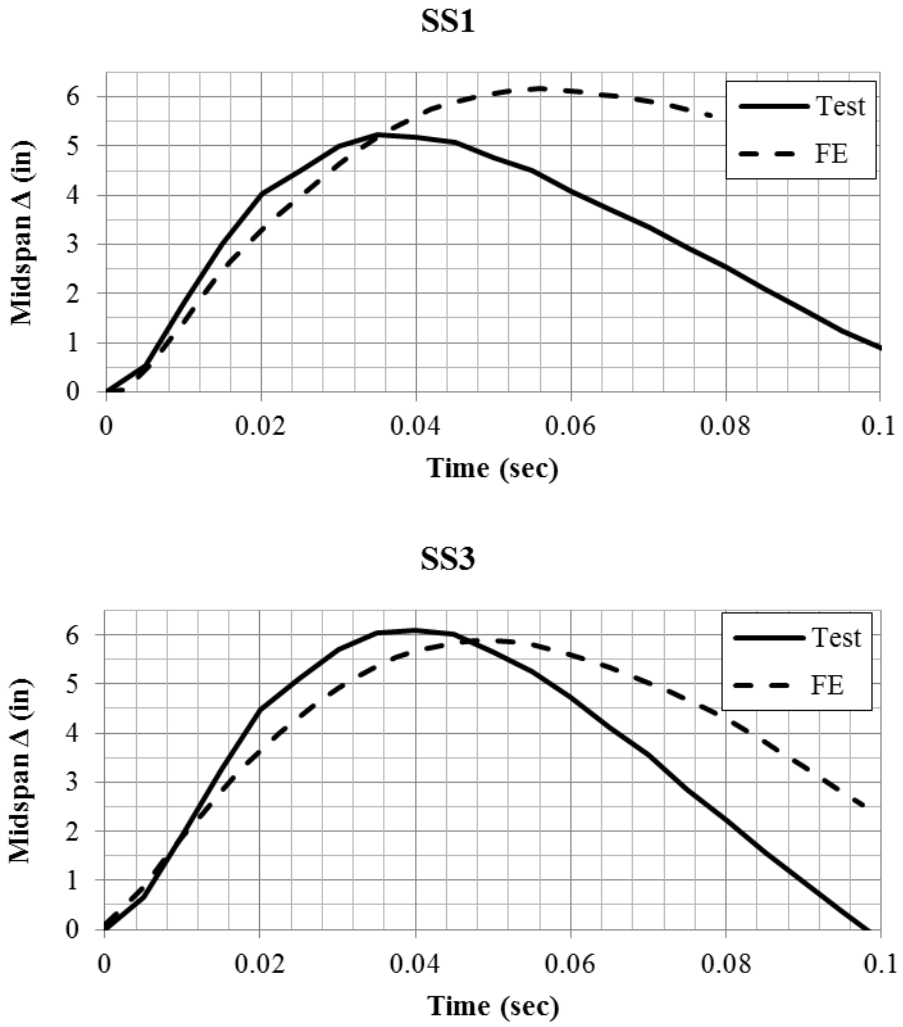

Figure 3-29: Test and FE Comparison of Primary Detonation Blast Response

3.5 Modeling Debonded Reinforcement

One parameter that the FE modeling methodology was to study was the effect that debonding the reinforcement from the concrete had on the failure mechanisms and ductility of the panels. This concept was implemented by sliding a piece of smooth Teflon tubing over a section of rebar at midspan, the location of greatest demand on the reinforcement for all cases, before the concrete was poured. By using this tubing, the concrete is unable to bond with the rebar over that section. When the reinforcement is allowed to bond with the concrete, the bond forces the concrete and reinforcement to strain together as the panel is loaded; however, if the

debond is applied, the reinforcement is free to strain independent of the concrete, resulting in slip between the concrete and reinforcement and uniform strain throughout the reinforcement in the debonded section. This technique was applied to tests of both conventionally reinforced and prestressed, solid and sandwich panels.

This debond effect provided another challenge to modeling these systems. In the models of the fully bonded panels, the concrete and reinforcement nodes were merged to simulate the bond between the concrete and reinforcement, but in order to model the debond effect another modeling technique was developed. For the panels with debonded sections, separate meshes were used for the bonded and debonded sections of reinforcement. In the bonded sections, the reinforcement nodes were merged with the concrete nodes as usual, but in the debonded section, the nodes were not merged but connected with a spring as seen in Figure 3-30. The spring was given an extremely large stiffness and applied only in the lateral or out-of-plane direction, so as the panel bends in flexure and deflects the concrete and reinforcement nodes move together in the direction of the deflection. The extremely large stiffness in essence constrained the nodes in that direction. The spring was only applied in the out-of-plane direction though, so the nodes were free to translate in the longitudinal direction independently, thus allowing for slip to occur between the concrete and reinforcement in that portion of the panel. The strain in the reinforcement was output from the FE results to show that this modeling approach was accurately simulating the effect of debonding the reinforcement.

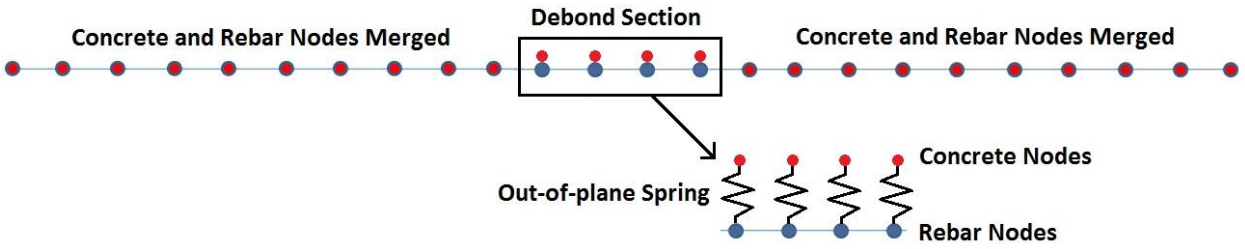

Figure 3-30: Debond Springs

3.5.1 Small, Debonded Solid Panel Test Results and FE Comparison

The original intent of the small and large solid panels presented previously was to serve as a control for comparison to debonded panels of the same layout that were also tested. The small solid panel was a singly-reinforced, non-PS panel with a four foot clear span. Two other sets of debonded panels with this same layout but varying debond lengths were also tested. One set of panels had a 7.5 inch debond length, and the other had a 15 inch debond length. Both of these panels were modeled in Abaqus/CAE using the same static modeling approach that was developed for the control panel. One slight difference between the tests and the FE models was the debond length. Because of the mesh resolution that was used, the FE models used a debond length of 8 and 16 inches instead of 7.5 and 15 inches. A comparison of the test and FE results is presented in Figure 3-31. The control panel results are also included in the figure even though they can also be seen in Figure 3-6.

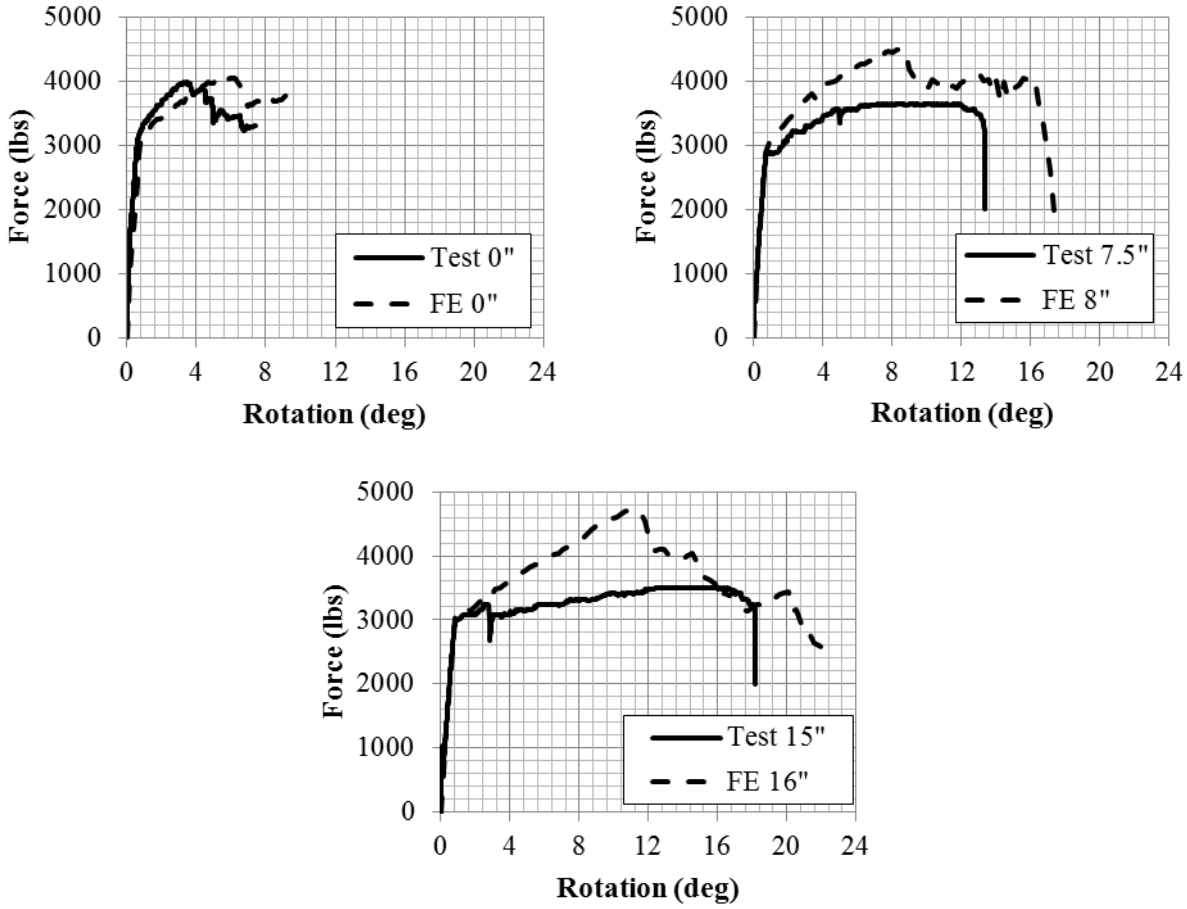

Figure 3-31: Small, Debond Solid Panel Test Results and FE Comparison

As seen before, the control model compared well with the testing; however, the debond models compared well in some ways but poorly in others. The initial stiffness and yield point from the models is very accurate. There is a slight difference in the plastic behavior of the test panels and FE models. In the test, the panels yielded and deformed almost perfectly plastically. It appears that there is almost no strain hardening in the debond test panels. This is untrue of the control panel. It yielded and deformed with a noticeable strain hardening slope until the concrete crushed. It can be assumed that the post-yield, plastic behavior of the debond panels must be a result of the debonded sections; however, the FE debond models did not capture this aspect of the post-yield behavior. The debond models maintained almost the same post-yield slope as the control mode; therefore, the peak force from the models was higher than the peak force from the

test. One difference between the debond panels and the FE models that could be attributed to this post-yield discrepancy is the region right outside the debonded section. In the models the concrete and reinforcement nodes are merged at the end of the debonded section, simulating a perfect bond between the concrete and steel; however, in reality there would be slip between the concrete and the reinforcement at the end of the debonded section as the bond stresses are developed. This difference would lead to higher stresses in the models than would actually occur in the tests.

The debond models did capture the increase of ductility from the debond section well though. The test and model of the control panel both showed crushing of the concrete and failure at approximately 4 to 6 degrees. Adding the debonded sections increased the ductility of the tested panels greatly, and the FE models agree with this increase in ductility. Although there was a noticeable difference in the ultimate strength of the debond test panels and models, the intention of debonding sections of reinforcement was to increase the ductility of the panels, and since the models captured this effect well, the modeling approach was considered valid and further used to investigate the effect of debonding reinforcement.

3.5.2 Large, Debonded Solid Panel Test Results and FE Comparison

The large solid panels were also tested in parallel with debonded panels to evaluate the effect of debonded reinforcement on doubly-reinforced panels. Non-PS and PS panels with a 20 inch debonded section were tested. A comparison of the test results is presented in Figure 3-32.

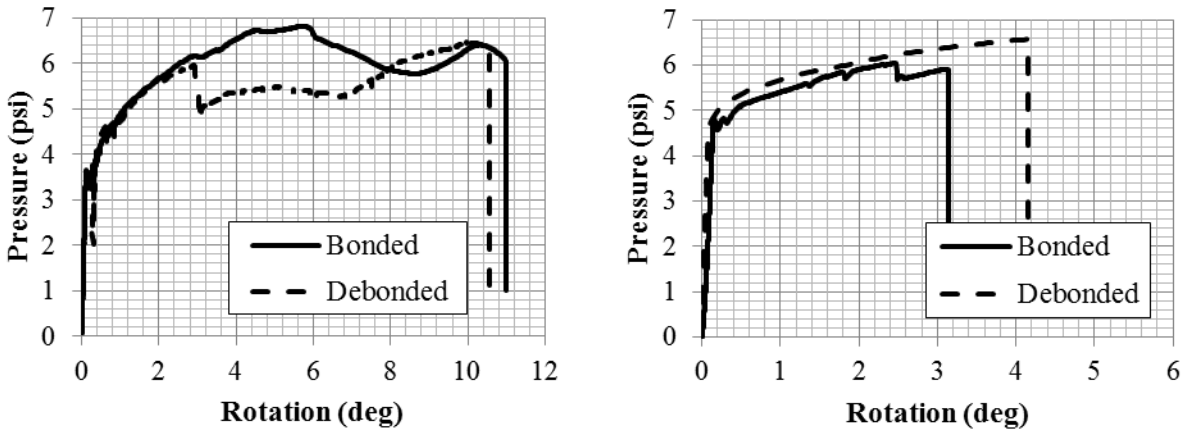

Figure 3-32: Debond Comparison of Large Solid Test Results – non-PS (left), PS (right)

The test results show that for the non-PS panel the debonded section causes a slight decrease in ultimate strength, similar to the small panels, but does not change the ductility of the panel. The debonded PS panel performed almost exactly the same as the bonded panel. Both panels failed due to fracture of the prestressing strand, except the debonded panel failed at 4 degrees of support rotation while the bonded panel failed at 3 degrees. This difference will be discussed further in Chapter 4.

Each of the debonded panels was modeled in addition to the control panels and the comparison of bonded non-PS and PS and debonded non-PS and PS is presented in Figure 3-33. The two graphs on the left are the non-PS results, and the graphs on the right are the PS results. Likewise, the top graphs are the bonded panels, and the bottom graphs are the debonded panels.

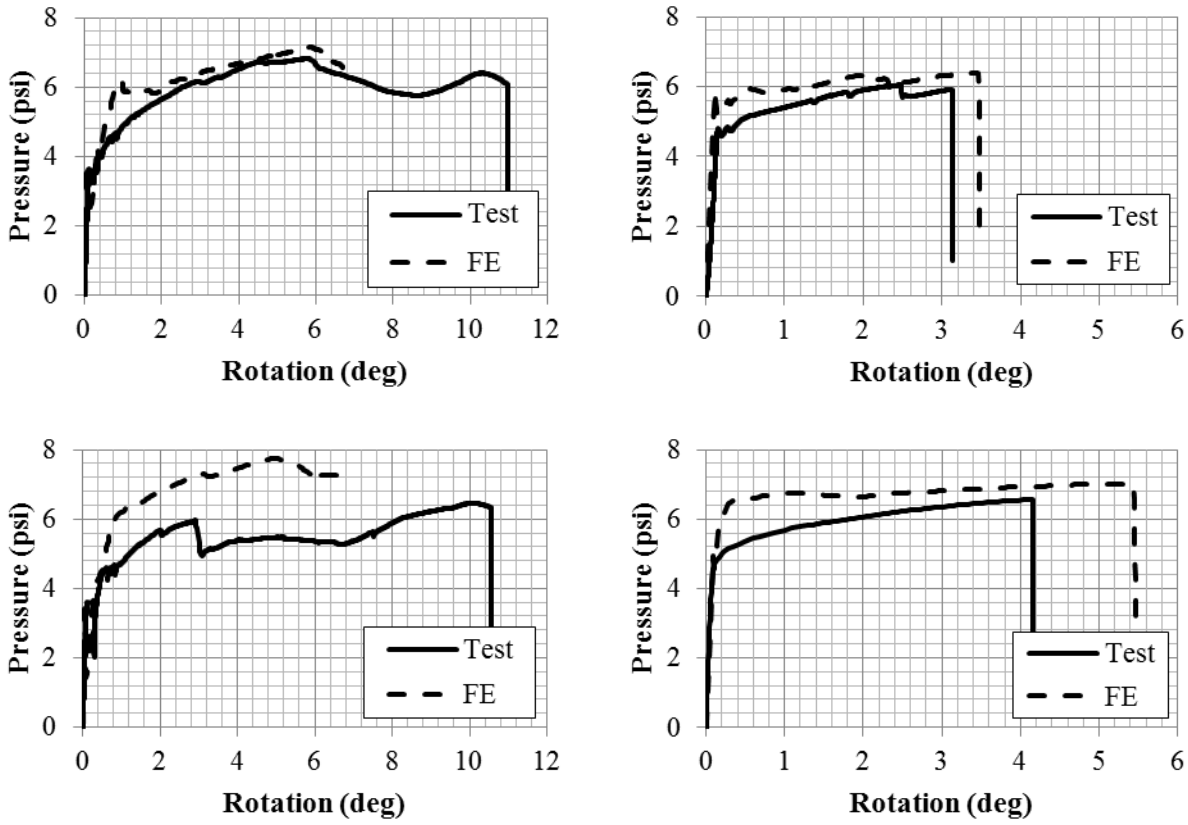

Figure 3-33: Comparison of Test and FE Results of Large Solid Panels

As presented before, the FE models of the non-PS and PS bonded control panels compare well to the test results; however, there was a significant difference in the peak strength of the FE models and test results of the non-PS and PS debonded panels. This was also the case in the small solid debond models but for different reasons. There is very little difference in the FE results from the bonded and debonded non-PS models, but the unbonded non-PS test showed a significant drop in strength. The FE model did not capture this drop in strength, but regardless, the non-PS FE models and tests show the same trend: debonding the reinforcement did not improve the ductility of the doubly-reinforced, non-PS section. There was one limitation to the non-PS models. After the concrete elements crushed and lost strength, a new flexural mechanism, a moment couple between the tension and compression steel, developed; however, the models were not able to capture this behavior. As this behavior developed in the model, the

resisted moment grew beyond the capacity of the section layout and material specifications, and the applied pressure was considered fictitious and not reported. This is why in both non-PS plots the FE curves seem to stop around 7 degrees of rotation. The PS debonded model also had slightly higher peak strength than the test results. Unlike the non-PS panels, this apparent increase is not because the debonded section caused the test panel to drop in strength. The strength of the bonded and debonded test panels was almost exactly the same. The debonded model has an increase in strength when compared to the bonded FE model and test as well. There was no reason to account for this increase in strength, so it was considered inaccurate. The debonded model did agree with the increase in ductility seen in the tests, although it was slightly exaggerated. The test showed about a 33% increase in support rotation before the strand fractured, while the FE results showed a 55% increase in support rotation. This slight difference could be due to discrepancy in the strain capacity of the prestressing strand in the test panel and FE model.

3.6 Modeling Load-Bearing Panels

Another parameter that was examined during this study was the effect that axial loads have on the flexural response of panels. In the course of this study, static and dynamic analyses, which are discussed in Chapter 5, were run to study this behavior. The same techniques as described previously for modeling solid and sandwich, conventionally reinforced and prestressed panels were implemented except an axial load was also applied to the panels. Similar to the initial condition used to model prestressing forces in the reinforcement, the axial load was applied in a preliminary analysis. In Abaqus/CAE the axial load was ramped up from zero to the full value, maintaining equilibrium throughout the preliminary analysis. The main flexural analysis was then initiated from the last equilibrium state with the axial load held constant

throughout the analysis. In LS-DYNA the axial load was applied as a step force in a preliminary analysis using dynamic relaxation. The analysis was run until the kinetic energy in the system dissipated below a tolerance level, and a quasi-static equilibrium state was reached. The main flexural analysis was then run, starting from the quasi-static equilibrium state, with the axial load held constant throughout the analysis. In both cases the axial load, typically thought of as a point load or distributed point load along the length of the panel, was applied as a uniform pressure across the whole section. The axial load was applied in this manner to avoid a local failure in the concrete than can occur when applying forces to just one line of nodes.

Chapter 4

Ductility of Prestressed Wall Panels

4.1 Overview

A very important concept in blast design is ductility. The developed FE modeling methodology was used to study the ductility of prestressed wall panels and their applicability in blast design. The general topics investigated in this chapter include ductility of solid vs. sandwich prestressed panels, general sandwich panel behavior, a shear tie parameter study, and the effect of debonding reinforcement.

4.2 Summary of Blast Design

Typical blast design differs from designing for other loads, such as, gravity, wind, etc., in that blast design is governed by levels of protection and response limits as opposed to strength requirements. Levels of protection specify an amount of structural damage that a building component will potentially experience. Acceptable levels of damage range from very low to high. A building component designed for a very low level of protection would potentially experience heavy to hazardous damage from the blast threat where as a component design for a high level of protection would potentially experience superficial damage. The component damage for each level of protection also depends on the type of component, i.e. primary, secondary, or non-structural component. For example, a low level of protection for a primary component allows for moderate damage while a low level of protection for a secondary component allows for heavy damage. The relationship between level of protection and component damage is summarized in Figure 4-1.

Building Level of Protection	Descriptions of Potential Overall Structural Damage	Component Damage (Response Limits)		
		Primary Components [3]	Secondary Components [4]	Non-Structural Components [5]
Below AT Standards [2]	Severe Damage - Progressive collapse likely. Space in and around damaged area is unusable.	Hazardous [6] (B3 – B4)	Blowout [7] (> B4)	Blowout [7] (> B4)
Very Low	Heavy Damage - Onset of structural collapse. Progressive collapse is unlikely. Space in and around damaged area is unusable.	Heavy [8] (B2 – B3)	Hazardous [6] (B3 – B4)	Hazardous [6] (B3 – B4)
Low	Unrepairable Damage - Progressive collapse will not occur. Space in and around damaged area is unusable.	Moderate [9] (B1 – B2)	Heavy [8] (B2 – B3)	Heavy [8] (B2 – B3)
Medium	Repairable Damage - Space in and around damaged area can be used and is fully functional after cleanup and repairs.	Superficial [10] (< B1)	Moderate [9] (B1 – B2)	Moderate [9] (B1 – B2)
High	Superficial Damage - No permanent deformations. The facility is immediately operable.	Superficial [10] (< B1)	Superficial [10] (< B1)	Superficial [10] (< B1)

1 - See Section 2 and Section 3 for complete discussion of Building LOP, Component Damage, and Response Limits

2 - This is not a level of protection, and should never be a design goal.

3 - Members whose loss would affect a number of other components supported by that member and whose loss could potentially affect the overall structural stability of the building in the area of loss.

4 - Structural component supported by a primary framing component.

5 - Components whose loss would have little effect on the overall structural stability of the building in the area of loss.

6 - Component has failed, and debris velocities range from insignificant to very significant.

7 - Component is overwhelmed by the blast load causing debris with significant velocities.

8 - Component has not failed, but it has significant permanent deflections causing it to be unrepairable.

9 - Component has some permanent deflection. It is generally repairable, if necessary, although replacement may be more economical and aesthetic.

10 - Component has no visible permanent damage.

Figure 4-1: Summary of Building LOP – Component Response Relationship (USACE 2008b)

Each damage level is bounded by response limits for particular types of construction. Response limits are either quantified as support rotation or ductility ratio. The response limits for reinforced concrete and prestressed concrete and the difference between them were of interest in this study. These limits as defined in the Protective Design Center Technical Report 06-08 (USACE 2008b) are presented in Tables 4-1 and 4-2. As highlighted in the tables, there is a significant difference in the response limits for reinforced concrete and prestressed concrete for any given level of protection. For a flexural reinforced concrete member without shear reinforcing or a tension membrane the maximum support rotation before blowout is 10 degrees, while the maximum support rotation before blowout for a flexural prestressed member without a

tension membrane is only 3 degrees. It is noted in the report that "prestressed members are normally considered very brittle for blast loads" (USACE 2008b).

Table 4-1: Response Limits for Reinforced Concrete (adapted from USACE 2008b)

Member		B1		B2		B3		B4	
		μ	θ	μ	θ	μ	θ	μ	θ
Flexure	No shear reinforcing/ without tension membrane	1	-	-	2°	-	5°	-	10°
	With compression face steel reinforcement and shear reinforcing/without tension membrane [2]	1	-	-	4°	-	6°	-	10°
	With tension membrane (L/h>=5) [3, 4]	1	-	-	6°	-	12°	-	20°
Combined Flexure & Compression [5]	No shear reinforcing/ without tension membrane	1	-	-	2°	-	2°	-	2°
	With compression face steel reinforcement and shear reinforcing/without tension membrane [2]	1	-	-	4°	-	4°	-	4°
Compression [5, 6]	Walls & Seismic Columns	0.9	-	1	-	2	-	3	-
	Non-Seismic Columns	0.7	-	0.8	-	0.9	-	1	-
Tension or Combined Flexure & Tension		No response limits in this report, see SBEDS Methodology Manual							

Table 4-2: Response Limits for Prestressed Concrete (adapted from USACE 2008b)

Member		B1		B2		B3		B4	
		μ	θ	μ	θ	μ	θ	μ	θ
Flexural members w/o tension membrane action, L/h>=5	$\omega_p > 0.30$ [2]	0.7	-	0.8	-	0.9	-	1	-
	$0.15 < \omega_p < 0.30$ [3]	0.8	-	$0.25/\omega_p$	1°	$0.29/\omega_p$	1.5°	$0.33/\omega_p$	2°
	$\omega_p < 0.15$ [4]	1	-	-	1°	-	2°	-	3°
Flexural members with tension membrane action, L/h>=5 [5]		1	-	-	1°	-	6°	-	10°

The strict limits for prestressed members make it difficult for engineers to design a cost effective prestressed member for blast loads when compared to a reinforced concrete design;

therefore, the modeling methodology previously developed was used to investigate the following questions: Are response limits for prestressed members too conservative? Can ductility of prestressed members be enhanced? Can sandwich panels be used in blast design? How can the design of sandwich panels be enhanced for blast loads?

4.2.1 Ductility of Solid Prestressed Members

The difference in response limits for reinforced concrete and prestressed members found in PDC-TR 06-08 can be attributed to the reinforcement used in these construction types. Reinforced concrete members use mild reinforcing steel that has a smaller stress capacity than prestressing strands and therefore require a larger steel area. Prestressing strands typically have about 3 times greater stress capacity than mild reinforcing steel; however the drawback of using prestressing strands is that they have a much smaller strain capacity and fracture sooner than mild reinforcing steel. A typical stress versus strain comparison of prestressing strands to mild reinforcing steel is show in Figure 4-2. This difference in strain capacity is the reason for stricter response limits for prestressed members. Reinforced concrete flexural members are usually designed to yield but since mild reinforcing steel has such a high strain capacity, crushing of the concrete typically controls failure of the member. The focus of prestressed design is usually the service load level, but in a large displacement scenario fracture of the prestressing strands can control failure and limit the ductility of the member. Thus, stricter response limits are specified.

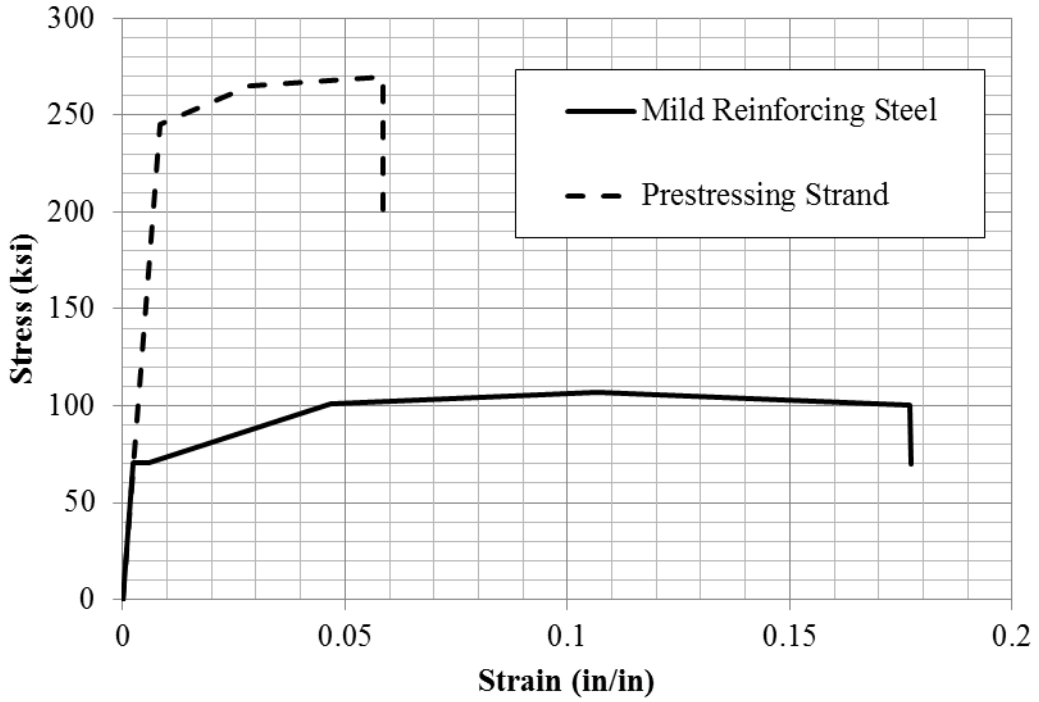

Figure 4-2: Stress-Strain Comparison of Prestressing Strands and Mild Reinforcing Steel (adapted from PCI 2004)

The results of testing and FEA of reinforced and prestressed concrete members presented in Chapter 3 agree with these observations. A comparison of reinforced versus prestressed concrete members is shown in Figure 4-3. Both testing and FEA show that while the reinforced concrete member goes out to large rotations and then crushes, the prestressed member fails at approximately 3 degrees because the prestressing strand fractures. These results support the use of the smaller response limits for prestressed members found in the PDC-TR 06-08.

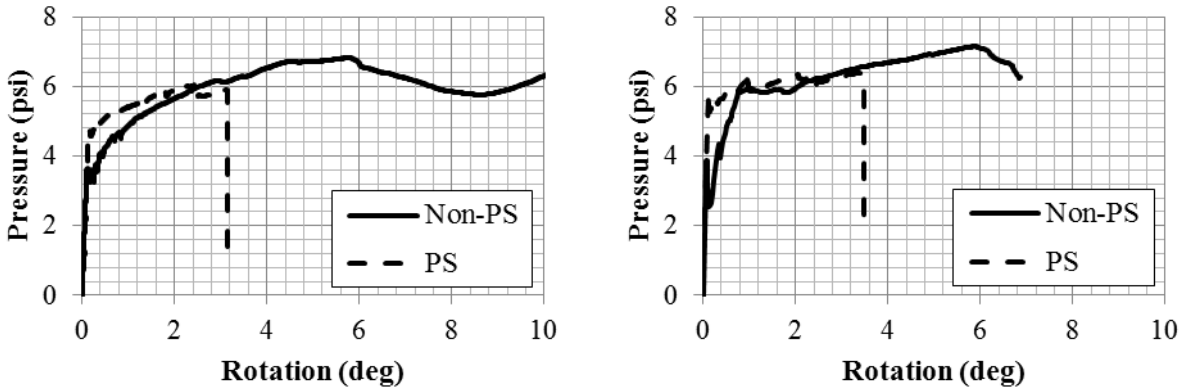

Figure 4-3: Reinforced vs. Prestressed Concrete Ductility - Testing (left), FEM (right)

4.2.2 General Sandwich Panel Behavior

It was observed during the development of a modeling approach for sandwich panels that failure of the shear tie system was the controlling flexural mechanism for sandwich panels. This observation is important to consider in regards to blast design, especially for prestressed members and how it relates to the prestressed response limits. In the previous section it was discussed how prestressing strands controlled the failure mechanism and limited the ductility of solid prestressed members. This failure mechanism has a direct result on the response limits for prestressed members; however, sandwich panels' flexural behavior is not controlled by this failure mechanism. Testing and FEA show that sandwich panels transition from their peak composite strength to a non-composite strength as the shear tie system fails. This is especially important for prestressed members because it is a much more ductile mechanism than strand fracture. Figure 4-4 shows a comparison of test results from the prestressed solid panel and the prestressed sandwich panel presented in Chapter 3 that were designed to have the same flexural strength. The figure shows that while the solid panel is stronger up until 3 degrees it has a very abrupt failure at 3 degrees; however, the sandwich panel holds some strength out to 10 degrees of support rotation. It begins transitioning from composite to non-composite strength at approximately 2 degrees of rotation, so it does not hold the design strength all the way out to

these large rotations; however, in blast design what is more important than peak strength is the area under the curve. The panel needs to dissipate the energy imparted by the blast shockwave, and the dissipated energy is proportional to the area under the pressure vs. rotation curve. Therefore, even though the sandwich panel is not quite as strong as the solid panel in the small rotation range, it holds some strength out to large rotations and dissipates more energy than the solid panel. This effect caused by the shear tie failure mechanism could make sandwich panels more suitable for blast loads than solid panels.

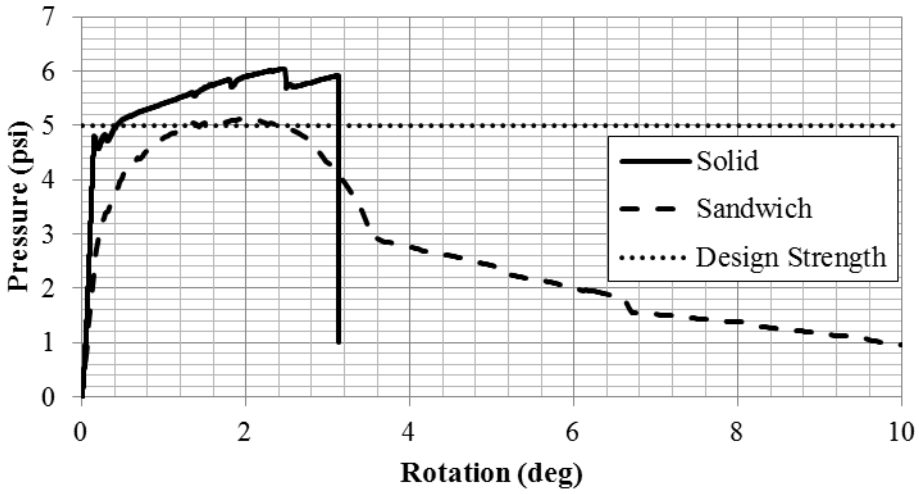

Figure 4-4: Comparison of Prestressed Solid vs. Sandwich Panel Ductility

The change in failure mechanism between solid and sandwich panels was observed in static FEA, but the same mechanism and effect also occurred in panels experiencing blast loads. In the sandwich panel blast tests used for LS-DYNA model validation, some of the prestressed sandwich panels rotated way beyond the 3 degree limit. Both single span PS sandwich panels rotated to approximately 6 degrees of support rotation, but some of the multi-span PS sandwich panels that were tested even rotated up to 10 degrees. Even though solid panels were not included in the matrix of panels tested, a PS solid panel with the same configuration and design strength was analyzed under the primary detonation blast loading using LS-DYNA in order to

observe how a PS solid panel would have compared to the PS sandwich panels. The FE response histories of the SS1 panel and the solid panel are presented in Figure 4-5.

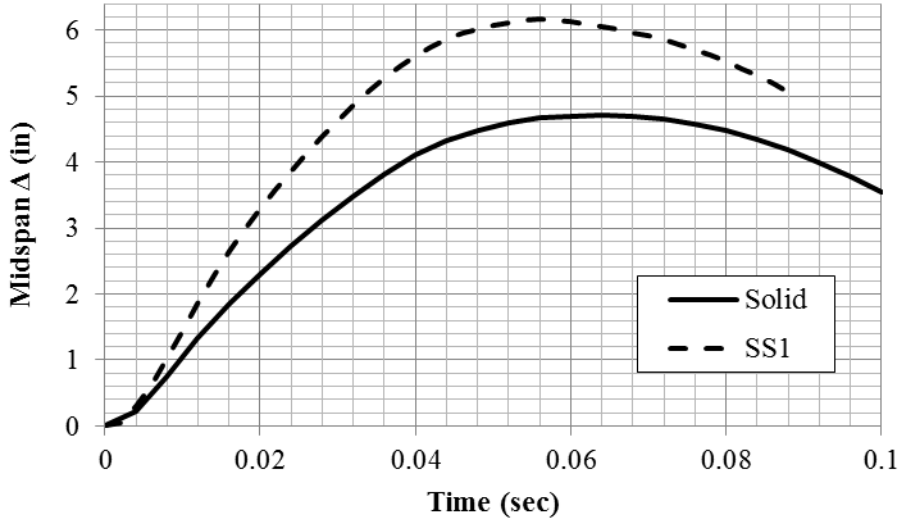

Figure 4-5: Comparison of SS1 and Solid Panel FE Response Histories

It appears from the figure that the PS solid panel outperformed the PS sandwich panel. The solid panel is stiffer than the sandwich panel, and its peak deflection is approximately 24% lower than the sandwich panel's peak deflection. However, what is not seen is this comparison is that even though the solid panel deflected less than the sandwich panel, the prestressing strands in the solid panel fractured. Figure 4-6 shows the stress in the prestressing strands versus time for the solid and sandwich panels. The comparison shows that while the stress in the sandwich panel prestressing strand levels off at approximately 260 ksi and then decreases once the panel begins to rebound, the stress in the solid panel prestressing strand rises very quickly, and the strand fractures within the first 10 milliseconds.

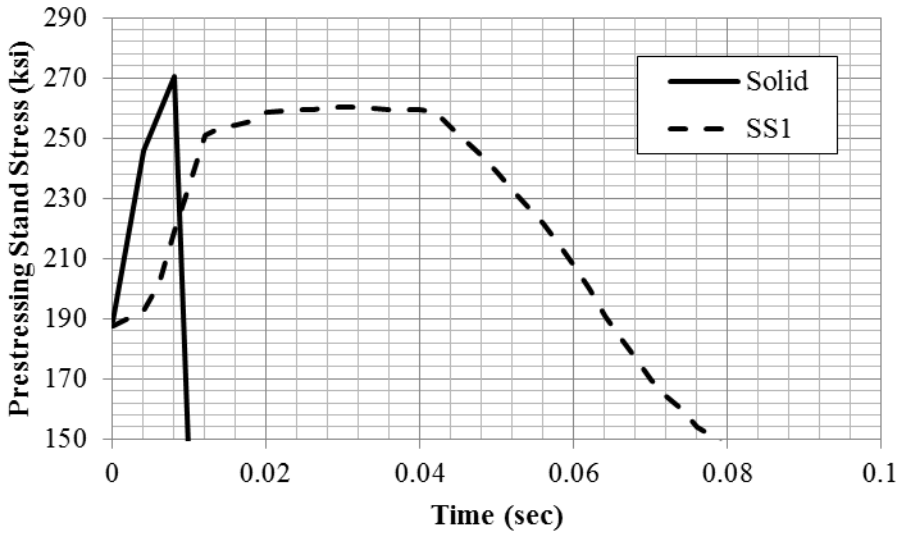

Figure 4-6: Comparison of Prestressing Strand Stress vs. Time for Solid and Sandwich Panels

Although the prestressing strands in the solid panel fractured, the solid panel still deflected less than the sandwich panel. It seems intuitive that if the solid panel's reinforcement fractured, it should at least have more deflection than the sandwich panel if not completely blowout. This unexpected result was due to the effect of the mass of the system on the dynamic response. Even though the resistance of the solid panel was theoretically equal to the sandwich panel's resistance and less than the sandwich panel's resistance once the prestressing strands fractured, the additional mass of the solid panel reduced the response of the solid panel compared to the sandwich panel. In order to take the mass into account, an additional solid panel model was analyzed with a reduced mass, equivalent to the mass of the sandwich panel. Figure 4-7 shows a comparison of the response histories of the sandwich panel and the solid panel with an equivalent mass.

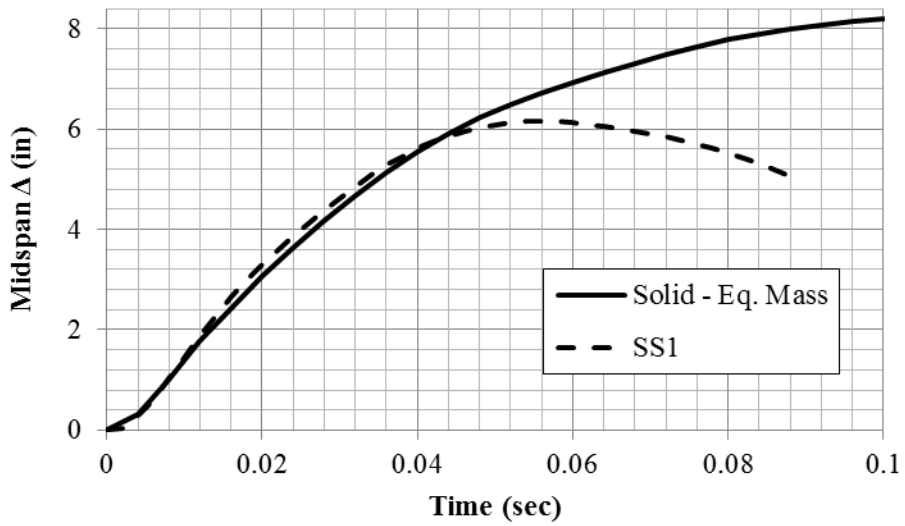

Figure 4-7: Comparison of SS1 and Equivalent Solid Panel FE Response Histories

As seen in the figure, the solid panel with the equivalent sandwich panel mass blows out, while the sandwich panel peaks at approximately 6 inches of deflection. Similar to the first solid panel, the prestressing strands fracture, but this solid panel does not have enough mass to withstand the blast load. This comparison shows that under this blast demand the mechanism that forms in the shear tie system of sandwich panels makes the panel more ductile and potentially more suitable to withstand blast loads than an equivalent solid panel.

4.2.3 Shear Tie Parameter Study

An advantage of using FEA is that once a modeling approach is validated, models can be developed that go beyond the scope of the testing matrix. It was discussed in the last section how the flexural mechanism that develops in sandwich panels can be advantageous for prestressed panels under blast loads. To further investigate this idea, the sandwich panel modeling methodology was used to conduct a shear tie parameter study to identify how the design of shear ties can be further improved specifically for panels with a blast demand.

Three characteristics of the ties were chosen as parameters for the study. These characteristics were the stiffness, strength, and ductility of the ties. A simplified, three-slope tie

definition which reasonably resembles the test results of one of the tested distributed ties was developed as a control. By having a simple, three-slope control tie definition versus a more complex control, the parameters of interest were able to be isolated by making slight modifications to the control tie definition. The control definition consists of an initial positive slope followed by a perfectly plastic portion at the peak strength of the tie. At one-tenth an inch of shear deformation the curve begins linearly degrading in strength until it reaches zero at one inch of shear deformation. A model with this tie definition was analyzed, and the results were used as a baseline for comparison as the tie definition was varied.

To investigate how the stiffness of the ties affects the behavior of the panel, two models were analyzed with a slightly different tie definition. The initial slope of the definition was amplified and reduced by a factor of four. This means that while the control definition has a stiffness of 13,750 lb/in/in the amplified definition has a stiffness of 55,000 lb/in/in and the reduced definition has a stiffness of 3,437.5 lb/in/in. The third part of the curve remained the same in all three curves with the peak strength degrading to zero from one-tenth to one inch of shear deformation. To investigate how the ductility of the ties affects the behavior of the panel, four different models were analyzed. The initial stiffness was kept the same as the control model, but the length of the perfectly plastic portion was modified. In the control model, the perfectly plastic behavior occurs between 0.02 and 0.1 inches of shear deformation. In these models four different lengths for the perfectly plastic portion were chosen after which the strength began to decrease linearly. The peak strength was held until 0.05, 0.2, 0.45, and 0.9 inches of shear deformation in these models. The negative slope of the third part of the curves was also modified. All of the curves were given a slope of -2750 lb/in/in. The slope was increased from the control slope of -305.6 lb/in/in in order to amplify the effect of the ties failing. Instead of a

slow transition from peak strength to complete loss of shear transfer, the curves drop quickly to replicate a sudden tie failure and emphasize the effect of a tie holding its strength longer. Finally, to investigate how the strength of the ties affects the behavior of the panel, three different models were analyzed. The initial stiffness was kept the same, but the peak strength was reduced by a factor of 0.5 and increased by a factor 1.5 and 2. The peak strength was held to one-tenth an inch deformation in all the curves and then reduced linearly, reaching zero at one inch deformation. Plots of the control definition and the three parameter definition sets are presented in Figure 4-8. The results from these analyses are presented in Figure 4-9.

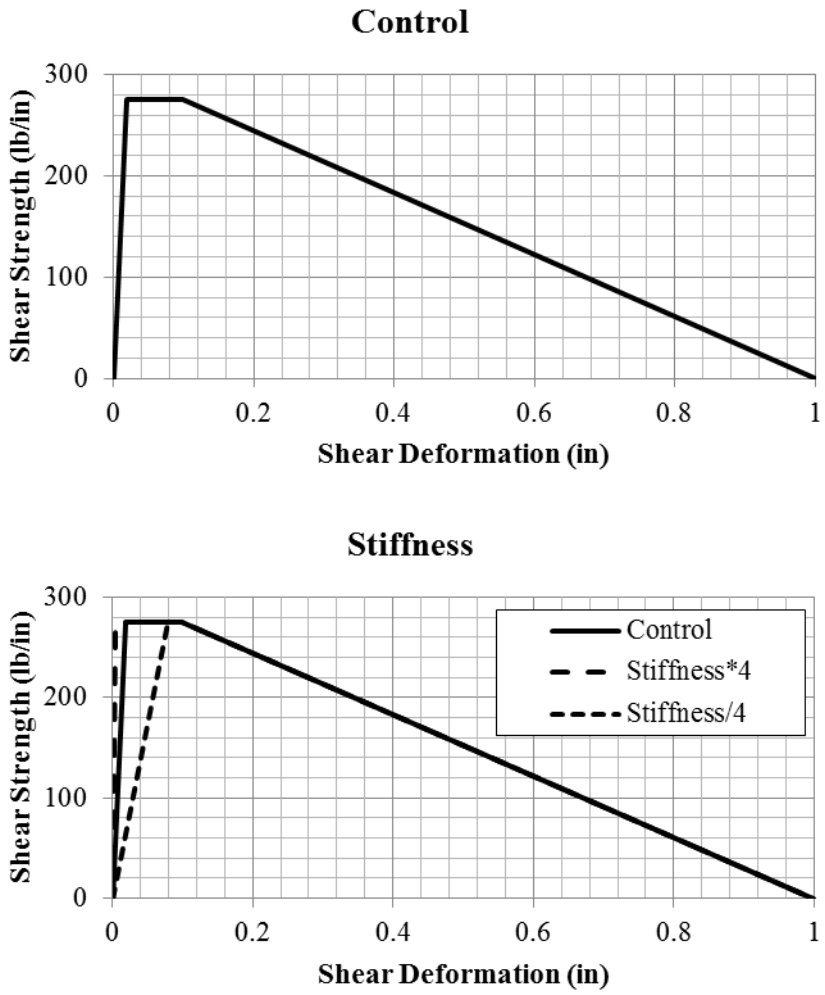

Figure 4-8: Shear Tie Definition Curves for Parameter Study

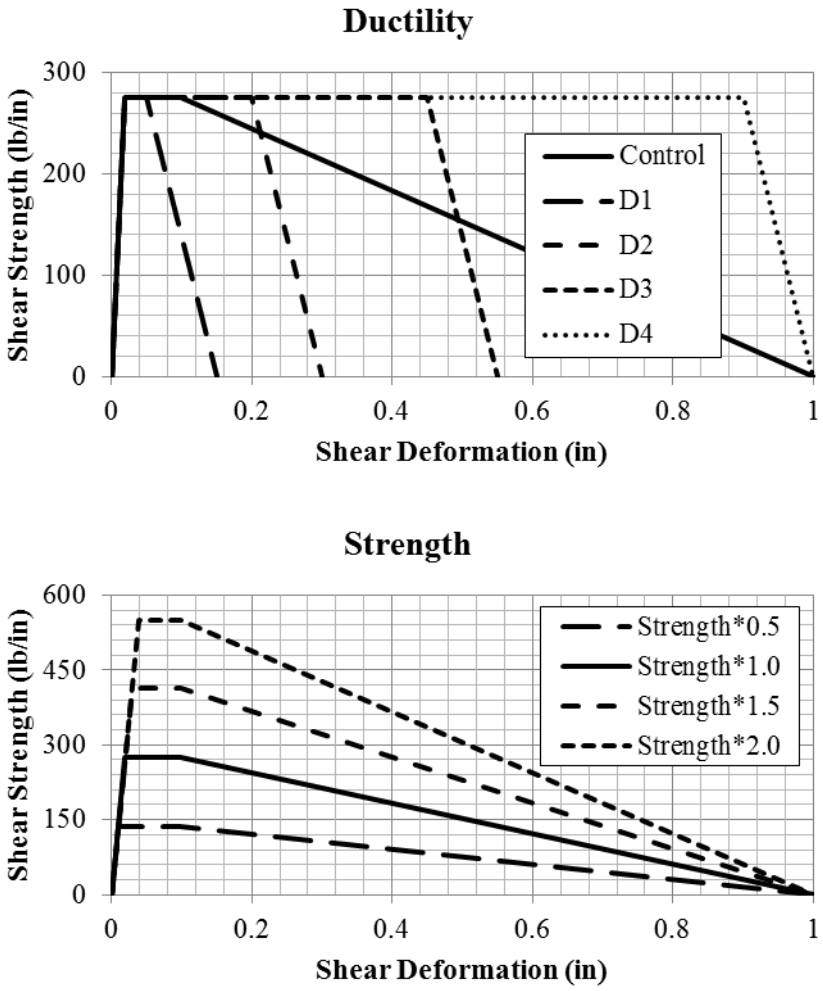

Figure 4-8 (Continued): Shear Tie Definition Curves for Parameter Study

4.2.4 Results and Observations from Shear Tie Parameter Study

Comparing these results gives an interesting indication of how to better design shear tie systems for panels subjected to blast loads. Increasing or decreasing the stiffness of the ties had little effect on the behavior of the panels. The panel with more flexible ties reached its peak strength later, which was expected; however, this change in stiffness had little to no effect on the peak strength or ductility of the panel. The panel with stiffer ties had a larger stiffness in the elastic range. This behavior is expected and would be of interest to engineers designing panels for service loads; however, it is not significant to the panel's resistance to blast loads. The

ductility of the ties had a significant effect on the behavior of the panel. The ductility of the ties directly correlated to the global ductility of the panel, e.g. the D3 tie had about twice as much ductility as the D2 tie, and resultantly the D3 model had about twice as much rotation capacity as the D2 model. The model D1, which held its shear strength over the shortest length, had a drop in peak strength compared to the control model. This illustrates that, even though the tie system had the desired shear strength, it needed to hold that strength through enough shear deformation for the panel to reach the design strength. The other models D2 through D4, which held the peak shear strength longer than the control model, not only maintained the design strength through larger rotations than the control but also increased in strength after the point where the control model started transitioning to the non-composite strength.

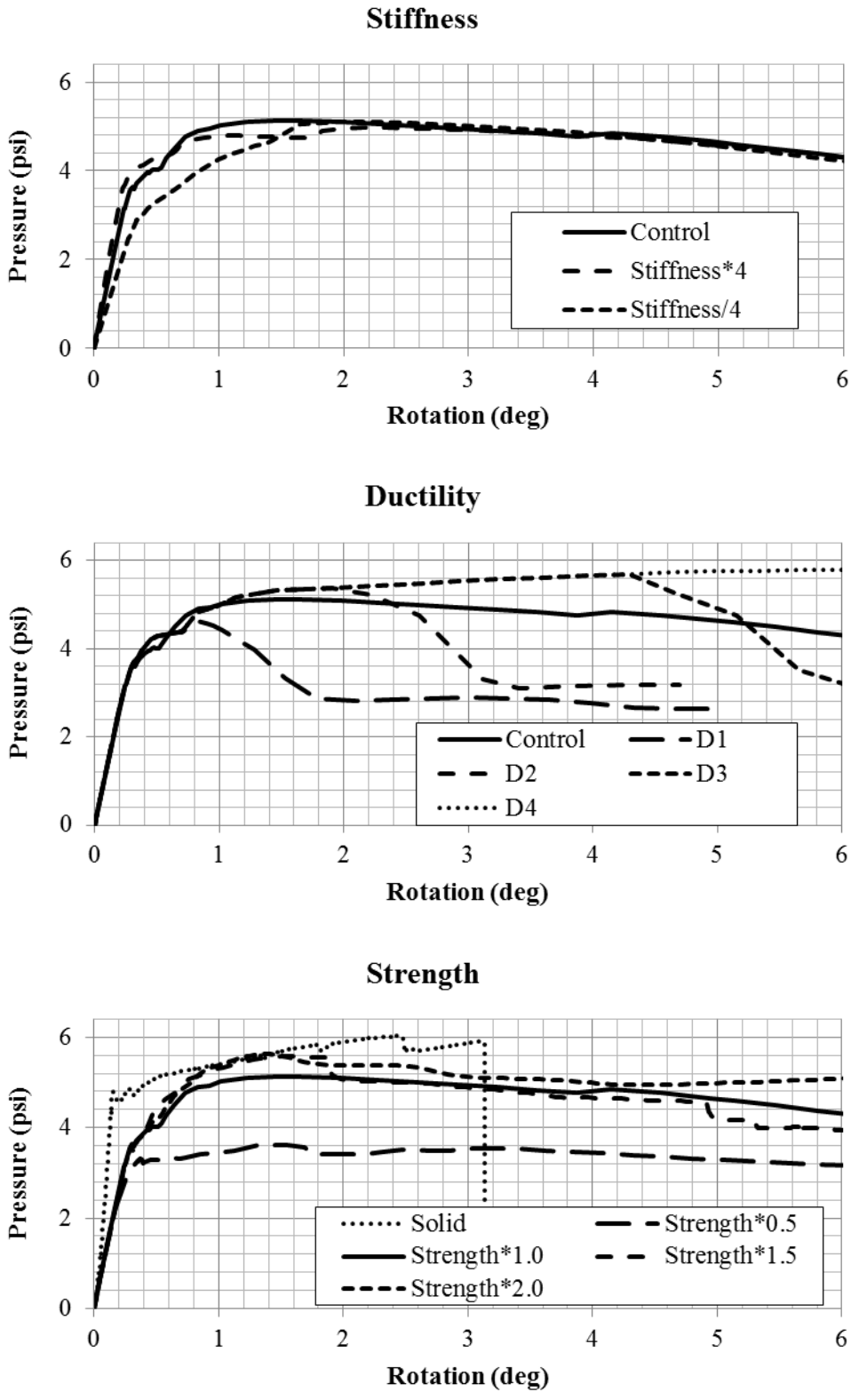

Figure 4-9: FE Results of Shear Tie Parameter Study

Finally, the tie strength parameter runs provided interesting results. Besides the different FE runs, 0.5, 1.0 (control), 1.5, and 2.0 Strength, the results of the solid PS panel with an equivalent layout and design strength were added to the strength parameter graph. The solid plot was added to demonstrate an important aspect of the strength of the shear ties. The design strength of the both the solid and sandwich panels, assuming composite action, was 5.0 psi. See Appendix A for all calculations related to these panels. The sandwich panel barely met this design strength, while the solid panel surpassed this strength, reaching an ultimate strength of 6.0 psi. This difference is an important observation considering that, as stated previously, the sandwich panel's ultimate strength was controlled by shear tie failure, while the solid panel's ultimate strength was controlled by material failure. The solid panel most likely exceeded the design strength for a couple reasons. First, material strength limits for concrete and reinforcement materials are specified in design, but actual strength limits in fabricated materials are commonly exceeded to ensure that the minimum specified strengths are met. This can result in higher moment couple forces than expected in design and thus higher shear forces that need to be transferred between wythes. Also, some assumptions used in design calculations, such as ignoring concrete in tension, are simplifications and can result in a higher strength than predicted in design. Therefore, because the shear ties were only designed to handle shear forces at the design ultimate strength, not the shear forces from the actual ultimate strength, the shear tie system failed and limited the ultimate strength of the panel. In light of this information the results of the strength parameter analyses make sense. As expected, the ultimate strength of the 0.5 Strength run was controlled and limited by the peak shear strength of the ties similar to the control panel. The 1.5 and 2.0 Strength models saw a slight increase in strength that matched the strength of the solid panel in the 1 to 2 degree range. The strength of these ties allowed the

composite action of the panel to fully utilize the strength of the concrete and steel materials and control the behavior in this range. However, at approximately 1.5 degrees the strength of the panels begins to drop. It was observed that this drop was not due to material failure but failure of the shear tie system. This shear tie failure was unexpected since these shear tie systems were designed to transfer shear forces from lateral pressures of 6.7 and 8.9 psi (see Appendix A). Upon further inspection of the models, it was discovered that local failure in the concrete elements around the shear tie beam elements was causing an effective failure of some of the springs. The springs were not meeting their strength limit, but they were unable to transfer shear between the wythes because the concrete failure was distorting the perpendicular orientation of the beams with the wythes. This effect is displayed in Figure 4-10.

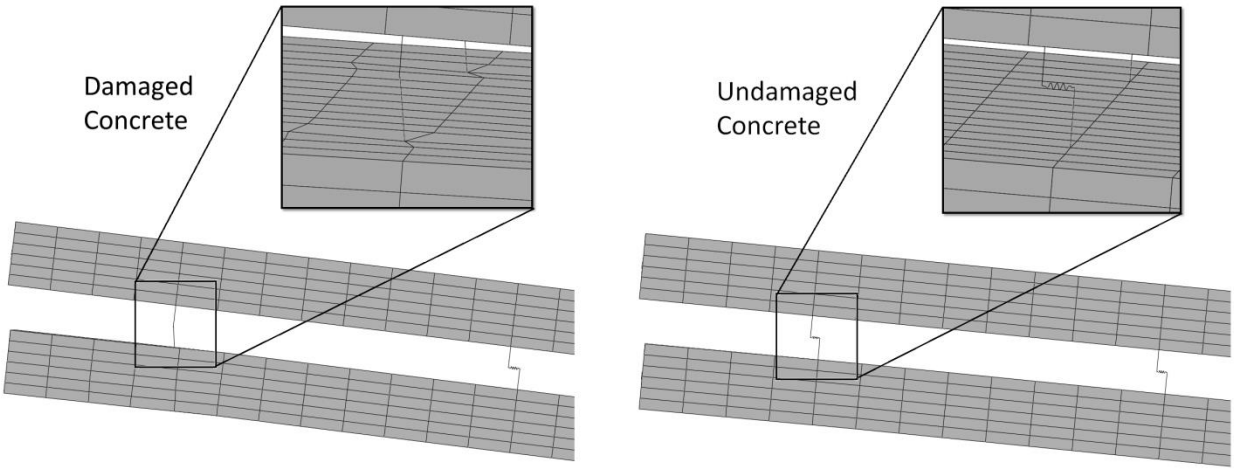

Figure 4-10: Effect of Local Concrete Failure on Shear Tie Modeling Approach

Although deformation and damage of the concrete surrounding the shear ties is possible, the effect that concrete has on the shear resistance was captured in the resistance curves developed from the direct shear tests of each tie connector. Therefore, it was desired that no local mechanisms would form in the concrete elements in the FE models. Since these local mechanisms did form, the results of these FE models were considered inaccurate. If no

mechanism had formed in the concrete elements and all of the shear deformation was concentrated in the spring elements, it was theorized that the material behavior and ultimately fracture of the prestressing strand would control the ultimate response of the behavior.

An important takeaway from the study is that a shear tie's ductility, or ability to maintain shear strength through shear deformation, has a direct effect on the global flexural ductility of a panel. The comparison between the control panel and the solid panel also demonstrated that even though shear ties are designed to handle the design strength of a panel, they will likely be the controlling mechanism in the panel since the concrete and steel materials are normally capable of resisting a demand greater than the design demand. As discussed previously, this response is favorable when compared to the brittle response of a solid panel, or potentially a sandwich panel with an overdesigned shear tie system, that is controlled by strand fracture. It is recommended that development of shear ties for blast design be focused on increasing the shear deformation capacity of the ties.

4.3 Effect of Debonding Reinforcement on Flexural Behavior

As described in Chapter 3, the FE modeling methodology was used to investigate the effect of debonding reinforcement on the flexural response of wall panels. The original goal of the debonding technique was to increase the ductility of the panel overall. The testing of debonded panels showed that it can have a variety of effects on different types of panels, and the FE models were used to study these effects and to understand the general behavior of debonded panels.

4.3.1 Response of Singly Reinforced Solid Panel to Debonding

The comparison of the small, singly reinforced panels in Chapter 3 showed that debonding the reinforcement increased the ductility of the panels. Furthermore, the longer the

debond length that was used, the more ductile the panel responded. The strains in the extreme fiber of the concrete and the rebar were compared along the length of the panels with debond=0" (fully bonded), debond=8", and debond=16" to study how debonding the reinforcement affected the ductility. Figure 4-11 displays this strain comparison at 4.8 degrees of support rotation. 4.8 degrees was chosen because the fully bonded panel crushed just beyond this point.

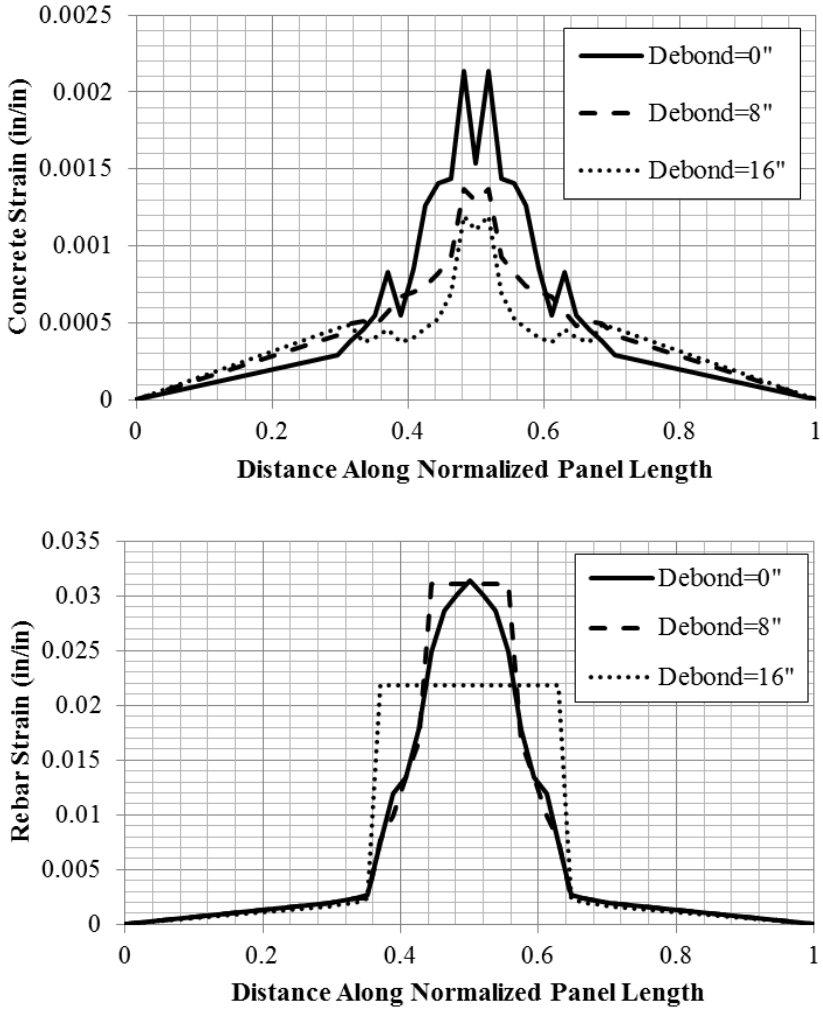

Figure 4-11: Strain Comparison at 4.8 Degrees of Support Rotation

The graph of the rebar strains shows that the debond forces the strain in the reinforcement to be uniformly distributed over the debond length. In general, this causes the peak strain in the debonded reinforcement to be less than the bonded reinforcement, although the peak strain value

in the 8 inch debonded reinforcement is very close to the value in the fully bonded reinforcement. This effect is better displayed in the panel with the longer 16 inch debonded section of reinforcement. Although the panels were designed to yield, crushing of the concrete was the controlling failure mechanism for each panel. Therefore, the effect that the uniform distribution of strain in the rebar has on the strain in the concrete is what causes a more ductile response. The graph of the concrete strains displays that the panels with debonded sections also have smaller peak strain values in the concrete compared to the fully bonded panel. This decrease in concrete strains delayed crushing of the concrete in the debonded panels and allowed these panels to hold their strength through greater rotations.

Similarly, the response of the debonded panels is compared in Figure 4-12. The strain comparison is presented at 8.5 degrees of support rotation. The fully bonded panel has failed prior to this rotation, so it is not included in the figure. Similar to before, the strain in the rebar is uniformly distributed across the debonded section, causing smaller peak values in the panel with the longer debonded section. The decrease in rebar strain results in smaller peak concrete strains as well. Therefore, while the panel with an 8 inch debond section is reaching its crushing limit state, the panel with a 16 inch debond section is still rotating with a stable concrete compression zone.

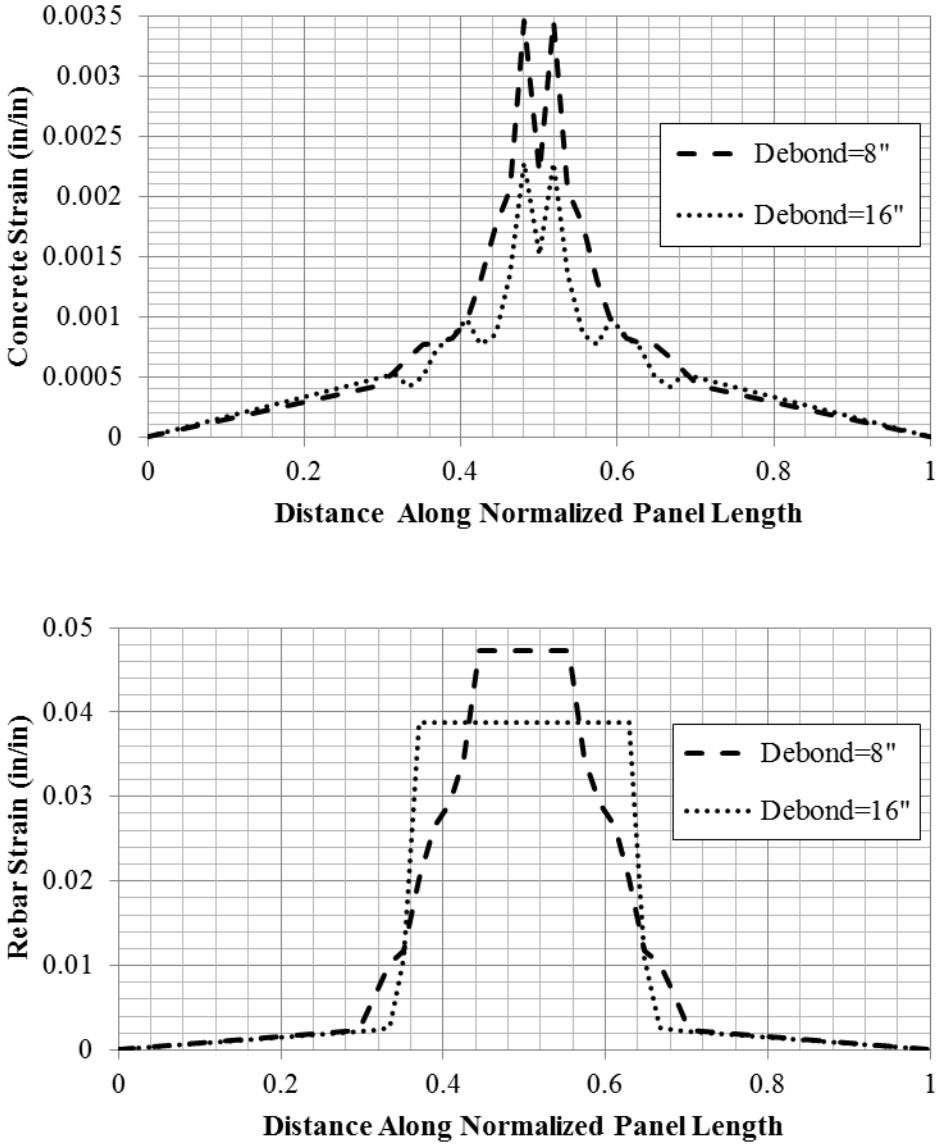

Figure 4-12: Strain Comparison at 8.5 Degrees of Support Rotation

4.3.2 Response of Doubly Reinforced Solid Panels to Debonding

The comparison of the large, doubly reinforced panels in Chapter 3 showed that debonding the reinforcement of the non-PS panel had almost no effect on its ductility, but debonding the reinforcement of the PS panel had a significant effect on its ductility. Similar comparisons of the concrete and reinforcement strains were used to study the difference in effect that debonding reinforcement had on these panels. Figure 4-13 shows the comparison for the

non-PS panel. 4.5 degrees of support rotation was chosen as the point for comparison because the debonded panel crushed shortly after this rotation.

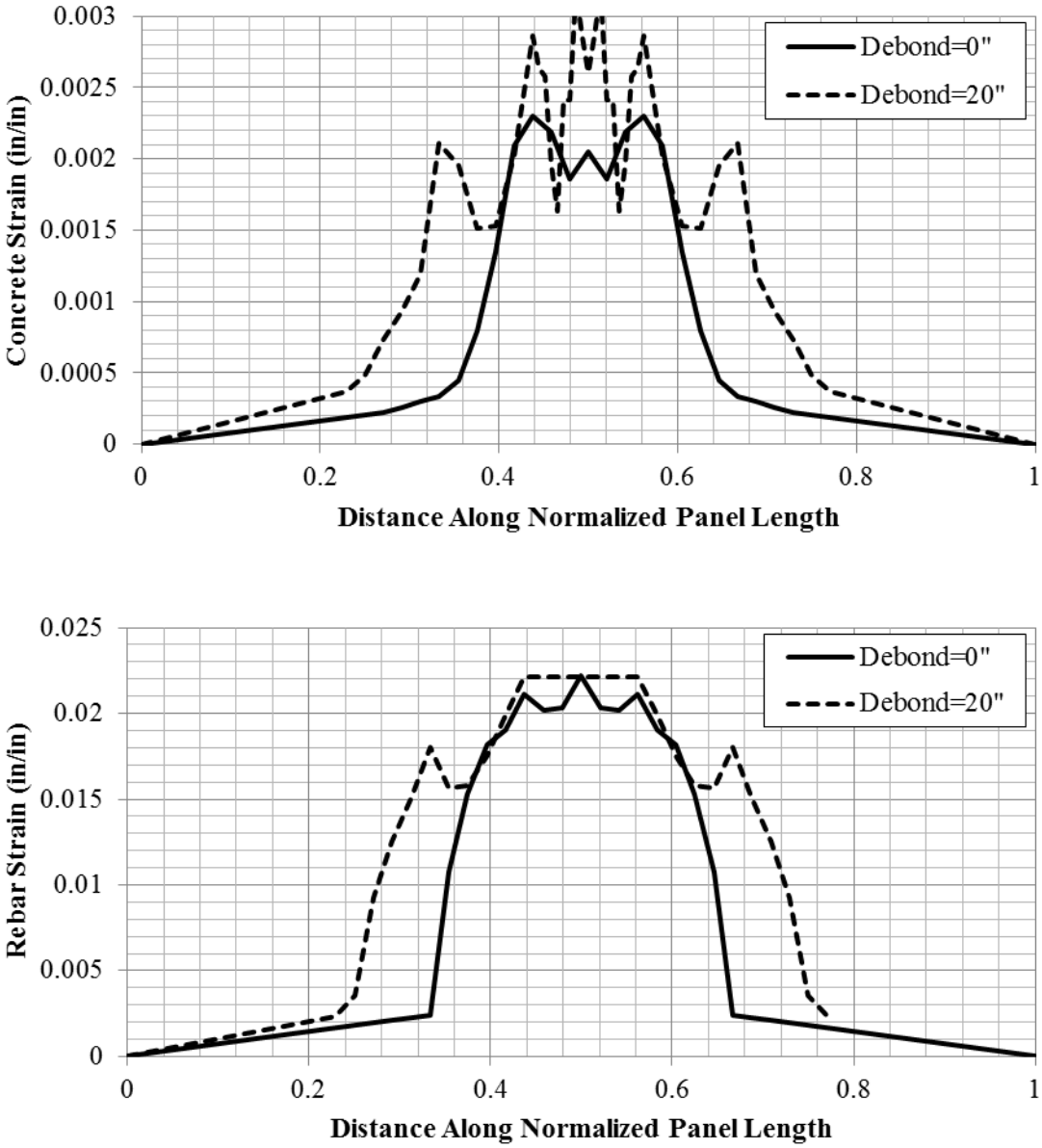

Figure 4-13: Strain Comparison of Non-PS Panels at 4.5 Degrees of Support Rotation

The graph of the rebar strains shows that although the rebar strain is uniformly distributed across the debonded section, the peak strain value in the bonded and debonded panels is the same. Also, unlike the singly reinforced, non-PS panels, the concrete strains actually increased in

the debonded panel compared to the fully bonded panel. This increase in concrete strain caused the debonded panel to crush at smaller support rotation, the opposite of the intended effect. The post-crushing behavior of tested panels was also significant since the compression and tension steel were able to form a moment couple. However, the FE models were not able to capture this behavior, so the models were not used to study the effect of debonding the reinforcement in this range of behavior.

While the effect that the strain distribution in the rebar had on the concrete strains was of interest in the non-PS panels, the strain distribution in the prestressing strand alone was primarily important in the PS panels, because strand fracture is the common failure mechanism in PS panels. The bonded panel failed at approximately 3.4 degrees of support rotation. Figure 4-14 shows the strain comparison of the PS panels at 3.0 degrees of support rotation, just prior to failure of the fully bonded panel. The strain in the strand is uniformly distributed across the debonded section, and the peak value is much lower compared to the peak value in the fully bonded panel. The strain in the bonded panel (4%) is very close to the strain limit used for the strands; thus, the bonded panel is about to fail, while debonding the strand reduced the strain by nearly 50% in the debonded panel. The strains in the concrete are fairly similar, but the effect on the concrete is not as important since the concrete is not part of the failure mechanism.

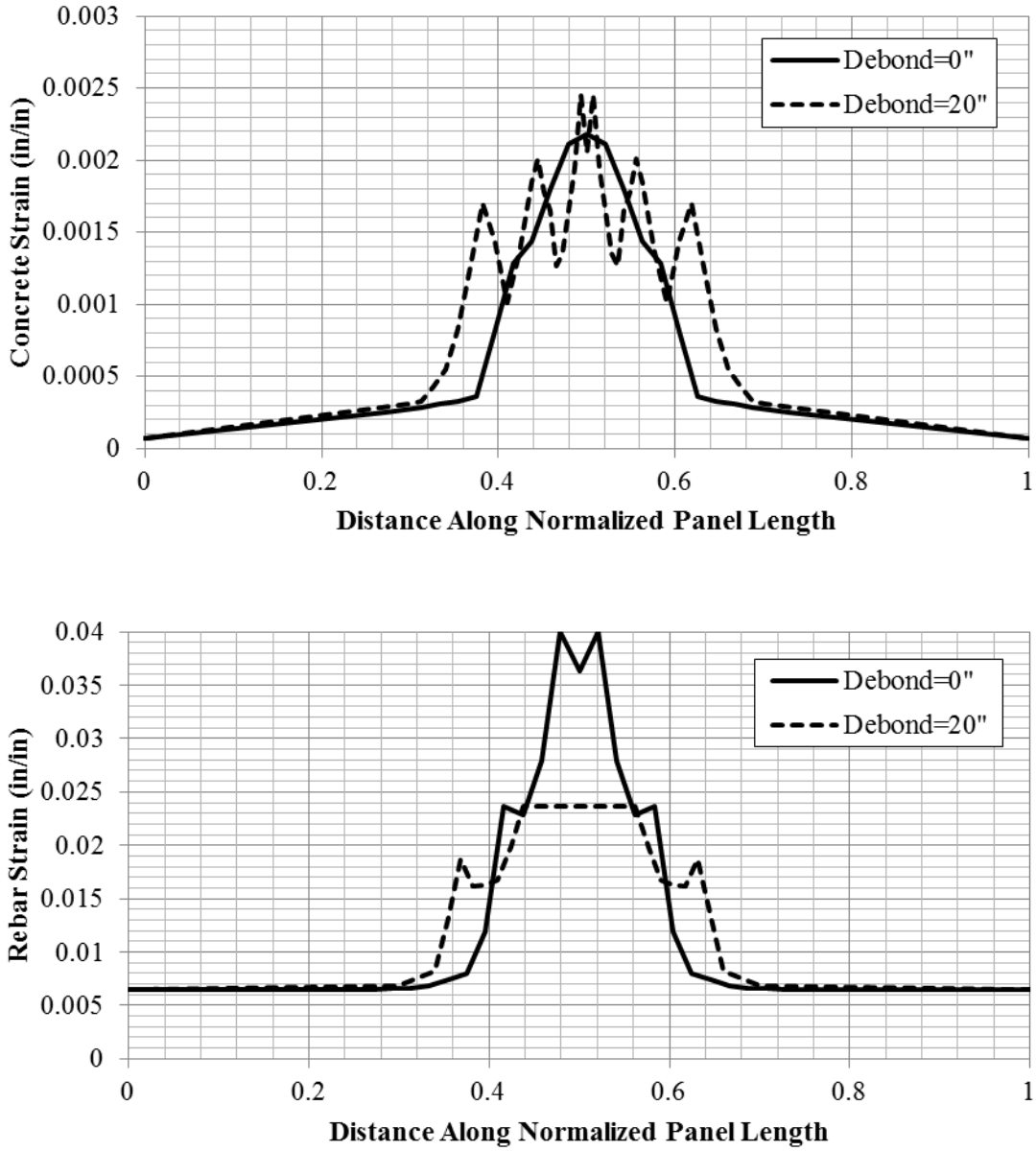

Figure 4-14: Strain Comparison of PS Panels at 3.0 Degrees of Support Rotation

Figure 4-15 shows similar plots of the concrete and rebar strains for the debonded panel at 5.0 degrees. The peak strain in the rebar is still less than 4% at this rotation. Fracture of the strand was still the controlling failure mechanism; however, debonding the strands allowed the panel to reach larger rotations before the strain capacity of the strand was met.

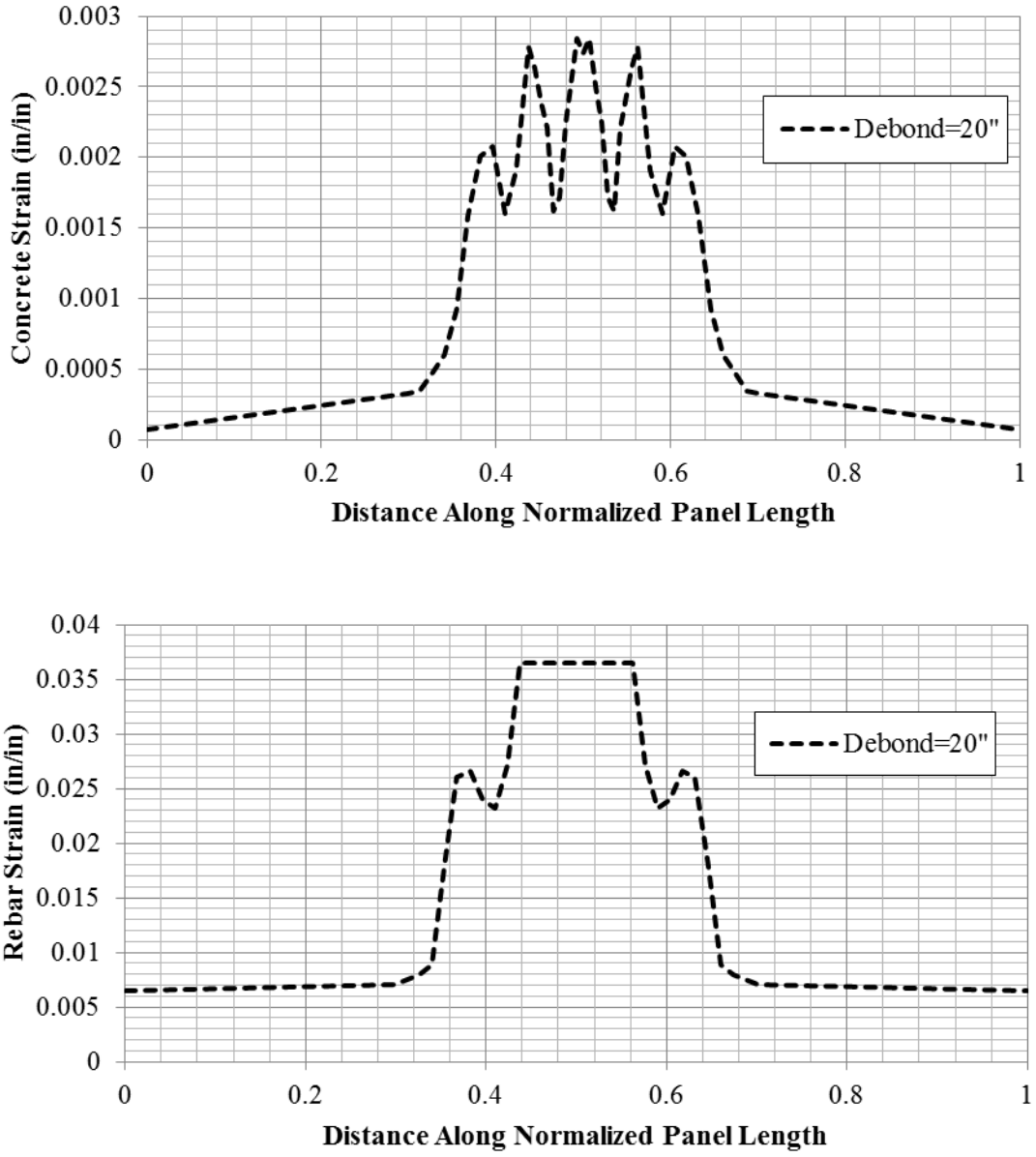

Figure 4-15: Strain Comparison of PS Panels at 5.0 Degrees of Support Rotation

Chapter 5

Quantifying Effects of Axial Load on Precast Wall Panels Subjected to Blast Loads

5.1 Introduction

Using a single degree of freedom (SDOF) process is the most common analysis method for blast design. The U.S. Army Corps of Engineers Protective Design Center developed a SDOF tool automated in an Excel spreadsheet, SBEDS (USACE 2008a). This design tool is often used in blast design of DOD buildings and was used in investigations for this study. In a typical design process a SDOF tool would be used to determine the maximum deflection and the corresponding support rotation or ductility ratio for a trial member. The support rotation or ductility ratio would then be related to the response limits to determine the potential damage sustained or level of protection provided by the trail member.

An inherent limitation of an SDOF analysis is that the response of the system has to be generalized into a single degree of freedom. In the case of wall panels, the lateral or out-of-plane response of the panel is of interest in design, and the applied loads must be related to this degree of freedom. A challenge of using a SDOF analysis for load-bearing panels is that the axial load does not have a direct correlation to the response of an out-of-plane load, such as a pressure, but the effects of an axial load on the lateral response still need to be indirectly incorporated into the analysis. The governing mode of response for a wall panel subjected to out-of-plane loading is normally flexure, and this study focused on how axial loads affect the flexural response of a panel subjected to blast loads. The axial loads would also affect the shear response of a panel, but this effect was not considered within the scope of this study.

5.2 Initial Dynamic FEA of Solid Load-Bearing Panels

As a starting point for the study on the effects of axial loads, solid non-PS and PS panels were analyzed dynamically with LS-DYNA. The same layouts used in the large solid panels from the modeling methodology development were used for these panels. These models were analyzed with various combinations of blast and axial loads. Although axial loads are generally thought of as point loads or distributed point loads, they were applied as a uniform pressure across the entire cross section of the member in order to avoid a local failure in the concrete at the load application point. Applying the load in this way also invokes a concentric loading condition. In reality axial loads are never applied perfectly concentrically, but as a starting point for the study it was better to study the behavior of the load-bearing system without eccentricity as an additional parameter. The panels were modeled as 12 feet high, but the supports were placed one foot from the top and bottom of the panel, resulting in a 10 foot clear span. The axial load was applied at the edge of the clear span instead of at the very top of the panel, so that as the panel rotates about the supports the axial load would remain concentric. The blast loads were applied as triangular impulse loads across the clear span with varying peak pressures and total impulses. Each blast load was also run with varying levels of axial load. In total 45 different load combinations were run, as seen in Table 5-1.

Table 5-1: Blast-Axial Load Combinations

Loading	1	2	3	4	5	6	7	8	9	10	11	12	13	14	15
Impulse (psi-ms)	100														
Peak Pressure (psi)	10					50					200				
Axial Load (kips)	0	44	88	176	352	0	44	88	176	352	0	44	88	176	352
Loading	16	17	18	19	20	21	22	23	24	25	26	27	28	29	30
Impulse (psi-ms)	200														
Peak Pressure (psi)	10					50					200				
Axial Load (kips)	0	44	88	176	352	0	44	88	176	352	0	44	88	176	352
Loading	31	32	33	34	35	36	37	38	39	40	41	42	43	44	45
Impulse (psi-ms)	300														
Peak Pressure (psi)	10					50					200				
Axial Load (kips)	0	44	88	176	352	0	44	88	176	352	0	44	88	176	352

The maximum out-of-plane deflection was monitored for each run, and the maximum deflections were used to calculate the maximum support rotations for each loading condition using Equation 3-4. For a ten foot clear span the support rotation can also be approximated as equal to the midspan deflection for small deflections. At ten inches of deflection, estimating the support rotation as ten degrees is only an error of about 5%. The results of the non-PS and PS analyses are presented in Table 5-2. Also, to demonstrate the effect of axial load on the flexural response of the panels, the maximum support rotations from Table 5-2 were plotted against axial load, as seen in Figure 5-1. The support rotations were normalized by the support rotation of a non-loading bearing panel to show the general trends in behavior as axial load is increased. The axial load was reported as a percentage of the factored nominal axial capacity with no eccentricity, ϕP_{no}, so that axial loads applied to different sections could be compared. The calculations used for ϕP_{no} are given in Equation 5-1 for reinforced concrete and Equation 5-2 for prestressed concrete.

$$\phi P_{no} = \phi * 0.8 * (0.85 * f_c^{'} * (A_g - A_s - A_s^{'}) + f_y * (A_s + A_s^{'})) \quad (5\text{-}1)$$

$$\phi P_{no} = \phi * 0.8 * (0.85 * f_c^{'} * (A_g - A_{ps} - A_{ps}^{'}) - (f_{pe} - 0.003 * E_{ps}) * (A_{ps} + A_{ps}^{'})) \quad (5\text{-}2)$$

Table 5-2: LS-DYNA Solid Non-PS and PS Blast-Axial Load Results

Impulse = 100psi-ms							
non-PS				PS			
Peak Pressure	10psi	50psi	200psi	Peak Pressure	10psi	50psi	200psi
%ΦPno	**Max Support Rotation (deg)**			**%ΦPno**	**Max Support Rotation (deg)**		
0	0.793	1.076	1.145	0	0.453	0.680	0.740
6	0.498	0.751	0.782	6.5	0.322	0.550	0.583
12	0.387	0.606	0.625	13	0.270	0.444	0.477
24	0.280	0.487	0.487	26	0.232	0.435	0.396
48	0.217	0.360	0.378	52	0.136	0.241	0.280
Impulse = 200psi-ms							
non-PS				PS			
Peak Pressure	10psi	50psi	200psi	Peak Pressure	10psi	50psi	200psi
%ΦPno	**Max Support Rotation (deg)**			**%ΦPno**	**Max Support Rotation (deg)**		
0	2.225	3.446	3.707	0	1.104	*rupture	*rupture
6	1.201	2.590	3.185	6.5	0.519	1.806	2.144
12	0.740	2.012	2.360	13	0.351	1.473	1.757
24	0.416	1.444	1.525	26	0.219	1.042	1.291
48	0.288	0.942	1.085	52	0.201	0.769	0.921
Impulse = 300psi-ms							
non-PS				PS			
Peak Pressure	10psi	50psi	200psi	Peak Pressure	10psi	50psi	200psi
%ΦPno	**Max Support Rotation (deg)**			**%ΦPno**	**Max Support Rotation (deg)**		
0	4.258	7.942 *rupture	8.691 *shear	0	*rupture	*rupture	*shear
6	2.345	*crush	*shear	6.5	0.852	*rupture	*rupture
12	1.066	*crush	*crush	13	0.490	*rupture/crush	*rupture
24	0.489	*crush	*crush	26	0.270	*crush	*crush
48	0.316	*crush	*crush	52	0.224	*crush	*crush

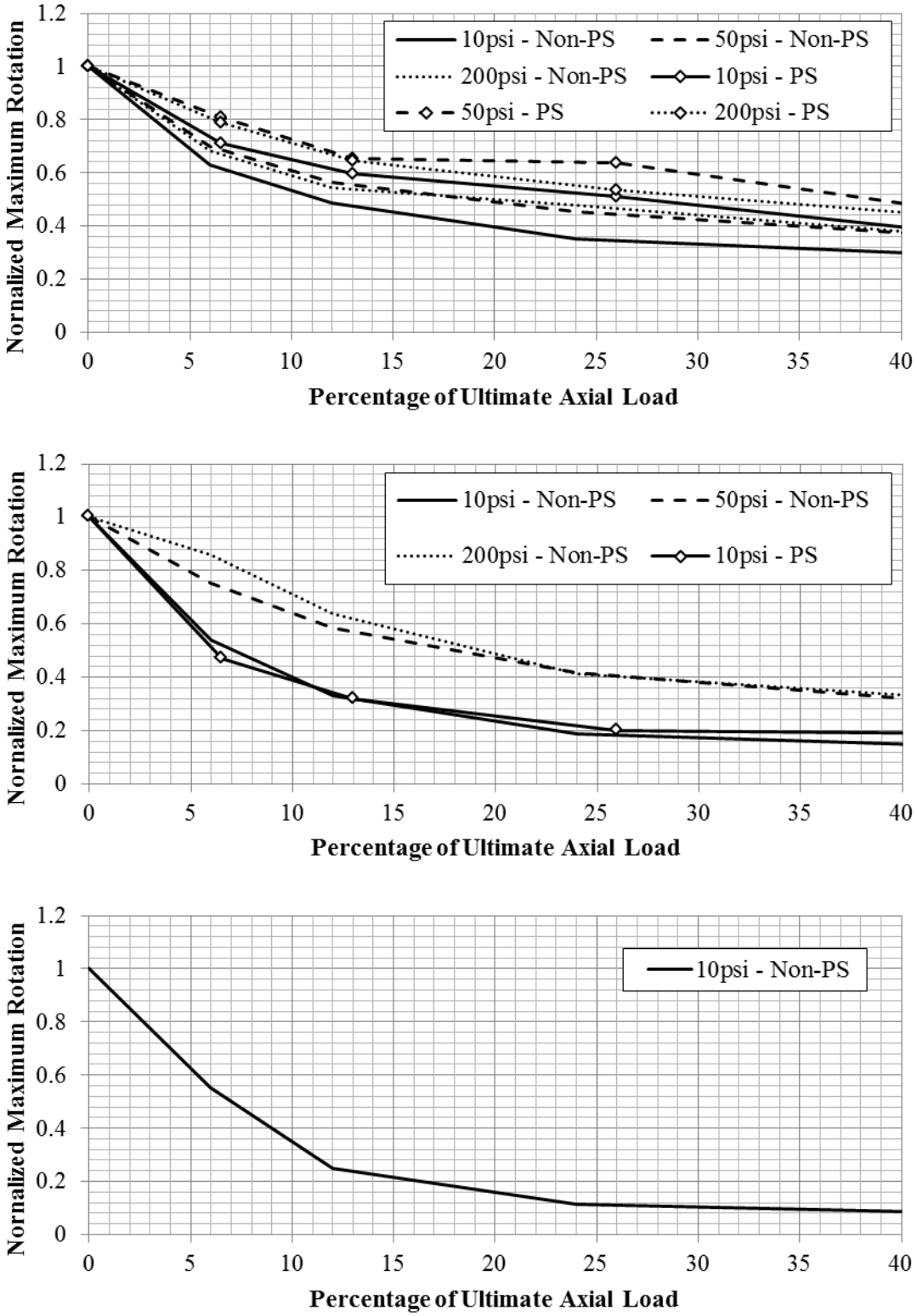

Figure 5-1: Effect of Axial Load on Flexural Response - 100 psi-ms Impulse (top), 200 psi-ms Impulse (middle), 300 psi-ms Impulse (bottom)

The plots in Figure 5-1 show that in general applying axial load to the panels caused smaller maximum rotations, which is beneficial in blast design. In some of the PS load sets (50 psi and 200 psi for 200 psi-ms impulse and 10 psi for 300 psi-ms impulse) the non-load-bearing panels failed while the load-bearing panels did not. Each of these non-load-bearing panels failed because the prestressing strand ruptured. This pattern indicates that an axial load can prevent a panel from failing that would have failed due to reinforcement reaching an ultimate strain limit. In these load sets, e.g. 50 psi/200 psi-ms, the non-load-bearing panel blew out, so the load-bearing results were not able to be normalized by the non-load-bearing case and were not incorporated into Figure 5-1. In other load sets the non-load-bearing and load-bearing panels all failed, but the failure mechanism changed depending on the axial load. For example, in the 50 psi/300 psi-ms set at low levels of axial load the panel collapsed because the prestressing strand ruptured, but at high levels of axial load the panel collapsed because the concrete crushed. In general this shows that the panel was unable to withstand that level of lateral loading but also supports the previous statement that axial load can be advantageous in regard to reinforcement failure. These observations will be discussed in more detail later.

These panel layouts were also analyzed using SBEDS to see if an SDOF analysis would show the same behavior as the FEA. For the non-PS panels, the Reinforced Concrete One-Way Slab input option was selected since this was the option closest to a wall panel. This input option allows for the user to input a static or dynamic axial load. For the RC One-Way Slab option the axial load is incorporated into the analysis as an equivalent lateral load calculated at each timestep. The PS FE results were unable to be compared to SDOF results because there is currently no input for axial load in the PS input option. The layout for the PS panel was run as a non-load-bearing panel, but no further runs were possible. The comparison of FEA to SDOF

analysis for the non-PS panel is shown in Figure 5-2. The results from the SDOF analysis were similarly converted to normalized support rotation versus percentage of factored nominal axial capacity. It is apparent from these results that the presence of axial loads shows opposite effects in the FEA and SDOF analysis. As stated previously, the FEA shows that in general the maximum support rotation will decrease as axial load is added to the panel; however, the SDOF analysis shows that the maximum support rotation will increase with axial load in all cases.

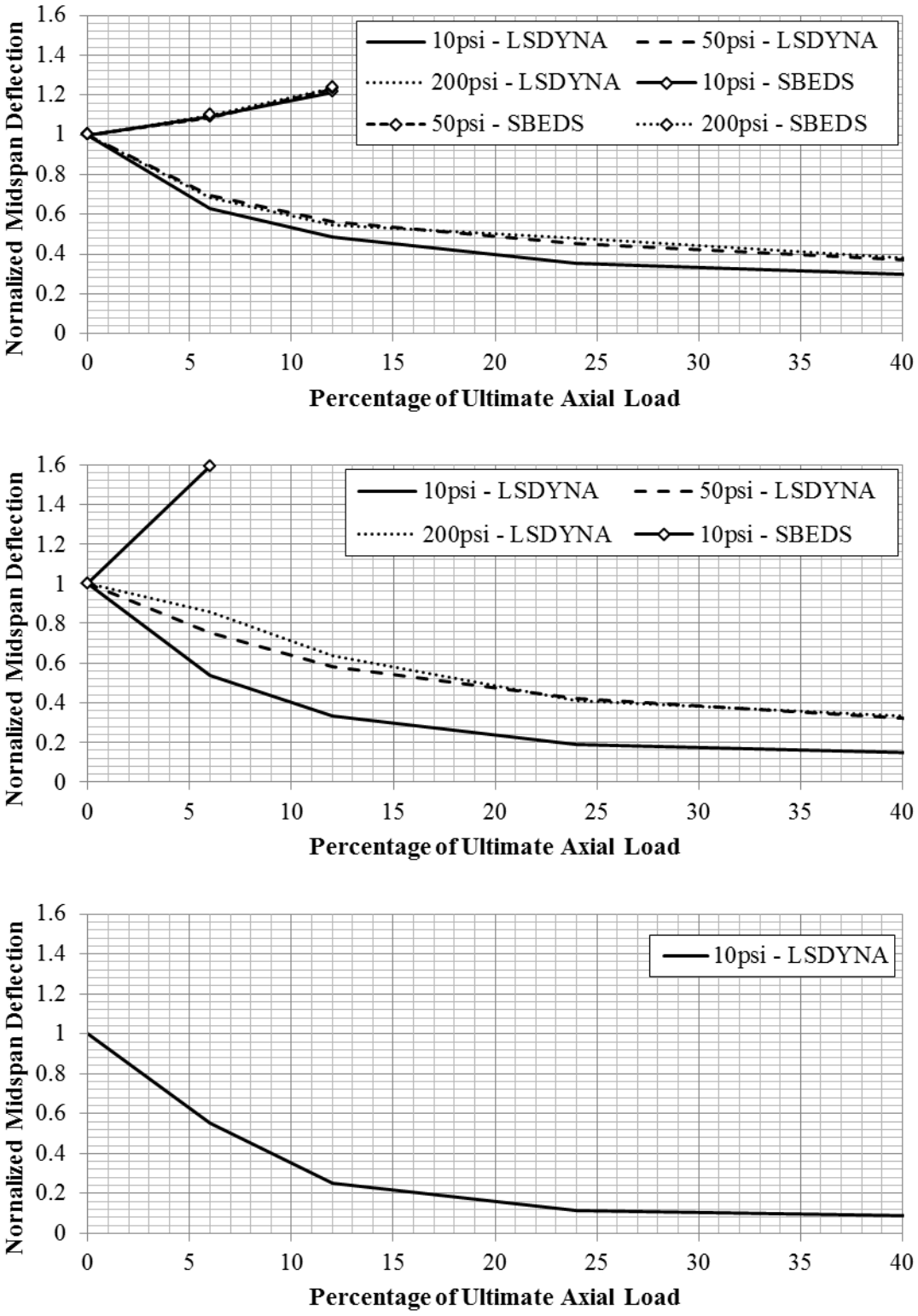

Figure 5-2: FEA vs. SDOF Analysis of Solid Non-PS Load-Bearing Panel - 100 psi-ms Impulse (top), 200 psi-ms Impulse (middle), 300 psi-ms Impulse (bottom)

For the 100psi-ms load sets, the deflections increased as 6% and 12% of ϕP_{no} were applied. At higher axial load levels the panel blew out so no results at these levels were able to be incorporated into Figure 5-2. The non-load-bearing panel was able to be analyzed at most of the larger lateral loads, but except for the 10 psi/200 psi-ms/6% of ϕP_{no} case applying any level of axial load caused the panel to blow out at the 200 and 300 psi-ms levels. In the 10 psi/200 psi-ms case, applying only 6% of ϕP_{no} caused the deflections to increase by about 60%. This is a large effect for such a small axial load.

The difference in these trends indicates that the current methodology for incorporating axial loads into the SDOF analysis is overly conservative for RC One-Way Slabs, because the effect of axial load on support rotations in the analysis is opposite of trend observed in the FE analyses. An ideal analysis would conservatively estimate the support rotation while proportionately incorporating the effect of axial load, whether that is beneficial or adverse. The reason for this disparity is that converting the axial load into an equivalent lateral load accounts for the additional second order moment applied to the member from the P-Δ effect, but it does not account for the change in moment capacity that results from axial-moment interaction. In SDOF analysis, the material input and layout is used to calculate a resistance curve that describes the static resistance of the member for the equation of motion at any given deflection. For the RC One-Way Slab analysis the resistance curve is calculated independent of the axial load, but in reality the interaction between axial forces and moment on a cross section has a large effect on the moment capacity and resultantly the resistance curve. The disparity in the results from the FEA and SDOF analysis show that this effect must be incorporated into the analysis for it to be done accurately.

5.3 Static Lateral Resistance of Load-Bearing Panels Using FEA

In order to quantify the lateral resistance of the non-PS and PS, load-bearing panels a static analysis was conducted using Abaqus/CAE. Similar to the dynamic analysis a concentric axial load was applied to the panels followed by a lateral pressure; however, in these analyses the pressure was applied statically, and a nonlinear solver was used to capture the full range of behavior of the member, including post-crushing softening and failure. Being able to capture the failure of the panels properly proved to be important in understanding how axial loads affect the ductility of the panels. Various levels of axial load were applied as before. The pressure was applied as a static ramp force and followed the resistance of the panels. An important parameter in the FE models was the nonlinear geometry feature. When nonlinear geometry is toggled on, the changes in geometry are considered, and the stiffness matrix is reformed throughout the analysis based on these changes. It seems intuitive that this feature should be included in the analysis because in reality the geometry is changing as loads are applied; however, the objective of the static analyses was to quantify the resistance of the panels, which is not affected by geometry. The models were run with and without nonlinear geometry. The comparison of these analyses was important in understanding the behavior of the systems.

5.3.1 Static Non-PS Solid Results

The results from the non-PS panel will be presented first. Figure 5-3 shows the results of the non-PS panels in terms of pressure versus rotation for varying levels of axial load with nonlinear geometry on and off. There are several important observations to be made from the figure. First, the peak pressure that the panel resists increases as axial load increases. This behavior was expected and can be described as the P-M interaction effect of the axial load. As can be seen in the generic P-M interaction diagram in Figure 5-4, as axial load is increased, the

moment capacity also increases until the balanced condition is reached. As axial load is further increased, the moment capacity then decreases until the pure compression state is reached. All of the axial loads that were applied were less than the axial load that would cause the balanced condition, so as expected the moment capacity, and resultantly the peak pressure, increased in each run as the axial load increased. Another important observation is the difference in the runs with and without nonlinear geometry. The pressure that the panel resists throughout the analysis is significantly less, especially at larger rotations, when nonlinear geometry is on. This difference is a result of the second-order moment caused by the axial load and the lateral deflection of the panel, or P-Δ effect. As the panel deflects, or rotates, the axial load is applying a moment along the length of the panel equal to the magnitude of the axial load times the deflection at any particular point along the length of the panel. This moment is initially negligible since the deflection is small but becomes significant as the member yields and reaches higher deflections. When nonlinear geometry is off, this effect is not captured. The moment from the P-Δ effect in essence decreases the available capacity of the cross section to resist moment from lateral pressure.

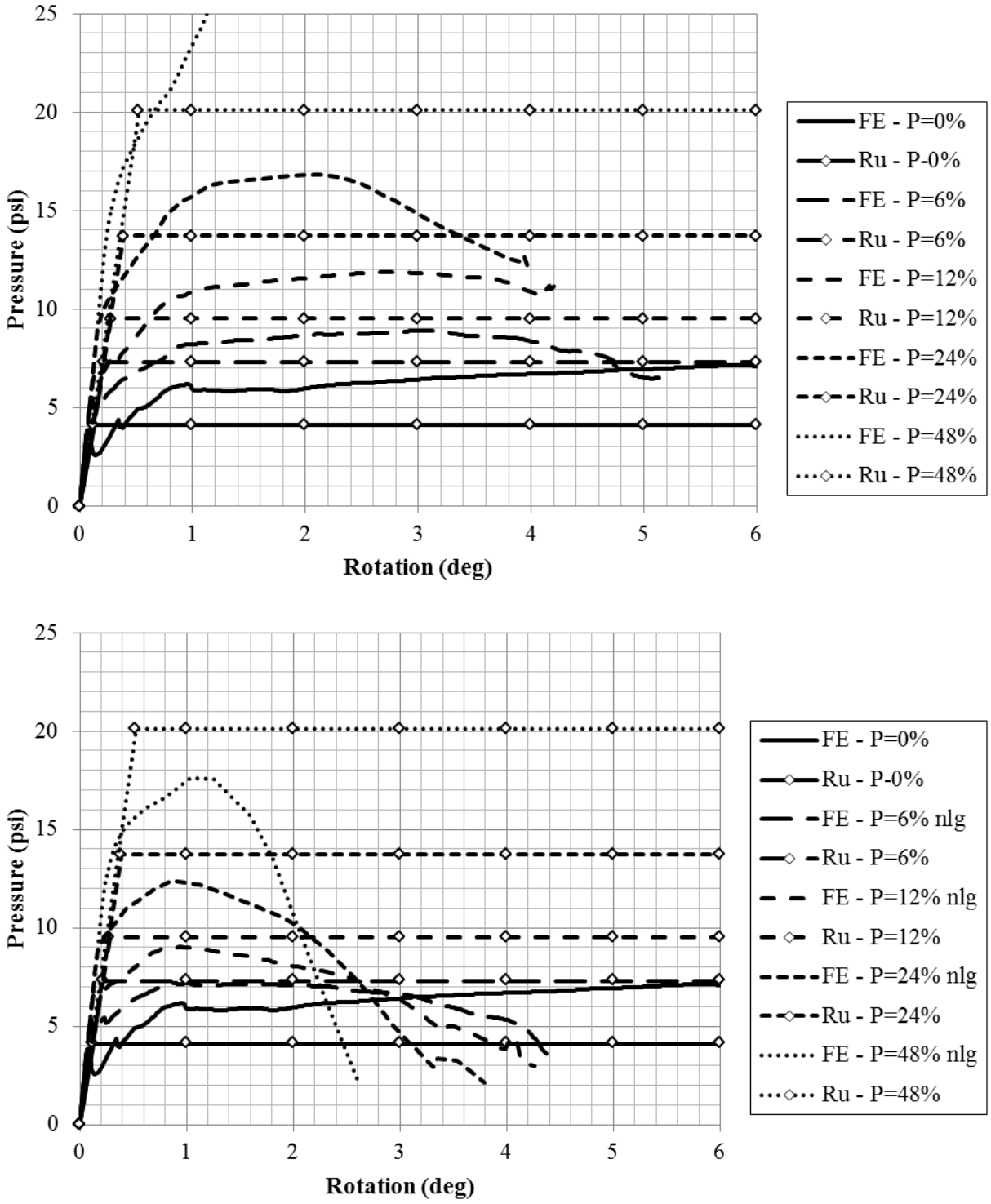

Figure 5-3: Static Resistance of Non-PS Load-Bearing Panels - Nonlinear Geometry Off (top), Nonlinear Geometry On (bottom)

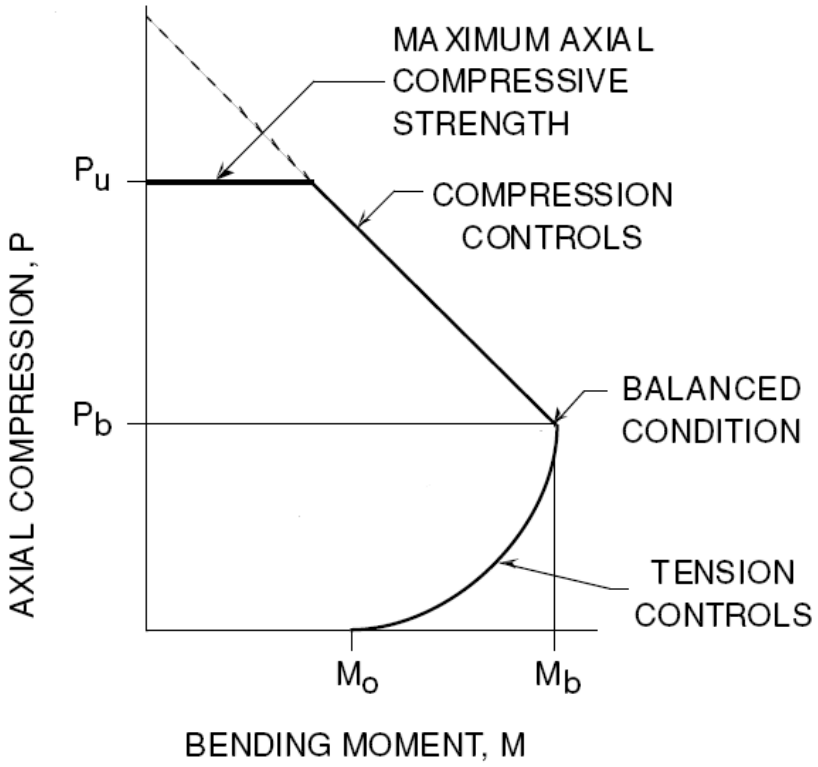

Figure 5-4: P-M Interaction Diagram (adapted from USACE 2008a)

In addition to the FE results, the graphs in Figure 5-3 include bilinear plots for each run labeled as Ru. These plots are resistant curves generated from hand calculations done in parallel with the FEA. The moment capacity of the panel was calculated for each level of axial load. To generate a P-M interaction diagram, typically several different strain profiles are assumed, and the axial load and moment are calculated for each profile and plotted together. For these calculations the axial loads were assumed and the corresponding moment capacities was calculated iteratively. These calculations were streamlined in an excel spreadsheet but are based on Equations 5-3 and 5-4. These equations correspond to the generic strain profile for a doubly reinforced cross section shown in Figure 5-5. The forces from the tension and compression steel are labeled as T_1 and T_2, but depending on the axial load, these forces could be either tensile or compressive. Determining the magnitude and orientation of these forces is part of the iterative

process. Resistance curves used in SDOF analysis are usually generalized as a multi-linear curve with different stiffnesses. In the SDOF investigations for this study the resistance curve for a simply supported member was approximated as a two-part curve with an initial elastic portion and a perfectly plastic portion, as seen in Figure 5-6. The curve is defined by the initial elastic stiffness, k_e, and the peak resistance, r_u, which is based on the moment capacity of the cross section. The moment capacities were calculated as described above. k_e, r_u, and x_e, the deflection at which the resistance transitions to plastic behavior, were calculated for each panel using Equations 5-5 through 5-7. The moment of inertia used in the stiffness calculation, I_a, is approximated as an average of the gross and cracked moment of inertia of the section.

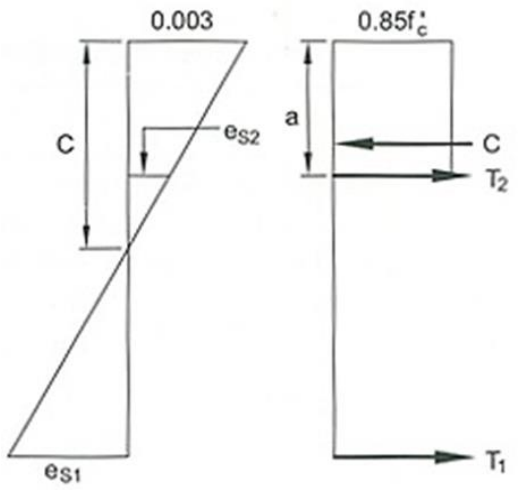

Figure 5-5: Strain Profile of Doubly-Reinforced Concrete Section (PCI 2004)

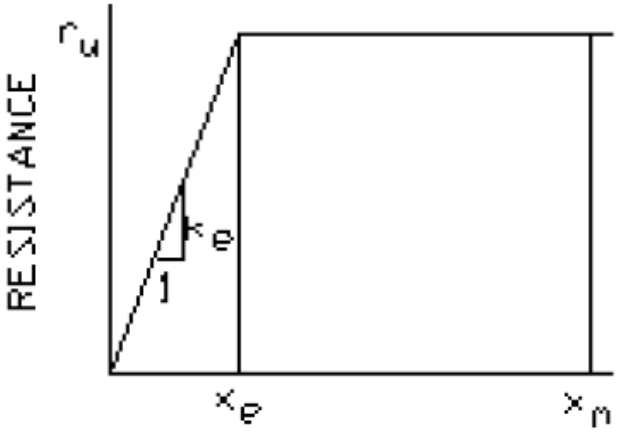

Figure 5-6: Resistance Curve for Simply Supported Member (USACE 2008a)

$$P = C - T_1 - T_2 \tag{5-3}$$

$$M_n = C * (\frac{h}{2} - \frac{a}{2}) + T_1 * (d - \frac{h}{2}) - T_2 * (\frac{h}{2} - d') \tag{5-4}$$

$$k_e = \frac{384 * E * I_a}{5 * b * L^4} \tag{5-5}$$

$$r_u = \frac{8 * M_n}{b * L^2} \tag{5-6}$$

$$x_e = \frac{r_u}{k_e} \tag{5-7}$$

These curves were developed to make sure that the comparison of calculations from RC theory and the FE results makes sense and to provide a way to incorporate the change in resistance due to axial load into SDOF analysis. It is important to note that the maximum pressure of the Ru curves is less than the maximum pressure of the FE results when nonlinear geometry was off, but greater than the FE results when nonlinear geometry was on. It is expected that the peak pressure of the Ru curve for each case would be less than the peak pressure of the FE results since the calculations make conservative assumptions, such as, no strain hardening in the reinforcement; therefore, in terms of pressure the comparison of the two makes sense in the nonlinear geometry off plot but does not make sense in the plot with nonlinear geometry on. These resistance curves really represent a moment that the midspan cross section is resisting, not a pressure. They need to be presented as an equivalent lateral pressure versus support rotation since the forcing function for a blast load in a SDOF analysis will be in terms of pressure. A better comparison of the all the FE results with the Ru curves can be made by plotting the results in terms of midspan moment versus rotation. These results are presented for each case individually in terms of moment versus rotation in Figure 5-7.

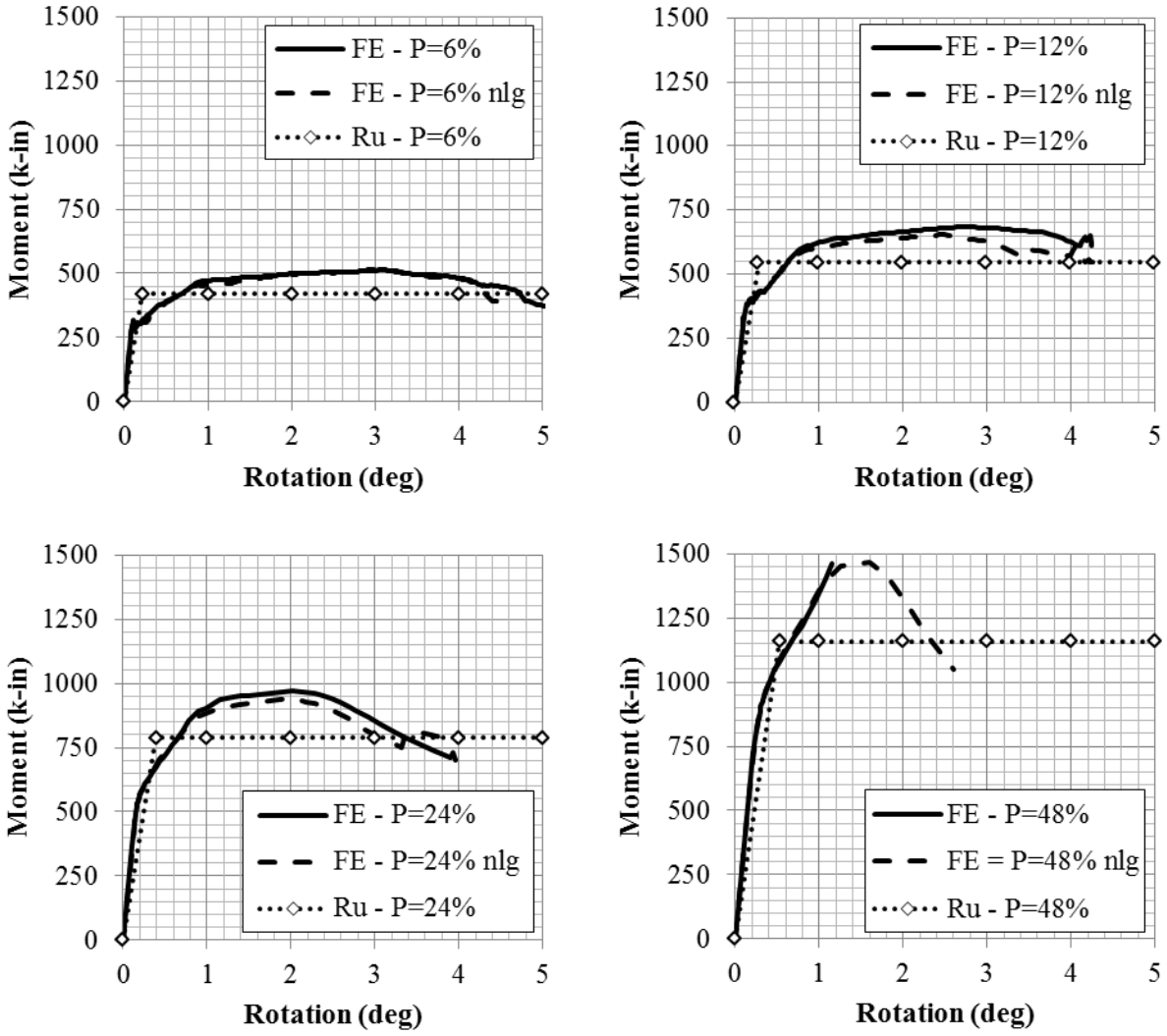

Figure 5-7: Static Moment Capacity of Non-PS Load-Bearing Wall Panels

In Figure 5-7, the solid lines are the results of the FE models without the nonlinear geometry feature. In these models all of the moment experienced by the member came from the lateral pressure, since there was no P-Δ effect; therefore, the moment was calculated by Equation 5-8. The dashed lines that follow a similar path as the solid lines are the results of the FE models with the nonlinear geometry feature on. In these models the moment experienced by the member came from a combination of the lateral pressure and the secondary P-Δ effect; therefore, the moment was calculated by Equation 5-9. The Ru curves are the same as before except that pressure was converted to moment using Equation 5-8.

$$M = \frac{p * b * L^2}{8} \tag{5-8}$$

$$M = \frac{p * b * L^2}{8} + P * \Delta \tag{5-9}$$

The FE results for each case with nonlinear geometry on and off compare very closely. This comparison shows that while incorporating P-Δ effects changes the way that loads are applied to the structure, the resistance of the member remains the same. This concept is important to understand when developing resistance curves for SDOF analysis. The peak moment was approximately 15 to 25% larger than the peak moment calculated for the resistance curves. This difference shows a reasonable amount of conservatism that would be expected when comparing hand calculations to actual results. There were no test results to compare to, but the comparison to hand calculations show the FE results are at least reasonable.

A discrepancy in the results that needs to be noted is the plot of the FE run for P=48% with nonlinear geometry off. The plot can be seen in the top graph of Figure 5-3 and in Figure 5-7 (FE - P=48%). The plot seems to stop abruptly at about 1.2 degrees of rotation, while all the other models ran out to 3 to 5 degrees. This difference was a result of convergence problems in the FEA. As discussed previously, an arc length solver was used in these analyses, which solves for loads and displacements simultaneously regardless of whether the response is stable or unstable. In this case the flexural response path became unstable, and the analysis started unloading the pressure elastically, as seen in Figure 5-8 (Low Viscosity). While this is a valid equilibrium path, it was not the desired result of the analysis.

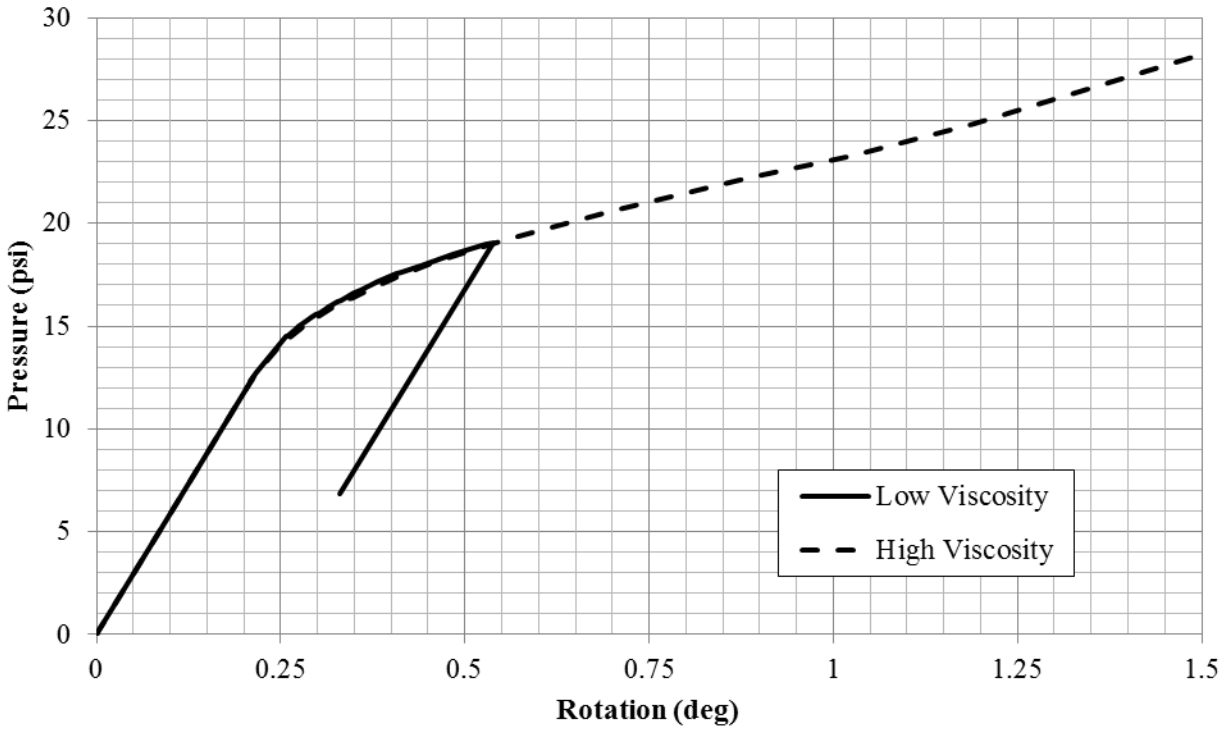

Figure 5-8: Elastic Unloading Equilibrium Path

Attempts were made to achieve a stable analysis through the entire flexural response of the panel by increasing the viscosity parameter in the Concrete Damaged Plasticity material model (see Section 3.2.1.1 for discussion of this feature). Increasing this parameter can result in a more stable run, but a trade-off of increasing the parameter is that if it is too high, it can result in fictitiously high compressive or tensile stresses in the concrete elements and consequently invalid results, as seen in Figure 5-8 (High Viscosity). Instead of failing in compression and tension, the stresses in the concrete increase beyond their ultimate limits. Ideally a stable run would be achieved using a low viscosity; however, a full stable run was not able to be achieved, so the results from the high viscosity case were used until the point where the tensile or compressive stresses reached their ultimate limit. Up until that point the results were considered valid and reported, while beyond that point the results were considered fictitious and ignored.

Fortunately, the model of the same case with nonlinear geometry was able to run a full analysis stably. The results from these two runs compare very well until the model without nonlinear geometry stops, which validates the use of this data.

5.3.2 Static PS Solid Results

Similar to Figure 5-3, Figure 5-9 shows the results of the PS panels in terms of pressure versus rotation for varying levels of axial load with nonlinear geometry on and off. The same trends that were seen in the non-PS results are also present in the PS results. The axial load increases the peak pressure that the panels are able to resist, and the moment from the P-Δ effect decreases the available capacity of the cross section to resist moment from lateral pressure. An observation that is unique to the PS results is a change in failure mechanism from the non-load-bearing to load-bearing panels. The non-load-bearing panel failed because the prestressing strands reached their ultimate strain capacity and fractured; however, all of the load-bearing panels failed because of crushing in the concrete. The compressive stress from the axial load reduced the tensile stresses and strain in the strands, allowing the concrete to reach its compressive strength before the strands fractured.

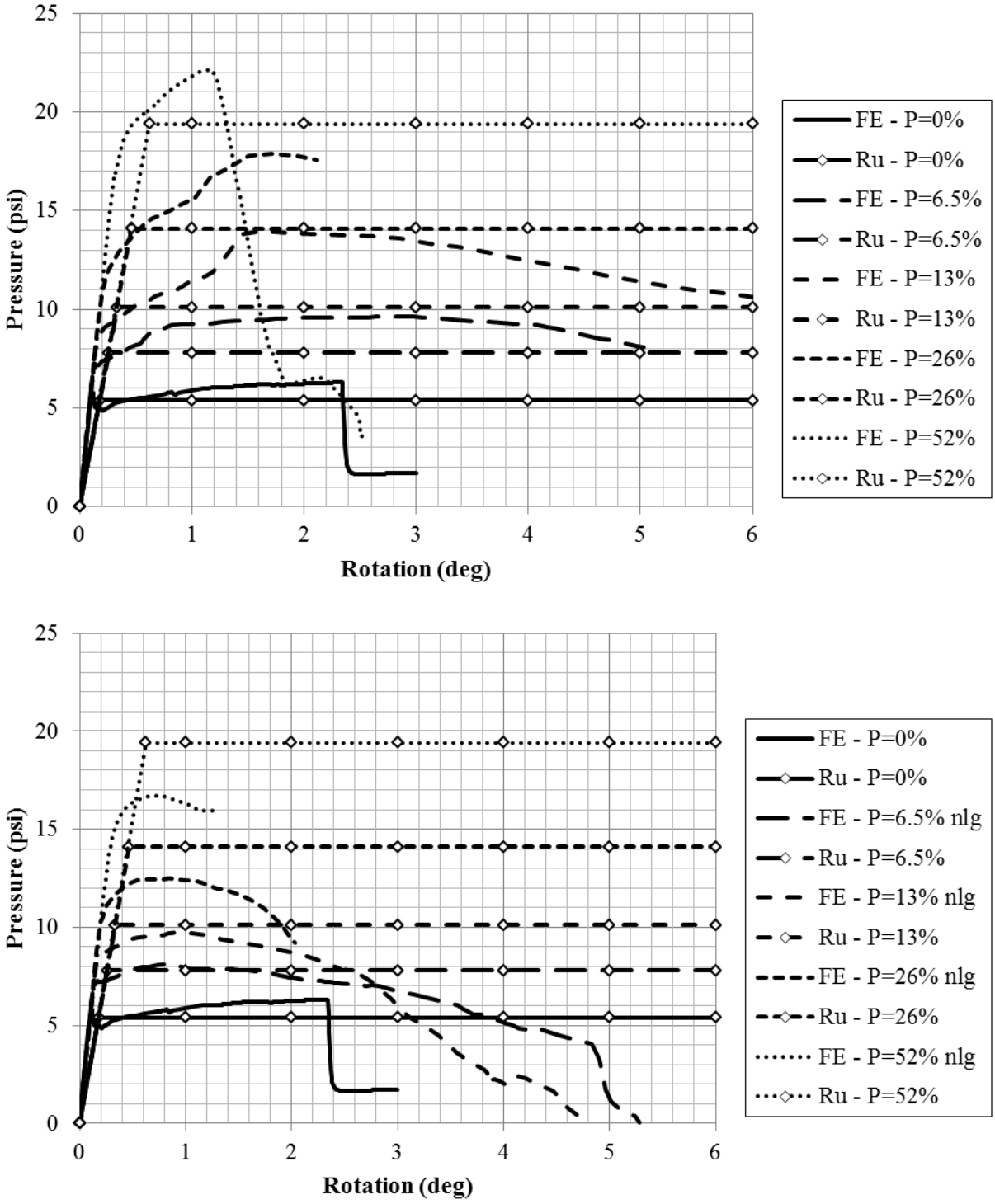

Figure 5-9: Static Resistance of PS Load-Bearing Panels - Nonlinear Geometry Off (top), Nonlinear Geometry On (bottom)

The PS results were also compared in terms of moment versus rotation as seen in Figure 5-10. The pressures were similarly converted to moments using Equations 5-9 and 5-10. The resistance curves developed from hand calculations for the PS panels also showed a reasonable amount of conservatism when compared to the FE results. Similar to before one of the models, P=52% with nonlinear geometry on, was unable to run stably, and only part of the results from this model that were considered valid and reported.

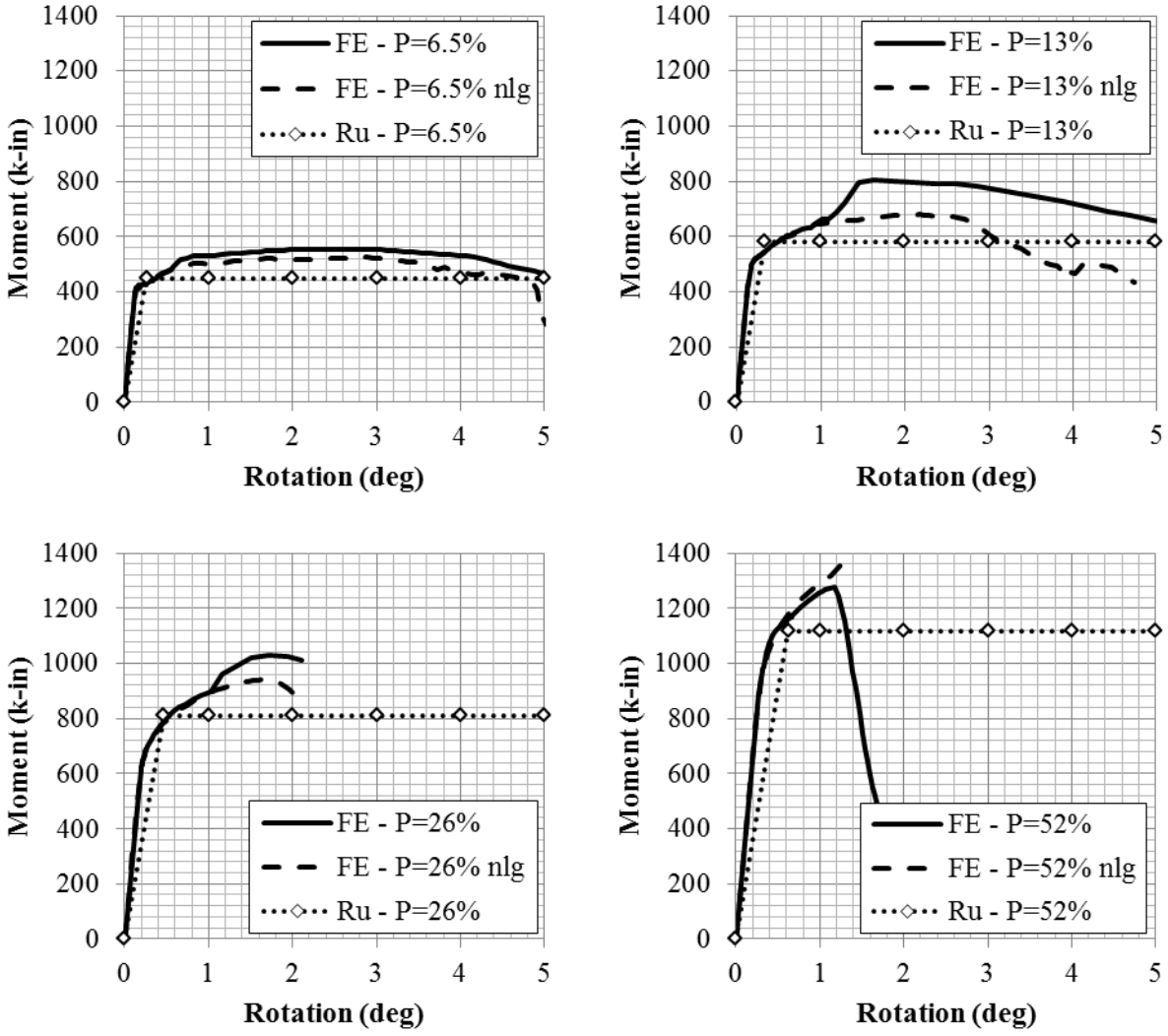

Figure 5-10: Static Moment Capacity of PS Load-Bearing Wall Panels

5.4 Incorporating the Effects of Axial Load on Resistance into SDOF

The next step in the study was to incorporate the effects of axial load quantified in the static analyses into the SDOF approach. The main two effects that need to be incorporated into the SDOF analysis are the P-M interaction and P-Δ effect. In the initial SDOF analyses the RC One-Way Slab input option was used for the non-PS panel. As discussed previously, this option accounts for the P-Δ effect using an equivalent lateral load but does not account for the P-M interaction effect on the panel resistance, which results in an overly conservative analysis. Since the SDOF tool was already programmed to incorporate the P-Δ effect for axial loads, the only modification that was needed was to the resistance curve. There is an input option with a user defined resistance that is available, but this option has no input for axial load; therefore, it does not compute the equivalent lateral load to account for the P-Δ effect. It is possible to indirectly account for the P-Δ effect by adjusting the resistance curve, but it was concluded that it would be simpler to use the RC One-Way Slab option and modify the resistance curve by using different input parameters. The inputs for steel areas, slab thickness, and concrete density were modified for each level of axial load to produce resistance curves that match the calculated resistance curves developed in parallel with the static analysis. The input for each run is presented in Table 5-3. The goal of changing the input was to keep the stiffness and mass of the resistance curve the same but change the peak resistance of the curve.

Table 5-3: SBEDS Modified Input

Axial Load (%Pno)	Axial Load (lb/in)	Calculated Resistance (psi)	Steel Area (in^2)	Slab Thickness (in)	Concrete Density (pcf)	SBEDS Resistance (psi)	Stiffness (psi/in)	Mass (psi-ms^2/in)
0	0	4.13	0.62	8	145	4.13	39.13	1737.3
6	1375	7.27	1.145	7.8	149	7.27	39.95	1740.6
12	2750	9.49	1.568	7.58	153	9.47	39.53	1736.9
24	5500	13.71	2.48	7.25	160	13.70	39.24	1737.3
48	11000	20.14	4.265	6.8	171	20.14	39.06	1741.5

Another option for the non-PS panel in SBEDS was to analyze the panel with the RC Beam-Column input option. This option not only accounts for the P-Δ effect using an equivalent lateral load but also modifies the resistance curve using a conservative simplification of the P-M interaction diagram. The moment capacity with no axial load, M_o, as well as the moment and axial load resulting in a balanced strain condition, i.e. concrete crushes and steel yields simultaneously, are calculated. Once these two points, (M_o, 0) and (M_b, P_b), are determined, the moment capacity for any amount of axial load between zero and P_b is calculated assuming a straight line between these two points. This concept is depicted in Figure 5-11 and can be quantified using Equation 5-10. This option was also used to analyze the panel since it was simple to run and provided another point of comparison, but the modified RC One-Way Slab input option provided more accurate and mechanically sound results for comparison.

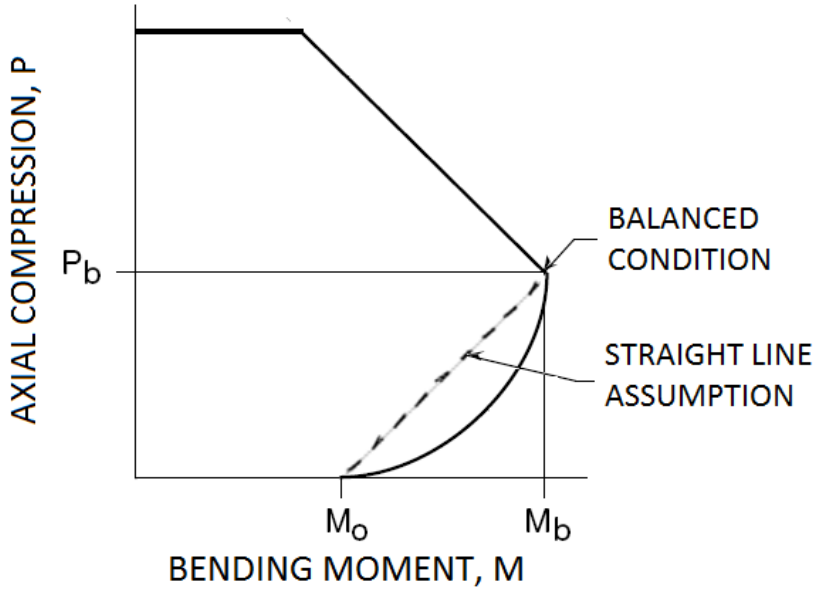

Figure 5-11: Straight Line Simplification of P-M Interaction Diagram (adapted from USACE 2008a)

$$M_n = \frac{P}{P_b} * (M_b - M_o) + M_o \qquad (5\text{-}10)$$

In the SDOF tool, there is only one input option for a PS panel, and it is unable to incorporate any axial load effects into the analysis; therefore, the only option for incorporating the effects of axial load into the analysis was by using the user-defined input option. As stated previously, this option has no input for axial load, so the effects of P-M interaction and P-Δ need to be incorporated into the resistance curve. In order to incorporate both of these effects, a slightly different bilinear curve was used. Similar to before, Equations 5-4 through 5-7 were used to calculate the peak resistance, r_u, for each panel and the deflection at which each panel reaches this capacity, x_e. For the second part of the curve, a perfectly plastic assumption was still made, except the resistance was reduced by the quantity of the magnitude of the axial load multiplied by the deflection. This quantity varies since the resistance is a function of the deflection resulting in the second part of the curve being linear with a negative slope equal to the negative of the magnitude of the axial load. The elastic part of the curve is still linear with a slightly smaller slope. In essence the resistance curves are the same as before except the resistance is reduced throughout the curve by the P-Δ moment. A comparison of a panel resistance curve with and without the P-Δ modification is shown in Figure 5-12, and all of the curves used for the PS panels used in the SDOF are shown in Figure 5-13.

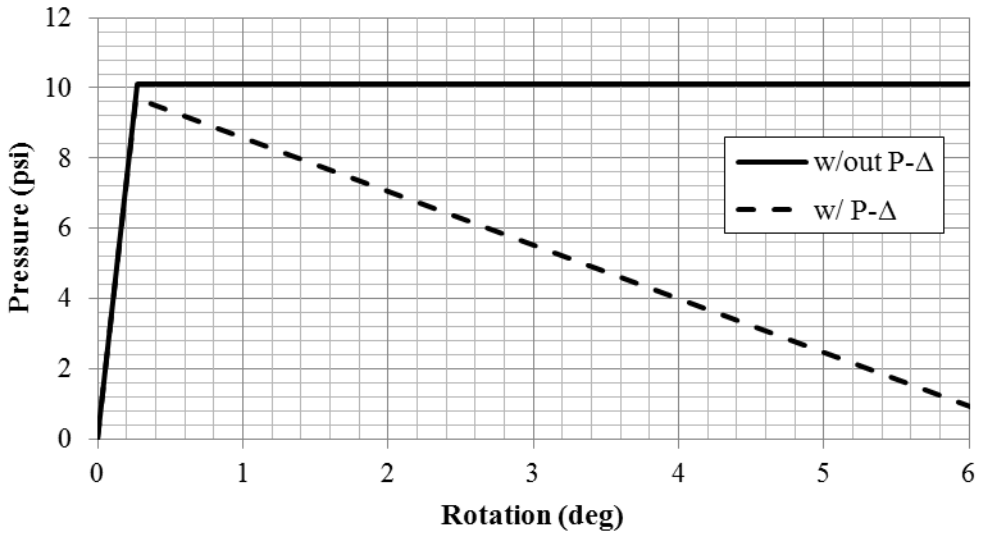

Figure 5-12: Comparison of PS Resistance Curve with and Without P-Δ Reduction (P=13%)

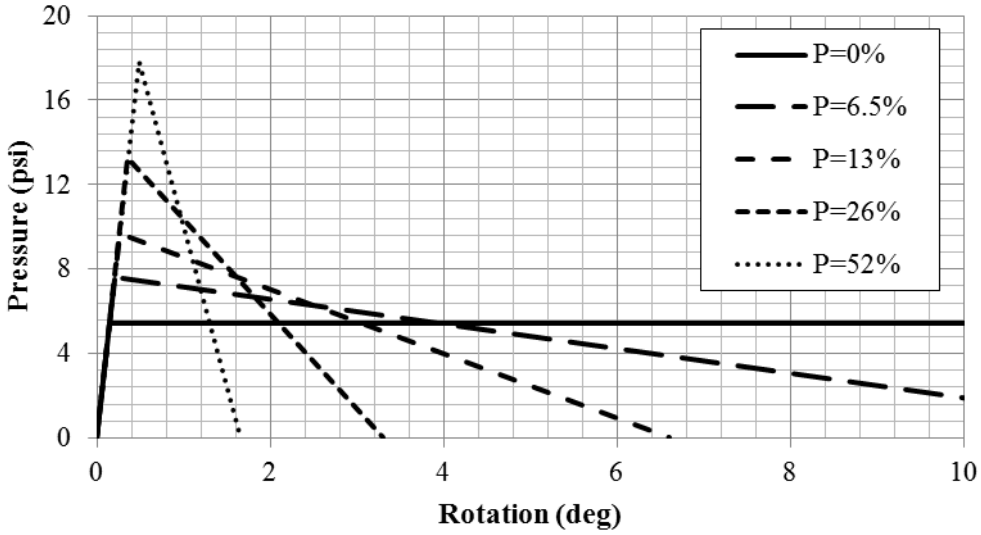

Figure 5-13: Resistance Curves for PS Panel Incorporating P-M and P-Δ Effects

The panels were analyzed with the SDOF analysis tool using the modified RC One-Way slab input and RC Beam-Column input for the non-PS panel and the user-defined input for the PS panel. The results from these analyses were compared with the original results of the FE and SDOF analyses as shown in Figures 5-14 and 5-15.

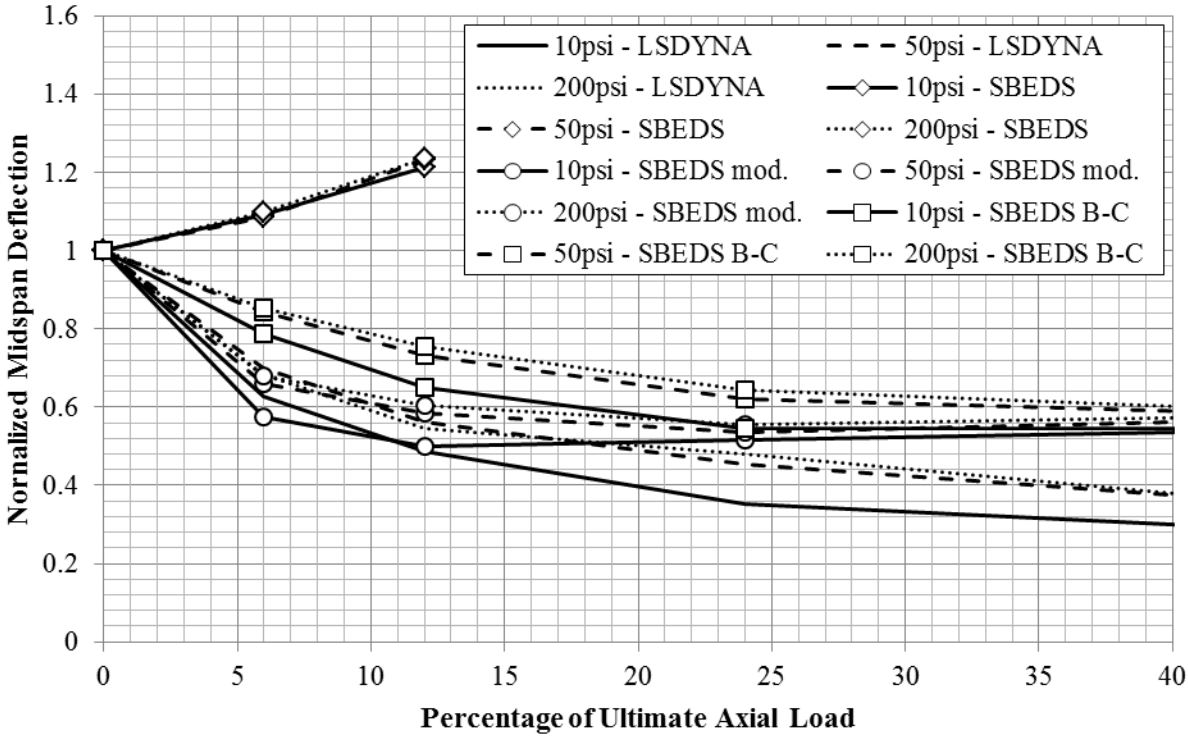
10psi - LSDYNA
50psi - LSDYNA
200psi - LSDYNA
10psi - SBEDS
50psi - SBEDS
200psi - SBEDS
10psi - SBEDS mod.
50psi - SBEDS mod.
200psi - SBEDS mod.
10psi - SBEDS B-C
50psi - SBEDS B-C
200psi - SBEDS B-C
Normalized Midspan Deflection
Percentage of Ultimate Axial Load
0
0.2
0.4
0.6
0.8
1
1.2
1.4
1.6
0
5
10
15
20
25
30
35
40

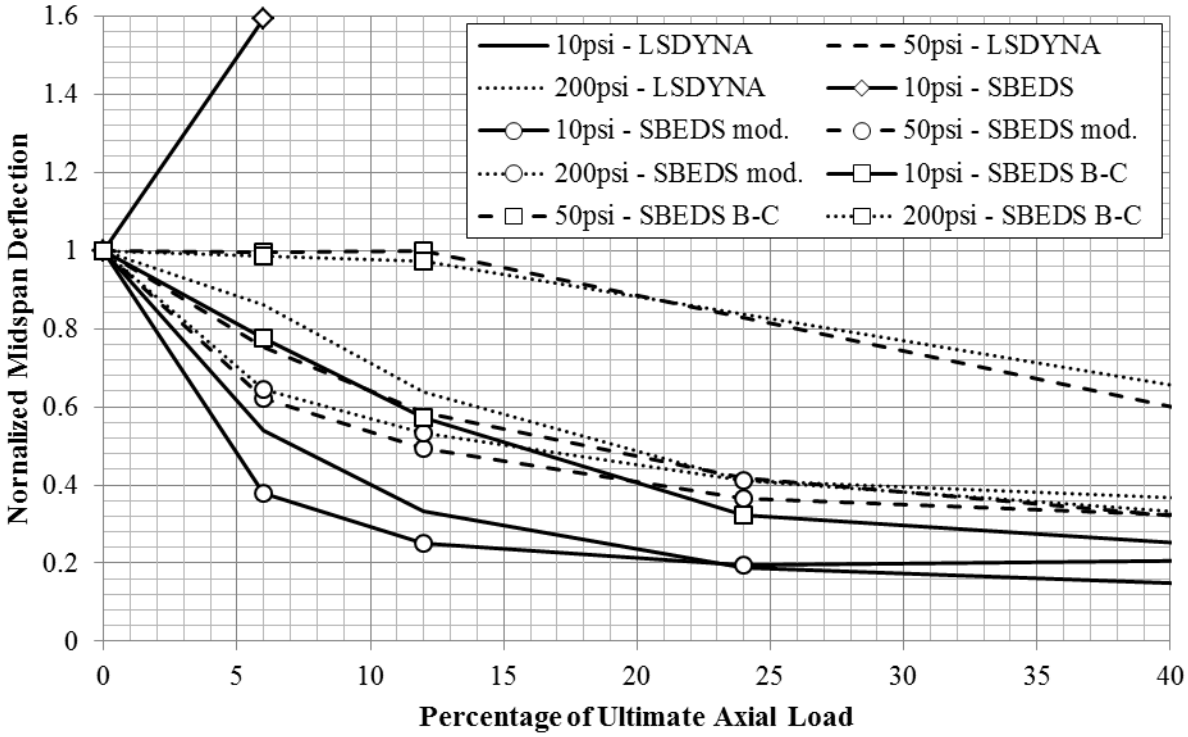
10psi - LSDYNA
50psi - LSDYNA
200psi - LSDYNA
10psi - SBEDS
10psi - SBEDS mod.
50psi - SBEDS mod.
200psi - SBEDS mod.
10psi - SBEDS B-C
50psi - SBEDS B-C
200psi - SBEDS B-C
Normalized Midspan Deflection
Percentage of Ultimate Axial Load
0
0.2
0.4
0.6
0.8
1
1.2
1.4
1.6
0
5
10
15
20
25
30
35
40

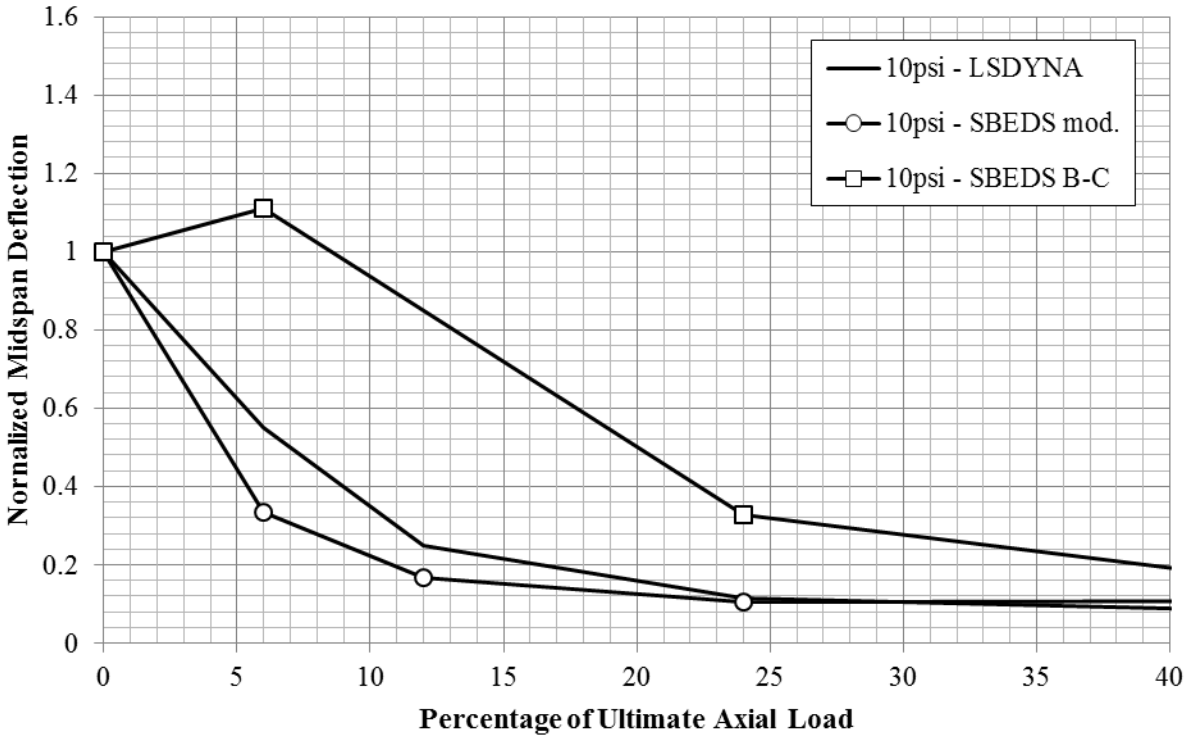

Figure 5-14: FEA and Modified SDOF Analysis Non-PS Comparison - 100 psi-ms Impulse (top), 200 psi-ms Impulse (middle), 300 psi-ms Impulse (bottom)

The results from these analyses compare much better to the FEA than the original SDOF analysis comparison. These results agree with the trend seen in the FEA that as the axial load increases the maximum support rotation decreases. The modified RC One-Way Slab input compares better to the FEA than the RC Beam-Column input, which was expected since the Beam-Column input uses a conservative simplification in calculating the moment capacity. At the 100psi-ms level, the Beam-Column input option was slightly conservative but still captured the general trend of how axial load affects the response correctly; however, at some of the higher load levels, such as, 50 psi/200 psi-ms or 10 psi/300 psi-ms the straight-line assumption was too conservative and resulted in no change or an increase in deflection for certain axial loads, while the deflections from the FEA and modified SDOF input based on a more accurate calculation for the moment capacity decreased for all levels of axial load. It would be advantageous to be able to

use the Beam-Column approach because the calculations are simpler, but the comparison shows that for some blast-axial load combinations, this approach is too conservative to capture the behavior properly. For the 50 psi/300 psi-ms and 200 psi/300 psi-ms sets, all of the axial loads cases blew out the panel for both SDOF input methods, which agrees with the FE results.

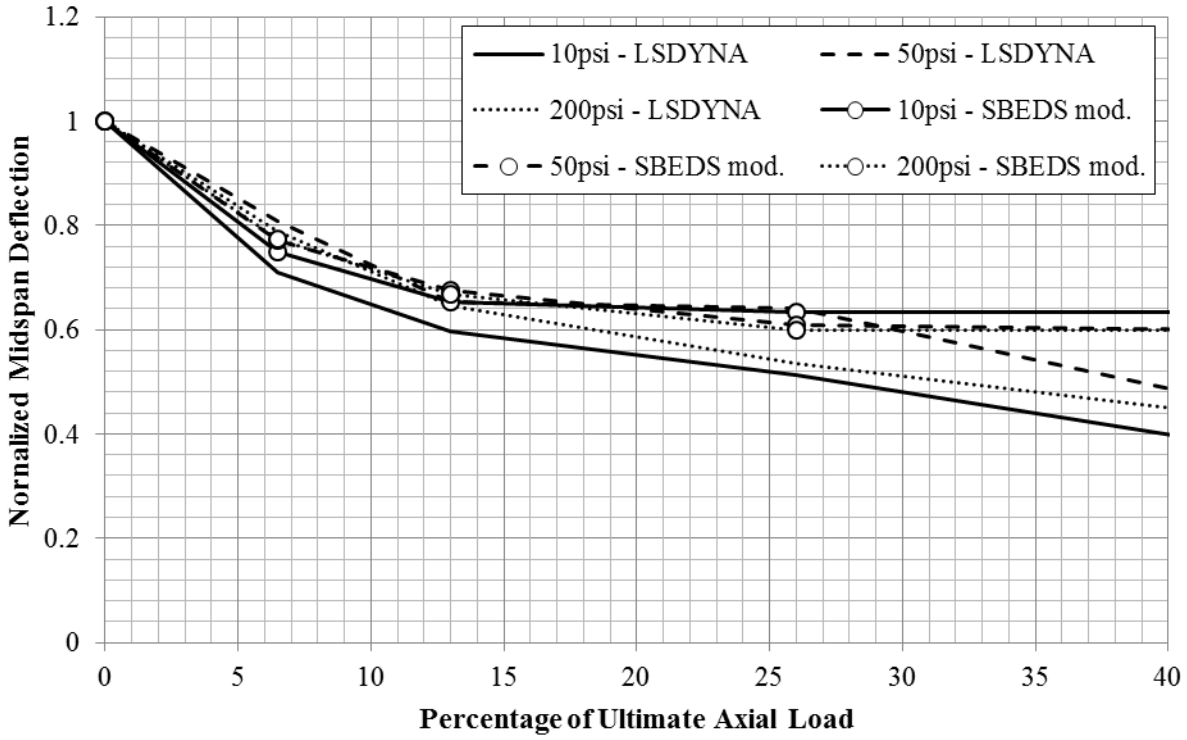
10psi - LSDYNA
50psi - LSDYNA
200psi - LSDYNA
10psi - SBEDS mod.
50psi - SBEDS mod.
200psi - SBEDS mod.
Normalized Midspan Deflection
Percentage of Ultimate Axial Load
0
0.2
0.4
0.6
0.8
1
1.2
0
5
10
15
20
25
30
35
40

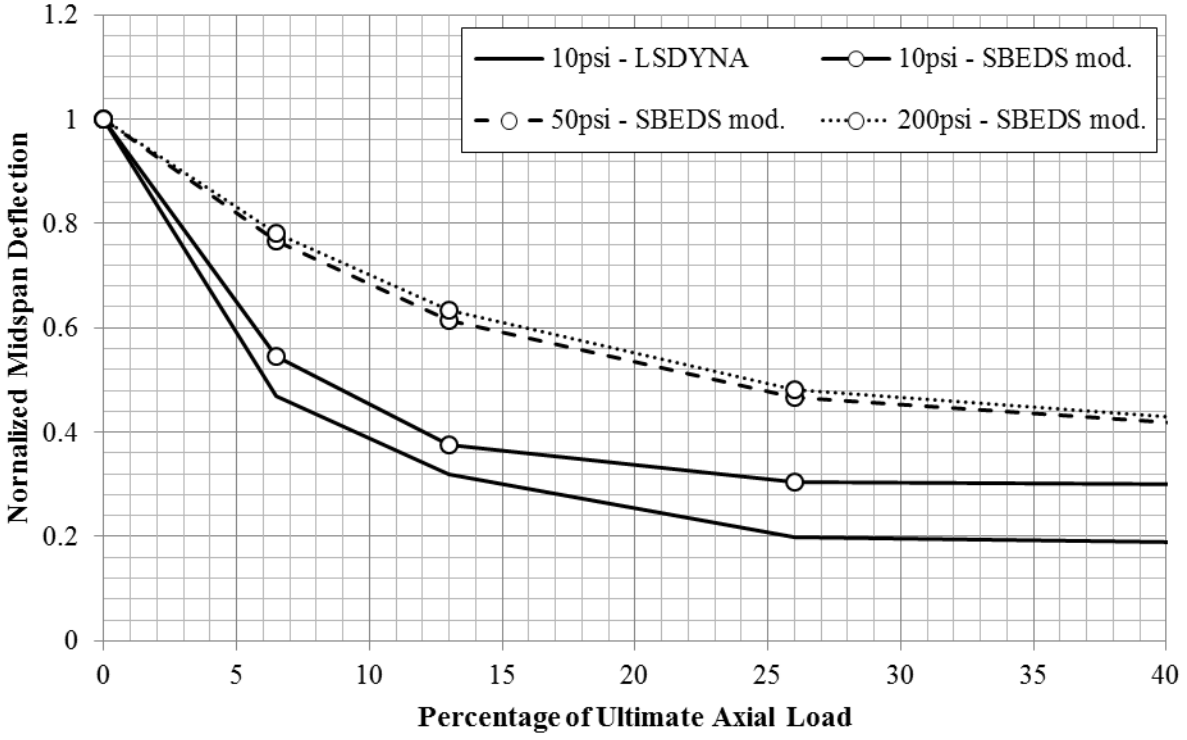
10psi - LSDYNA
10psi - SBEDS mod.
50psi - SBEDS mod.
200psi - SBEDS mod.
Normalized Midspan Deflection
Percentage of Ultimate Axial Load
0
0.2
0.4
0.6
0.8
1
1.2
0
5
10
15
20
25
30
35
40

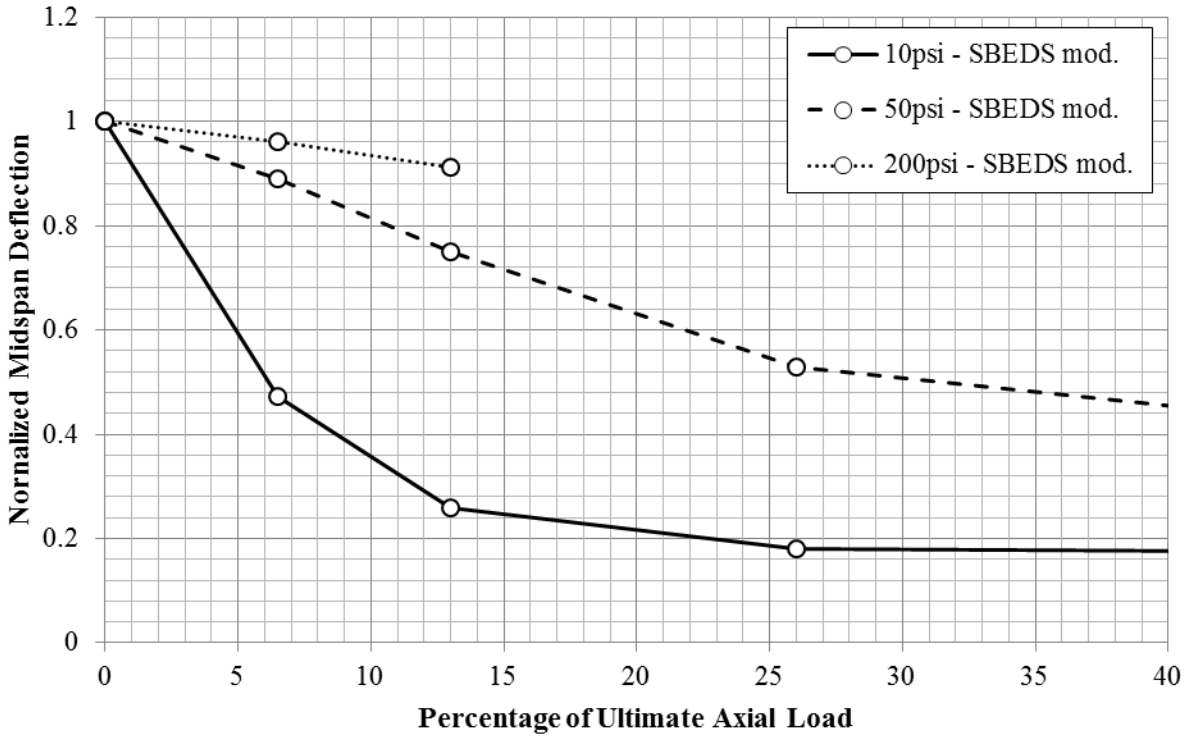

Figure 5-15: FEA and Modified SDOF Analysis PS Comparison - 100 psi-ms Impulse (top), 200 psi-ms Impulse (middle), 300 psi-ms Impulse (bottom)

The user-defined input option for the PS panel also compares well with the FEA. The results agree with the trend seen in the FEA. The only notable difference between the SDOF and FE results is that there are some load sets where the FE results could not be normalized and plotted because the non-load-bearing panel blew out while the SDOF panel did not. This difference is due to the fact that the non-load-bearing resistance curve used in the SDOF analysis was perfectly plastic with no rotation or ductility limit, so while the beam elements in LS-DYNA reached a strain limit, the panel maintained its resistance in the SDOF analysis. Although in these cases, the results might be fictitious, the issue of ductility is handled by response limits in blast design instead of incorporating ductility limits into the resistance curves. These plots were still presented, even if there were no FE results available for comparison, in order to show that

this particular method for incorporating the effects of P-M interaction and P-Δ forces into an SDOF analysis was effective for their load cases.

5.5 Observations from Static and Dynamic Analyses of Solid Load-Bearing Panels

These analyses and comparisons show that there are multiple viable options for incorporating the effects of axial load into a dynamic SDOF analysis. The resistance of the panel needs to be amplified to incorporate the effects of P-M interaction. The secondary P-Δ moment also needs to be incorporated in some way. The two methods for accounting for it in this study were by adding an additional equivalent lateral load or reducing the resistance curve. Both methods provided satisfactory results and could be used for future SDOF analysis. If the SDOF analysis tool has an algorithm for incorporating the axial load as an equivalent lateral load, it is recommended to account for the P-Δ effect using this method since it makes forming the resistance curves simpler.

Axial load increases the panel's strength but changes ductility of response. Compressive forces reduce the available strain energy of the member causing the panels to reach the compressive limit state at smaller rotations. The vertical lines in Figure 5-16 show the point for each panel at which the concrete crushes. The figure shows that as the axial load increases the crushing rotation decreases. This explains why increasing the axial load in the dynamic analysis either reduced the panel rotation or caused the panel to fail. The beneficial effect of an increase in ultimate strength outweighed the adverse effect of P-Δ forces, resulting in smaller rotations, except in cases where the axial load reduced the available strain energy enough to cause crushing of the concrete and failure of the panel. It is important to note though that for every PS load case where the 26% or 52% axial load caused failure due to crushing of the concrete, the non-load-bearing panel and the 6.5% and 13% panels also failed by other mechanisms. There were no

pressure-impulse load cases where a PS panel did not fail until a large axial load was applied; however, there were a few cases where a non-load-bearing PS panel blew out but the load-bearing panel withstood the blast. This suggests that an axial load is advantageous in a blast environment.

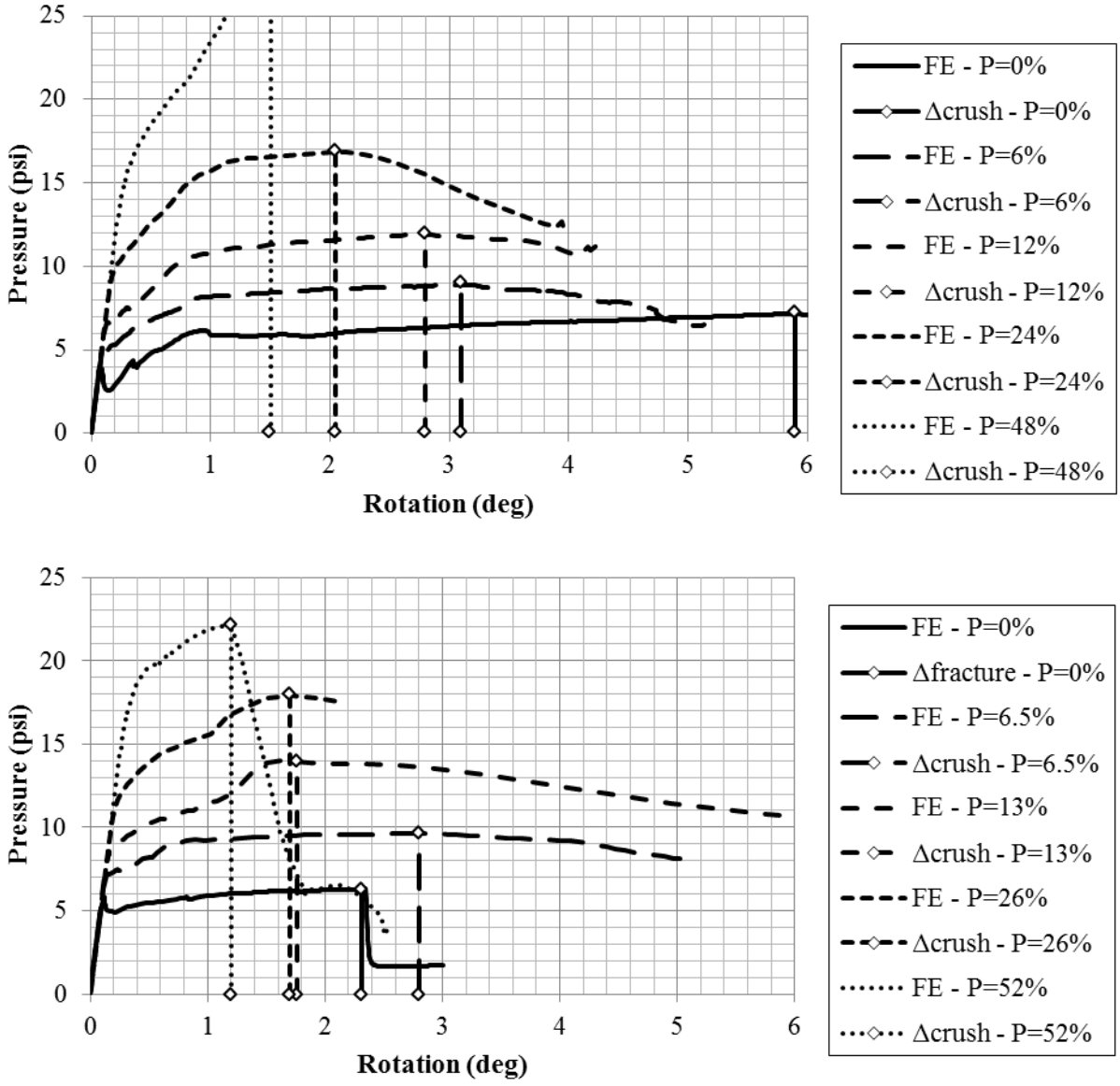

Figure 5-16: Static Ductility of Load-Bearing Panels – Non-PS (top), PS (bottom)

Another aspect of design besides the analysis approach that needs to be evaluated is the response limits used for load-bearing panels in blast design. According to the Protective Design

Center Technical Report 06-08, the response limits for panels in flexure can be used for panels in combined flexure and compression, or load-bearing panels, if the axial demand is less than twenty percent of the panel's axial capacity. If the axial demand is more than twenty percent of the panel's axial capacity, the component is restricted to the response limit for a moderate level of damage even if the design allows for heavy or hazardous damage; for example, a prestressed component with a reinforcement index less than fifteen percent would be limited to a support rotation of one degree when three degrees would normally be the limit.

Several observations from the static FEA shed light on the appropriateness of the current response limits for load-bearing panels. In regard to panels with axial loads less than the twenty percent limit, the ductility of the non-PS and PS panels was affected differently. In this category the response limits would be the same as the limits for flexural design. The blowout limit for a non-PS panel in flexure is 10 degrees. This limit assumes that the concrete will crush and a moment couple between the tension and compression steel will provide some post-crushing ductility. The two analyses of non-PS panels in this category show that even a small level of axial load reduces the ductility of the panels; however, the analyses were not able to accurately capture the post-crushing range of behavior, so it is uncertain if the 10 degree limit is too liberal for panels in this range of axial load. The axial load showed an inverse effect on the PS panels in the less than twenty percent category. The two analyses of PS panels in this category reached much larger rotations than the non-load-bearing PS panel. The blowout limit for a PS panel in flexure is 3 degrees. As discussed previously, this limit is smaller than the non-PS limit because of the tensile strain capacity of prestressing strands. The compressive stress from the axial load in essence increased the tensile stress capacity of the prestressing strands, similar to how prestressing forces increase the tensile stress capacity of concrete. The tensile stress/strain

material limits of the strands do not change, but the compressive stresses allow the strands to absorb more tensile stress as the panel bends in flexure. This effect was significant enough to change the failure mechanism seen in the non-load-bearing panel. Allowing the panel to crush and undergo post-crushing softening results in the panel reaching much higher support rotations and a more ductile response than fracture of the prestressing strands. This effect supports the use of the flexural response limits for load-bearing PS panels in this category, if not more liberal limits.

In regard to panels with axial loads greater than the twenty percent limit, the ductility of the non-PS and PS panels were affected similarly. Crushing of the concrete was the controlling failure mechanism for both of these panel types, and increasing the axial load forced crushing to occur at small rotations. This behavior warrants the use of the smaller response limit (moderate level of damage) for panels in this axial load category; however, using this response limit does not necessitate a more robust design if the analysis method incorporates the effects of axial load properly. For example, the non-PS solid panel subjected to a blast load with a peak pressure of 10 psi and an impulse of 300 psi-ms demonstrates this concept. The non-load-bearing panel rotated approximately 4 to 5 degrees in the FE and SDOF analyses. If a low or very low level of protection was specified in the design, the panel would meet the 5 or 10 degree response limit for reinforced concrete. If the panel had an axial demand greater than twenty percent of the axial capacity though, it would be limited to the 2 degree response limit. Even though the non-load-bearing panel rotated 4 to 5 degrees, all of the support rotations for the load-bearing panels in this range from the FE and SDOF dynamic analyses were less than 1 degree. Therefore, the panel meets the different response limits whether it's load-bearing or not without needing to a more robust design. The PS solid panel subjected to a blast load with a peak pressure of 50 psi and an

impulse of 200 psi-ms provides another interesting example to look at. The non-load-bearing panel blew out due to strand fracture. The two load-bearing panels in the less than twenty percent category rotated in the 1.5 to 2 degree range. The panel with a load equal to 26% of ϕP_{no} rotated just over 1 inch, and the panel with a load equal to 52% of ϕP_{no} rotated less than 1 inch. It's interesting that the non-load-bearing panel would need to be redesigned, while the 6.5%, 13%, and 52% load-bearing panels not only withstood the blast but also met the response limits (1 degree for >20% ϕP_{no} and 2 or 3 degrees for <20% ϕP_{no} depending on specified level of protection). The 26% load-bearing panel withstood the blast but would need slight changes in the design to meet the 1 degree response limit. Both of these examples support the idea that using the moderate damage response limit in blast design of certain load-bearing panels does not have to be over-conservative if the analysis method is developed properly.

5.6 Effect of Axial Load on Sandwich Panels

All of the load-bearing analyses discussed so far have been very informative into understanding the effect of axial load on the lateral response of wall panels; however, the scope of the analyses has been limited to solid panels. Solid panels were analyzed first for a couple reasons. First, understanding the behavior of load-bearing vs. non-load-bearing solid panels in a blast environment was in itself of interest in this study. Also, it was considered preferable to study the general behavior of load-bearing panels subjected to blasts using solid panels in order to eliminate additional parameters that come with the complexity of sandwich panels. The next step in the study therefore was to apply the static and dynamic analysis methods for load-bearing panels to sandwich panel models.

5.6.1 Static Load-Bearing Sandwich Panels

The PCS2 prestressed, sandwich panel model (see Section 3.3.4) was used for the static analyses. Similar to before, various levels of axial load were applied in a preliminary analysis and then held constant as a lateral pressure was applied. There was a slight difference in how the axial load was applied to the sandwich panel versus the solid panel. In the solid panel models, the axial load was applied across the whole section of the panel, but in the sandwich panel models, the axial load was only applied across the bottom and top concrete wythes. Figure 5-17 shows the static resistance of the panel subjected to the various levels of axial load.

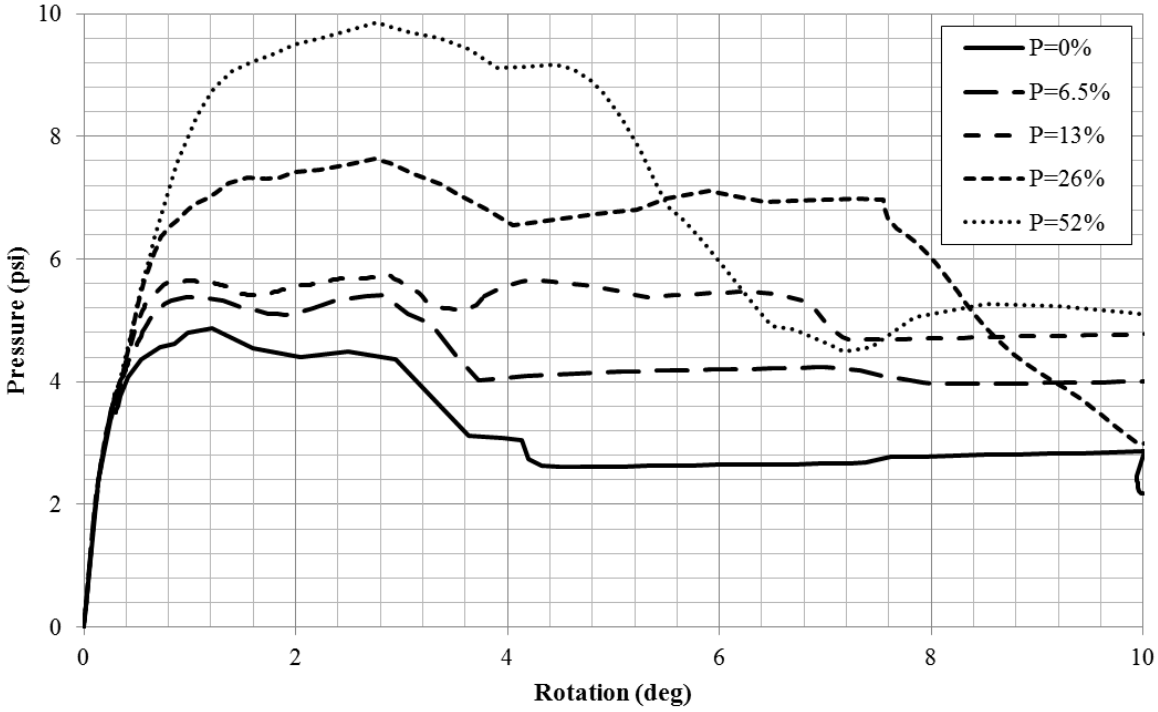

Figure 5-17: Static Resistance of Load-Bearing Sandwich Panels

The figure shows that, similar to solid panels, the ultimate flexural resistance of sandwich panels increases as the applied axial load increases, although the effect is less significant. For example, in the static analysis of a prestressed, solid panel with an axial load equal to 26% of ϕP_{no}, the ultimate strength of the panel increased over 150%, but the ultimate strength of a

prestressed sandwich panel with the same axial load only increased by approximately 55%. Similar to how the shear tie system limits the strength of the non-load bearing panel, this difference between the load-bearing solid and sandwich panel is caused by the effect of shear ties on ultimate strength. In each case, the ultimate strength was not limited by crushing of the concrete or fracture of the strands but failure of the shear ties. For this reason, the panel was not able to reach the ultimate strengths seen in the solid panel analyses. Although limited, the increase in strength was still significant. However, the analyses did not include the effect of second-order P-Δ forces; therefore, these analyses alone are not conclusive on whether an axial load will have an overall beneficial effect on the lateral response of sandwich panels.

At lower levels of axial load, the shear ties controlled the strength of the panel, and after the shear ties failed, the panel held a non-composite strength out to large rotations. At higher levels of axial load though, the shear ties were not the sole factor affecting the strength of the panel. For the 26% and 52% cases, the ultimate strength was limited by the shear ties, but at larger rotations, crushing of the concrete still occurred. It is interesting that the concrete does not crush as the panels reach their peak strengths at approximately 2 to 3 degrees but does crush at larger rotations even after the strength has dropped off. This can be explained in light of the percent composite action provided by the shear tie system. In the early stages of loading, the shear ties allow the top and bottom wythes to flex compositely, applying a certain compressive stress to the concrete elements. In these cases, the compressive stress demand on the concrete was within the material limits at the peak strength, the point when the shear ties began to fail. As the shear ties fail, the panel begins to transition from composite to non-composite action. As this transition occurs, the strength decreases because the top and bottom concrete wythes begin to flex independently, but even though the strength is decreasing, the compressive stresses from the

non-composite flexure may still be increasing. In the 26% and 52% cases, the compressive stress reached the concrete limit state, and crushing occurred in the non-composite range of behavior.

5.6.2 Load-Bearing Sandwich Panels Subjected to Blast Loads

The final step was to analyze load-bearing sandwich panels dynamically to see how axial load affected sandwich panels subjected to blast loads. It was previously concluded that axial load had a beneficial effect on the lateral response of the solid wall panels for each of the load cases that was analyzed, because the positive effect of P-M interaction on the panel's resistance outweighed the negative effect of P-Δ forces. However, as noted in the previous section, the enhancement of the panel's resistance due to P-M interaction is limited in sandwich panels due to the shear tie mechanism. Thus, it is not guaranteed that, like the solid panels, the axial load will have an overall beneficial effect on the lateral response of sandwich panels.

It was proposed that instead of analyzing the sandwich panels under all of the blast-axial load combinations from Table 5-1, the pre and primary detonation blast loadings from the full-scale blast testing combined with the previous axial load levels (44, 88, 176, and 352 kips) be used to study the sandwich panels' response to blast-axial load combinations. However, these analyses have not been completed but are recommended as part of future research.

The goal of these future analyses is to answer the following important questions related to design of load-bearing sandwich panels subjected to blast load: Is the trend seen in load-bearing solid panels, an axial load decreases the support rotation in laterally loaded wall panel, also seen in load-bearing sandwich panels? Although no method for quantifying the increase in the lateral resistance of sandwich panels due to P-M interaction is presented here, it would be overly conservative to only account for P-Δ forces and not P-M interaction in a SDOF analysis for a blast design of a sandwich panel.

5.7 Residual Axial Capacity

Another component of the study focused on how lateral loads affect the axial capacity of the wall panels. In this phase of the study Abaqus was again used to study the static behavior of the panels first. Similar to previous static analyses the models were loaded axially in a preliminary analysis, and then the panels were loaded laterally with a uniform pressure. In the previous analysis the models were loaded through failure of the panel; however, the goal of this analysis was to evaluate the residual axial capacity of a panel after it's been damaged in flexure from a lateral load. The panels were loaded laterally to certain levels of damage. After reaching the desired damage level, the analyses were stopped, and an additional analysis was run. In this analysis the lateral pressure was unloaded from the point the previous analysis was stopped. After the pressure was completely unloaded, the axial load was increased until the panel collapsed. The phases of the analysis are depicted in Figure 5-18.

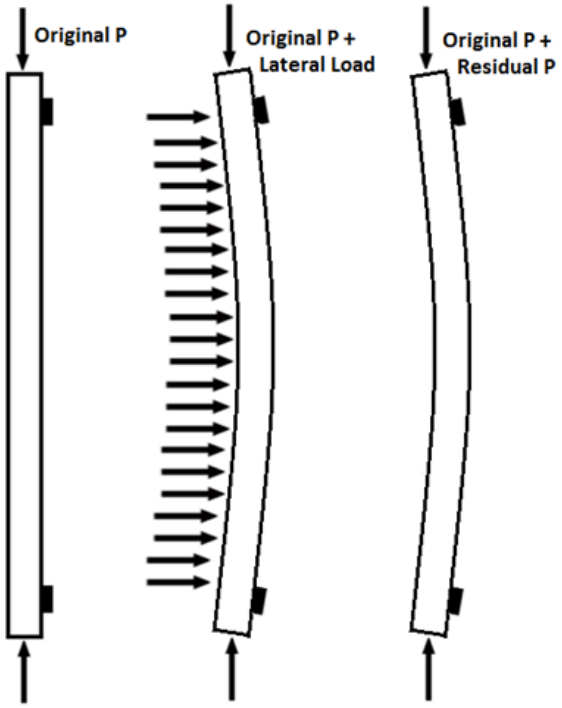

Figure 5-18: Phases of Residual Axial Capacity Analysis

The analyses were run for non-PS and PS solid panels. Five different damage levels were chosen to evaluate the effect of lateral damage on the axial capacity. The points where yield and crushing occurred, Δyield and Δcrush, were determined for each panel. These points and three intermediate points, one-fourth, one-half, and three-fourth the way between Δyield and Δcrush were the five points from which the lateral analysis was restarted. The pressure was unloaded from these five points while maintaining the initial axial load. The initial level of axial load that was chosen for this study was 6% of ϕP_{no} (6.5% of ϕP_{no}). The five deflection points that were chosen to represent different damage levels for the non-PS and PS panel are depicted in Figure 5-19.

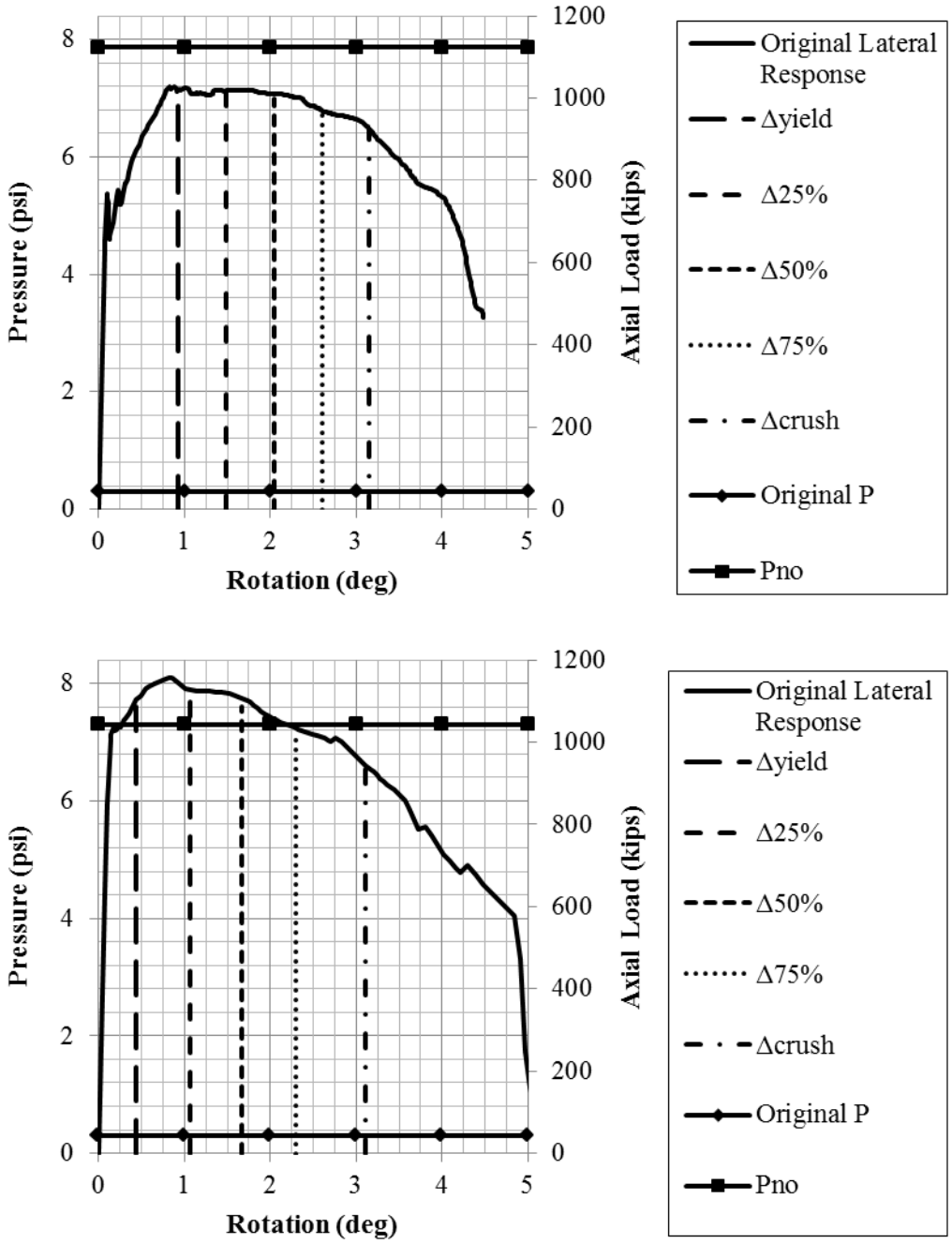

Figure 5-19: Five Damage Levels vs. Response History – Non-PS (top), PS (bottom)

The load histories for the non-PS and PS solid panels are shown in Figures 5-20 and 5-21. The solid horizontal lines in the plots represent the maximum axial capacity of the panels, P_{no}. The original response histories of the non-PS and PS panels are included in the figure to

compare with the results of the residual analysis. The dashed lines with no markers in the figure show the pressure versus rotation response of the panels. Notice that the plots follow the same path as the solid line in the original response plot until they are stopped at certain points, Δyield, Δ25%, Δ50%, Δ75%, and Δcrush. The plots then unload elastically from these points until there is no lateral pressure. The dashed lines with diamond markers represent the axial load versus rotation response of the panels. The initial level of axial load in the response histories is 6% of ϕP_{no} (6.5% of ϕP_{no}). Notice that the axial load increases from the same point of rotation where the panel is unloaded laterally. The axial load then increases until it reaches a maximum level. In the plot the axial load levels off, and the panel seems to rotate plastically; however, this behavior is fictitious. Although in reality the panel would lose all axial capacity and collapse, the level that the axial load levels off at is representative of the residual axial capacity.

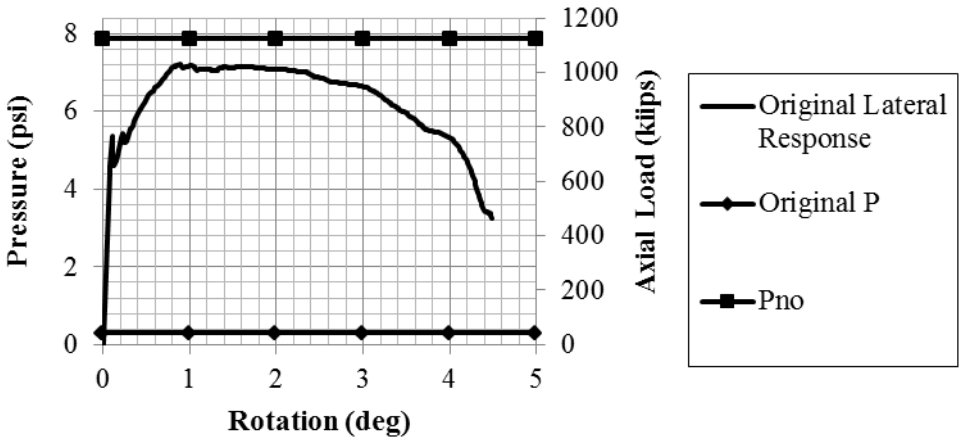
Pressure (psi)
Axial Load (kips)
Rotation (deg)
Original Lateral Response
Original P
Pno

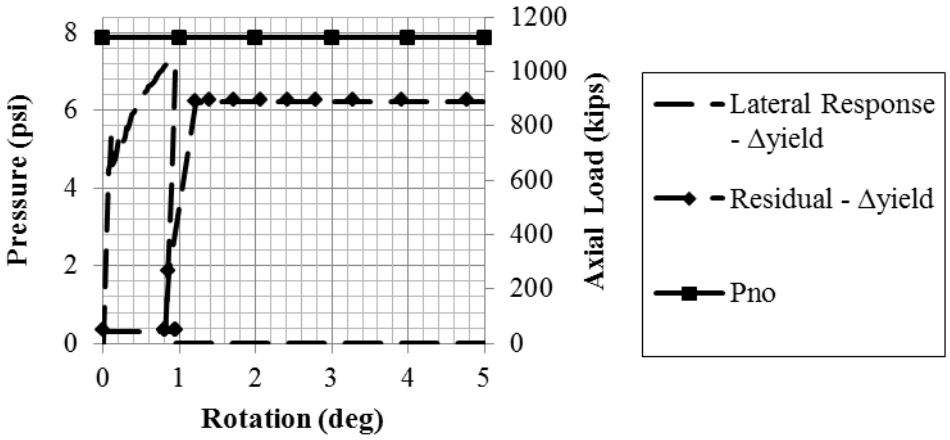
Pressure (psi)
Axial Load (kips)
Rotation (deg)
Lateral Response - Δyield
Residual - Δyield
Pno

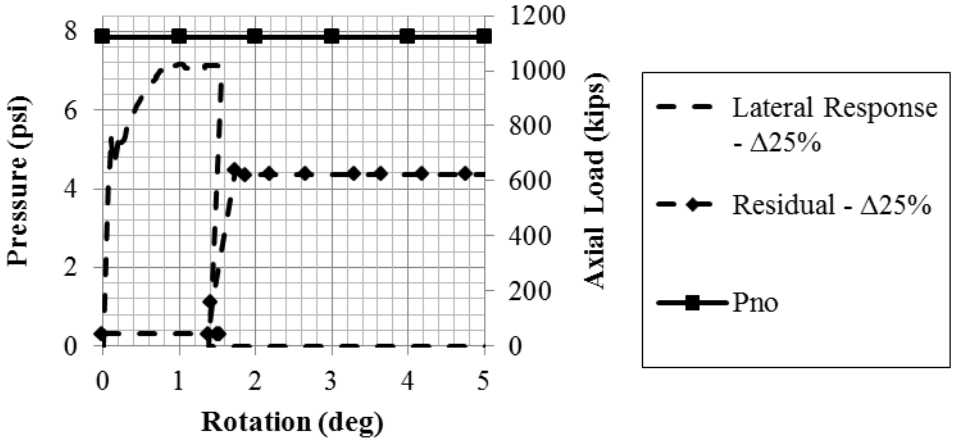
Pressure (psi)
Axial Load (kips)
Rotation (deg)
Lateral Response - Δ25%
Residual - Δ25%
Pno

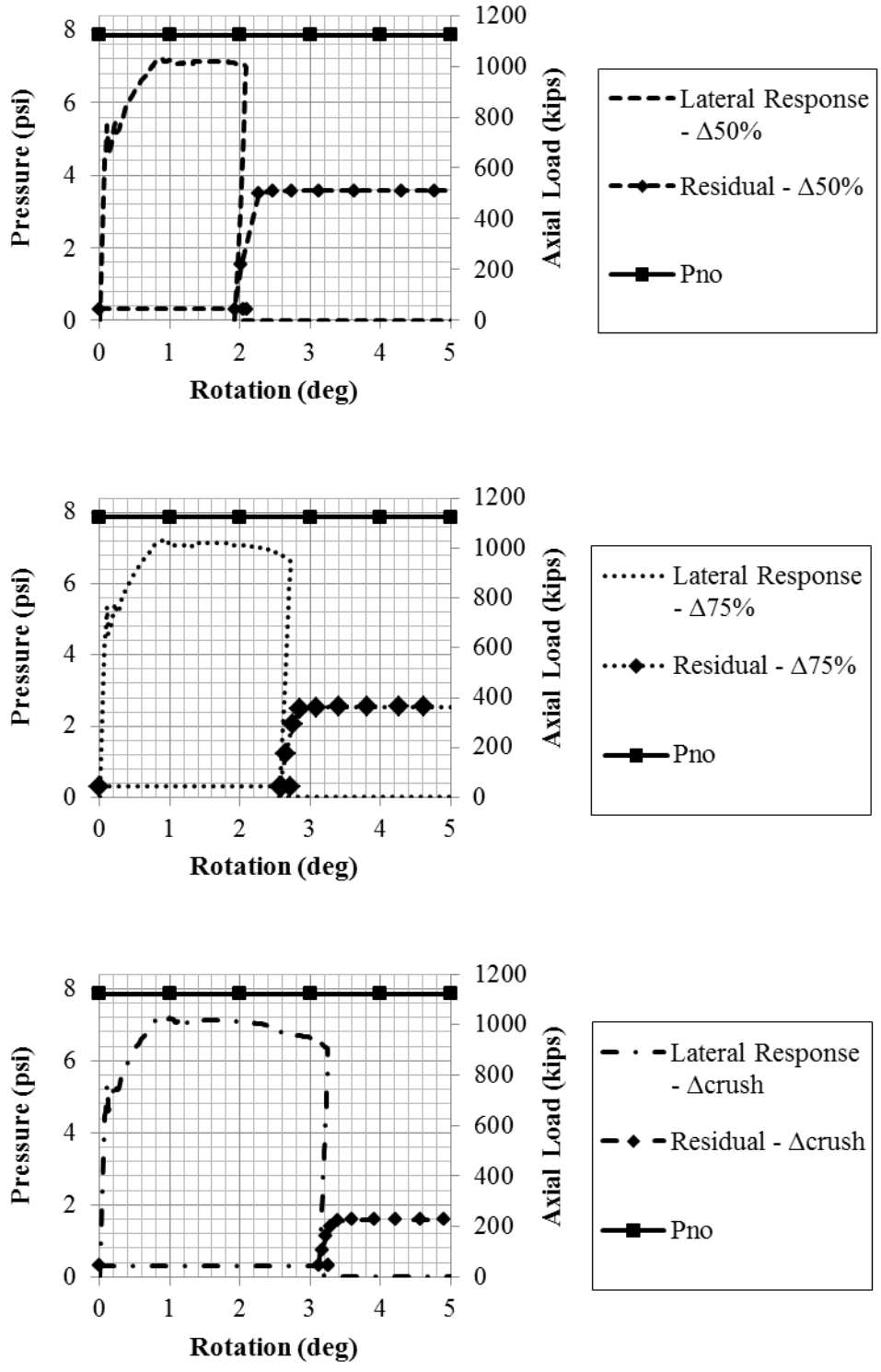

Figure 5-20: Load Histories of Residual Axial Capacity Analyses - Non-PS

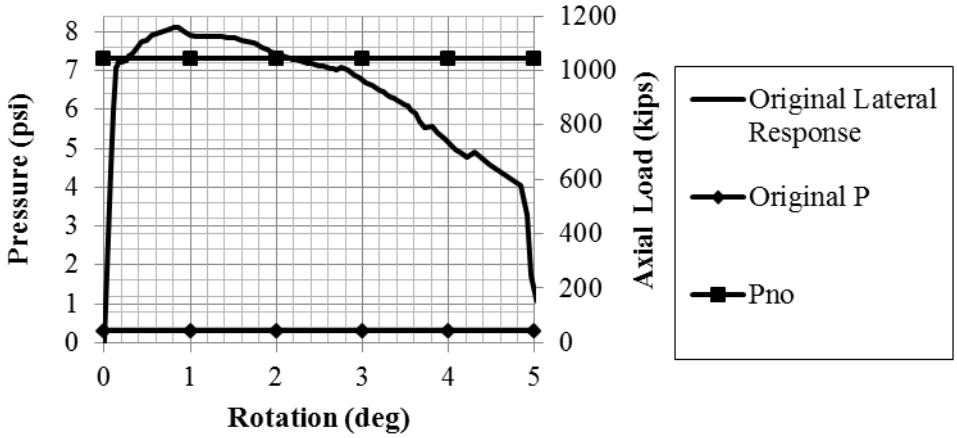
Pressure (psi)
Axial Load (kips)
Rotation (deg)
Original Lateral Response
Original P
Pno

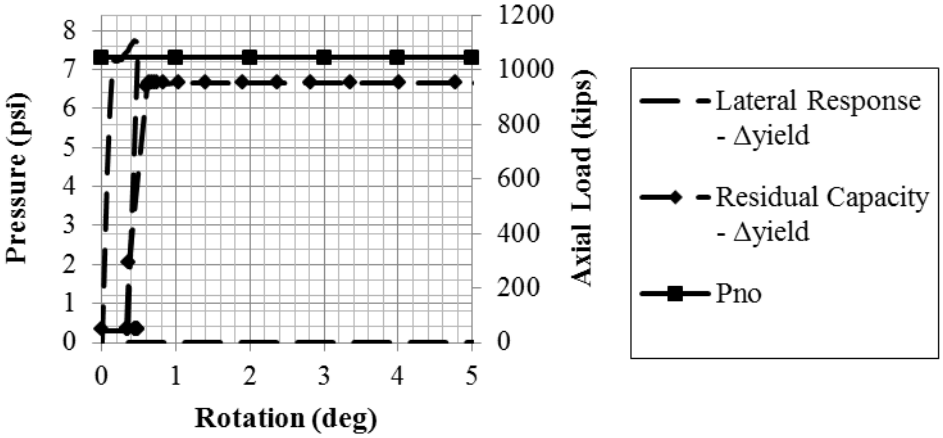
Pressure (psi)
Axial Load (kips)
Rotation (deg)
Lateral Response - Δyield
Residual Capacity - Δyield
Pno

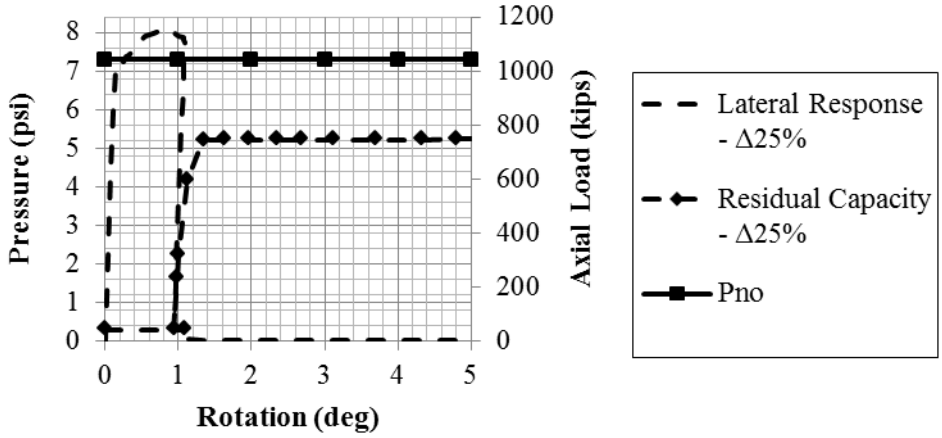
Pressure (psi)
Axial Load (kips)
Rotation (deg)
Lateral Response - Δ25%
Residual Capacity - Δ25%
Pno

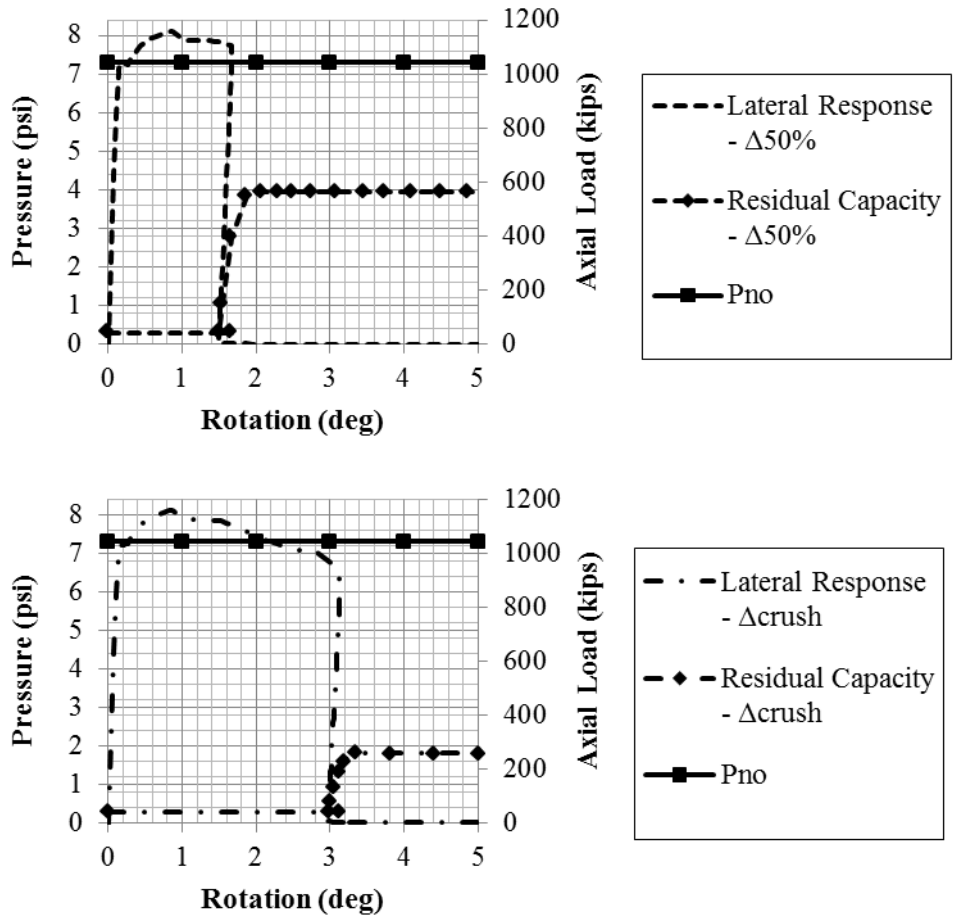

Figure 5-21: Load Histories of Residual Axial Capacity Analyses - PS

5.7.1 Observations from Residual Axial Capacity Analyses

The results in Figures 5-20 and 5-21 show that these panels have residual axial capacity even after sustaining lateral damage. A comprehensive representation of these results is contained in Figure 5-22. The figure shows that as the panels are pushed to higher levels of damage from a lateral load, the residual axial capacity of the panel decreases. This pattern is true of the non-PS and PS panel. When the panels were loaded until they reached their yield point, they were still able to maintain 90% or more of the calculated nominal axial capacity. As the panels were loaded more, the axial capacity decreased, but even when the panels reached the point of the concrete crushing, a significant amount of axial capacity remained.

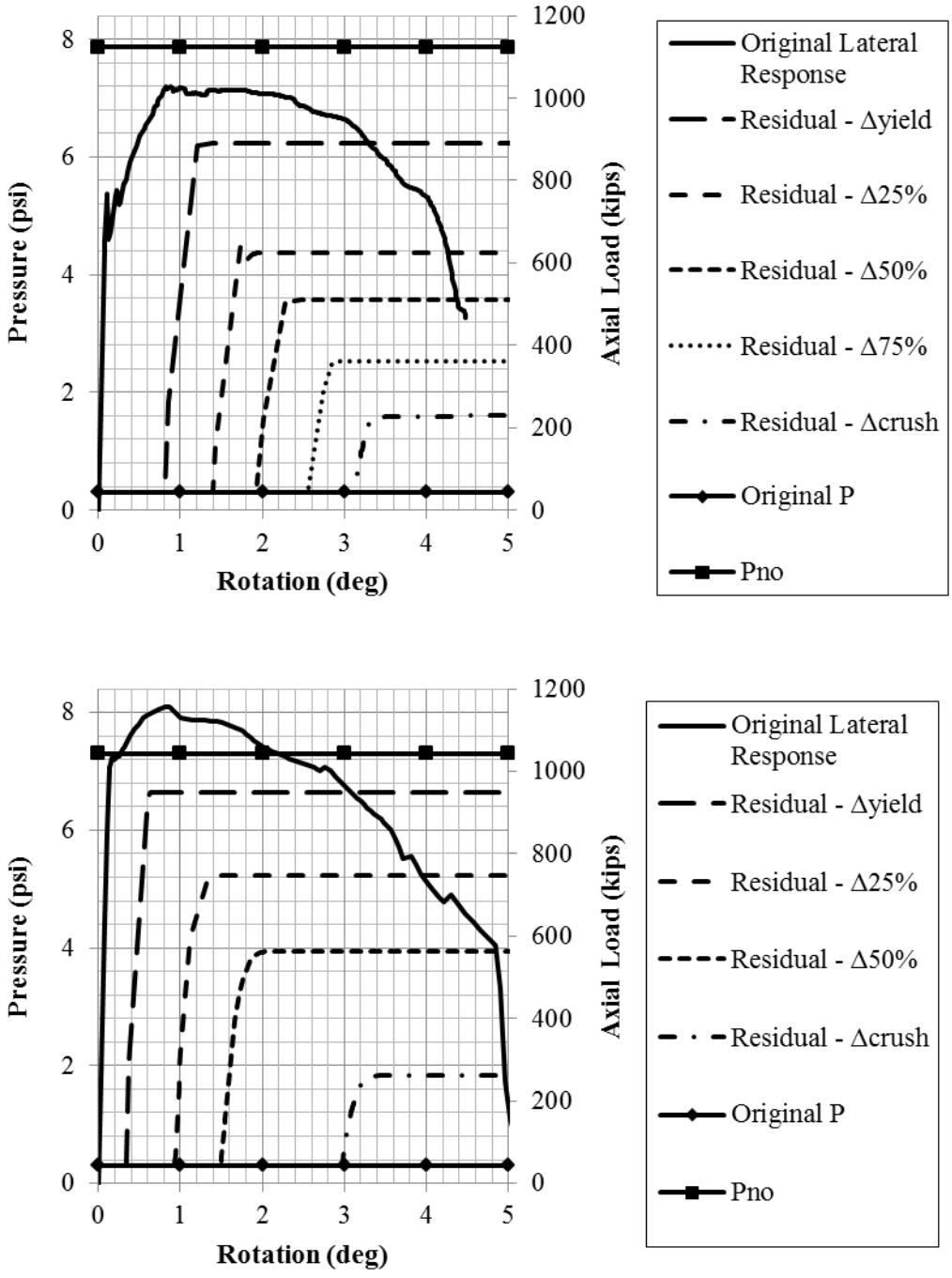

Figure 5-22: Summary of Residual Axial Capacity Results – Non-PS (top), PS (bottom)

Chapter 6

Conclusions and Recommendations

6.1 Conclusions

A finite element modeling methodology for prestressed, insulated sandwich panels, which captured the large displacement behavior of the sandwich panel system, was developed. Static testing of solid panels and sandwich panels, component level testing of shear connectors, and dynamic testing of sandwich panels was used to validate the modeling approach. Use of a beam-spring system to capture the shear transfer between concrete wythes of various shear connectors accurately was a primary focus of the modeling approach.

The developed FE modeling approach was then used to address the following questions related to blast design:

- **Are response limits for prestressed members used in blast design too conservative?**

  Results: Testing and FE modeling of prestressed members both indicated that fracture of prestressing strands limited the ductility of solid, prestressed members. It was concluded that the general assumption that "prestressed members are normally considered very brittle for blast loads" and the response limits currently used for blast design (limits in PDC-TR-06-08 were investigated) are appropriate for *solid*, prestressed members.

- **Can sandwich panels be used in blast design?**

  Results: It was observed that failure of shear connectors governed the global behavior of the tested panels. This observation contrasted the behavior of solid panels, which was governed by material failure of the concrete or reinforcement. The static and dynamic

performance of prestressed solid panels and prestressed sandwich panels was compared. The contract between the ductile failure of shear ties in prestressed sandwich panels and the brittle failure of prestressing strands in prestressed solid panels led to the conclusion that designing for failure of shear connectors in sandwich panels at ultimate strength allows the sandwich panel system to absorb more energy than a solid panel and may prevent collapse under a blast load.

- **How can the design of sandwich panels be enhanced for blast loads?**

  Results: A parameter study of shear connector properties was conducted using the prestressed sandwich panel FE model. The effect of the stiffness, strength, and ductility of shear connectors on sandwich panel behavior as it relates to blast design was investigated. It was concluded that designing shear ties to maintain strength through large shear deformations would be favorable for constructing blast resistant panels. It was also postulated that over-designing the strength of the shear tie system would be unfavorable for blast design, because it would cause fracture of the prestressing strands to act as the controlling failure mechanism.

- **Can debonding sections of reinforcement increase the ductility of wall panels?**

  Results: Debonding reinforcement in concrete panels was investigated as a method for increasing the flexural ductility of wall panels. Strain output of concrete and rebar elements from FE models was used to study the effect of debonding reinforcement on conventionally reinforced and prestressed panels. Debonding reinforcement displayed benefit in some conventionally reinforced panels but not others; however, debonding reinforcement in prestressed panels increased the ductility of the panels slightly by delaying fracture of the strands.

- **How do axial loads affect the response of load-bearing wall panels subjected to blasts?**

  Results: Static and dynamic analyses of solid, load-bearing wall panels were performed. Static analyses were conducted to quantify the effect of P-M interaction and P-Δ forces on the flexural resistance of solid panels. It was also concluded that low levels of axial load, which are typical in wall panel design, limit the ductility of conventionally reinforced solid panels but increase the ductility of prestressed panels; however, it was still concluded that low levels of axial load are beneficial to the lateral response of both types of solid wall panels to blast loads and could even prevent collapse.

  Similar static analyses of sandwich panels were conducted to quantify the effect of axial load on flexural resistance. It was observed that axial load increased the flexural resistance of the sandwich panels as well; however, the increase was less significant being limited by the capacity of the shear ties. Dynamic analyses of load-bearing sandwich panels subjected to blast loads were proposed but not completed.

- **How should the effects of axial load be incorporated into current SDOF analysis tools used in blast design?**

  Results: Comparison of FE and SDOF analysis results showed that using the equivalent lateral load approach to account for axial loads in SDOF analysis was overly conservative, because it neglected the effect of the axial load on the flexural resistance of load-bearing wall panels. Various alternative methods for incorporating the effects of axial load into SDOF analysis tools were proposed, and results from dynamic FE and SDOF analyses of load-bearing panels were shown to be in good agreement. It was recommended that the P-M interaction effect of axial loads be incorporated into SDOF

analyses by a modification of the resistance curve and the P-Δ effect of axial loads be incorporated into SDOF analyses with an equivalent lateral load method.

- **How do lateral loads affect the residual axial capacity of wall panels?**

  Results: A residual axial capacity analysis of solid panels was conducted. It was concluded that the residual axial capacity of the panels depended upon the amount of damage the panels sustained, but the panels maintained some axial capacity even when loaded to the point of crushing of the concrete.

6.2 Recommendations

It is recommended that the scope of the study of sandwich panel behavior be expanded to include panels with different insulation thicknesses and fenestrations. This would include component level testing of shear connectors with different insulation thicknesses and static and dynamic tests of full-scale sandwich panels with different insulation thicknesses and fenestration layouts, e.g. M-shaped panels, L-shaped panels, etc.

Further FE investigation into the dynamic response of load-bearing sandwich panels to a variety of blast loads is recommended. Static and dynamic testing of load-bearing solid panel and sandwich panels would also be beneficial for validation of the results of the load-bearing FE models and the proposed methods for incorporating the axial loads into SDOF analysis tools. The scope of the investigations of load-bearing wall panels was limited to a concentric axial load, while in reality most load-bearing wall panels are eccentrically loaded; therefore, it is also recommended to incorporate eccentricity into future investigations of load-bearing wall panels.

References

Alaoui, S., and Oswald, C. (2007). "Blast-resistant Design Considerations for Precast, Prestressed Concrete Structures." *PCI Journal*, Vol. 52, No. 6, 53-65.

American Society of Civil Engineers (ASCE). (1997). "Design of Blast Resistant Buildings in Petrochemical Facilities." Reston, VA.

Benayoune, A., Samad, A. A., Trikha, D. N., Ali, A. A., and Ashrabov, A. A. (2006). "Structural Behaviour of Eccentrically Loaded Precast Sandwich Panels." *Construction and Building Materials*, Vol. 20, Issue 9, 713-724.

Benayoune, A., Samad, A. A., Trikha, D. N., Ali, A. A., and Ellinna, S. H. (2008). "Flexural Behaviour of Pre-cast Concrete Sandwich Composite Panel – Experimental and Theoretical Investigations." *Construction and Building Materials*, Vol. 22, Issue 4, 580–592.

Bush, T. D., and Stine, G. L. (1994). "Flexural Behavior of Composite Precast Concrete Sandwich Panels with Continuous Truss Connectors." *PCI Journal*, Vol. 39, No. 2, 112-121.

Bush, T. D., and Wu, Z. (1998). "Flexural Analysis of Prestressed Concrete Sandwich Panels with Truss Connectors." *PCI Journal*, Vol. 43, No. 5, 76-86.

Brun, M., Batti, A., Limam, A., and Gravouil, A. (2012). "Explicit/implicit Multi-time Step Co-computations for Blast Analysis on a Reinforced Concrete Frame Structure." *Finite Elements in Analysis and Design*, Vol. 52, 41-59.

Department of Defense (DOD). (2008). "Structures to Resist the Effects of Accidental Explosions." Unified Facilities Criteria 3-340-02.

El-Dakhakhni, W., Mekky, W., and Rezaei, S. (2010). "Validity of SDOF Models for Analyzing Two-Way Reinforced Concrete Panels under Blast Loading." *Journal of Performance of Constructed Facilities*, Vol. 24, Issue 4, 311-325.

Frankl, B. A., Lucier, G. W., Hassan, T. K., and Rizkalla, S. H. (2011). "Behavior of Precast, Prestressed Concrete Sandwich Wall Panels Reinforced with CFRP Shear Grid." *PCI Journal*, Vol. 56, No. 2, 42-54.

Gara, F., Ragni, L., Roia, D., and Dezi, L. (2012). "Experimental Tests and Numerical Modelling of Wall Sandwich Panels." *Engineering Structures*, Vol. 37, 193-204.

Hassan, T. K., and Rizkalla, S. H. (2010). "Analysis and Design Guidelines of Precast, Prestressed Concrete, Composite Load-bearing Sandwich Panels Reinforced with CFRP Grid." *PCI Journal*, Vol. 55, No. 2, 147-162.

Jankowiak, T., and Lodygowski, T. (2005). "Identification of Parameters of Concrete Damage Plasticity Constitutive Model," *Foundations of Civil and Environmental Engineering*, No. 6, 53-69.

Jenkins, R. S. (2008). "Compressive Properties of Extruded Expanded Polystyrene Foam Building Materials." M.S.C.E. report, University of Alabama at Birmingham.

Kabir, M. Z. (2005). "Structural Performance of 3-D Sandwich Panels Under Shear and Flexural Loading." *Scientia Iranica*, Vol. 12, No. 4, 402-408.

Livermore Software Technology Corp. (LSTC). (2006). *LS-DYNA Theory Manual*. Livermore, CA.

Livermore Software Technology Corp. (LSTC). (2009). *LS-DYNA Keyword User's Manual*. Version 971, Rel. 4. Livermore, CA.

Losch, E. (2005). "Precast/Prestressed Concrete Sandwich Walls." *STRUCTURE Magazine*, April, 16-20.

Malvar, L. J., Crawford, J. E., Wesevich, J. W., and Simons, D. (1997). "A Plasticity Concrete Material Model for DYNA3D." *International Journal of Impact Engineering*, Vol. 19, Issues 9-10, 847–873.

Malvar, L. J., and Ross, C. A. (1998). "Review of Strain Rate Effects for Concrete in Tension." *ACI Materials Journal*, Vol. 95, No. 6, 735–739.

Naito, C.J., Dinan, R. J., Fisher, J. W., and Hoemann, J. M. (2008). "Precast/Prestressed Concrete Experiments – Series I (Volume I)." Air Force Research Laboratory Report, AFRL-RX-TY-TR-2008-4616.

Naito, C. J., Hoemann, J. M., Bewick, B. T., and Hammons, M. I. (2009). "Evaluation of Shear Tie Connectors for Use in Insulated Concrete Sandwich Panels," Air Force Research Laboratory Report, AFRL-RX-TY-TR-2009-4600.

Naito, C. J., Hoemann, J. M., Shull, J. S., Saucier, A., Salim, H. A., Bewick, B. T., and Hammons, M. I. (2011a). "Precast/Prestressed Concrete Experiments Performance on Non-Load Bearing Sandwich Wall Panels." Air Force Research Laboratory Report, AFRL-RX-TY-TR-2011-0021.

Naito, C., Beacraft, M., Hoemann, J., Shull, J., Bewick, B., and Hammons, M. (2011b). "Dynamic Performance of Insulated Concrete Sandwich Panels Subject To External Explosions (Volume II)." Air Force Research Laboratory Report, AFRL-RX-TY-TR-2011-0039.

National Research Council. (1995). "Protecting Buildings from Blast Damage: Transfer of Blast-Effects Mitigation Technology from Military to Civilian Applications." Committee on Feasibility of Applying Blast Mitigating Technologies and Design Methodologies from Military Facilities to Civilian Buildings. National Academy Press. Washington, D.C.

Newberry, C. (2011). "Finite Element Simulation and Assessment of Single-Degree-of-Freedom Prediction Methodology for Insulated Concrete Sandwich Panels Subjected to Blast Loads." M.S.C.E. thesis, Auburn University.

Nijhawan, J. C. (1998). Insulated Wall Panels - Interface Shear Transfer. *PCI Journal*, Vol. 43, No. 3, 98-101.

Pessiki, S., and Mlynarczyk, A. (2003). "Experimental Evaluation of the Composite Behavior of Precast Concrete Sandwich Wall Panels." *PCI Journal*, Vol. 48, No. 2, 54-71.

PCI Committee on Precast Sandwich Wall Panels. (2011). "State of the Art of Precast/Prestressed Sandwich Wall Panels." 2nd Ed. *PCI Journal*, Vol. 56, No. 2, 131–176.

Precast/Prestressed Concrete Institute (PCI). (2004). "PCI Design Handbook: Precast and Prestressed Concrete." 6th Ed. L. D. Martin and C. J. Perry, eds., 11-32.

Salmon, D. C., Einea, A., Tadros, M. K., and Culp, T. D. (1997). "Full-Scale Testing of Precast Concrete Sandwich Panels." *ACI Structural Journal*, Vol. 94, No. 4, 354-362.

SIMULIA. (2010a). "Abaqus Analysis User's Manual - Vol. II: Analysis."

SIMULIA. (2010b). "Abaqus Analysis User's Manual - Vol. III: Materials."

SIMULIA. (2010c). "Abaqus Analysis User's Manual - Vol. IV: Elements."

SIMULIA. (2010d). "Abaqus Analysis User's Manual - Vol. V: Prescribed Conditions, Constrains, & Interactions."

SIMULIA. (2010e). "Abaqus Theory Manual."

U.S. Army Corps of Engineers (USACE). (2008a). "Methodology Manual for the Single-Degree-of-Freedom Blast Effects Design Spreadsheets (SBEDS)." Protective Design Center Technical Report 06-01.

U.S. Army Corps of Engineers (USACE). (2008b). "Single Degree of Freedom Structural Response Limits for Antiterrorism Design." Protective Design Center Technical Report 06-08.

Yongxiang, D., Shunshuan, F., Changjing, X., and Lele, G. (2009). "Dynamic Behaviour of Concrete Sandwich Panel under Blast Loading." *Defence Science Journal*, Vol. 59, No. 1, 22-29.

Appendix A

A.1 Design Strength Calculation of Prestressed Solid or Composite Sandwich Panel

$fc := 5\ ksi \quad \varepsilon cu := 0.003\ in/in \quad b := 32\ in \quad L := 120\ in \quad dp := 6.5\ in \quad Aps := 0.17\ in^2$

$fse := 189.4\ ksi \quad \varepsilon se := \frac{fse}{29000} = 6.531 \times 10^{-3}\ in/in$

Assume: $c := 0.5\ in$

$\varepsilon sa := \frac{\varepsilon cu}{c} \cdot dp - \varepsilon cu = 0.036\ in/in \qquad \varepsilon ps := \varepsilon sa + \varepsilon se = 0.0425\ in/in$

$a := \frac{fps(\varepsilon ps) \cdot Aps}{0.85 \cdot fc \cdot b} = 0.334\ in \qquad c := \frac{a}{0.8} = 0.418\ in$

Assume: $c = 0.418\ in$

$\varepsilon sa := \frac{\varepsilon cu}{c} \cdot dp - \varepsilon cu = 0.0437\ in/in \qquad \varepsilon ps := \varepsilon sa + \varepsilon se = 0.0502\ in/in$

$a := \frac{fps(\varepsilon ps) \cdot Aps}{0.85 \cdot fc \cdot b} = 0.336\ in \qquad c := \frac{a}{0.8} = 0.419\ in$ **Assumption is close enough

$T := Aps \cdot fps(\varepsilon ps) = 45.6\ kips$

$M := T \cdot \left(dp - \frac{a}{2} \right) = 289\ kip\text{-}in \qquad p := \frac{M \cdot 8 \cdot 1000}{b \cdot L^2} = 5.02\ psi$

$$
\begin{aligned}
\text{fps}(\varepsilon\text{ps}) := \;& \varepsilon\text{py} \leftarrow \frac{245}{29000} \\
& \text{fps} \leftarrow \varepsilon\text{ps} \cdot 29000 \quad \text{if} \quad \varepsilon\text{ps} \le \varepsilon\text{py} \\
& \text{fps} \leftarrow 245 + (\varepsilon\text{ps} - \varepsilon\text{py}) \cdot \frac{(265 - 245)}{(0.02845 - \varepsilon\text{py})} \quad \text{if} \quad \varepsilon\text{ps} > \varepsilon\text{py} \wedge \varepsilon\text{ps} \le 0.02845 \\
& \text{fps} \leftarrow 265 + (\varepsilon\text{ps} - 0.02845) \cdot \frac{(270 - 265)}{(0.05845 - 0.02845)} \quad \text{if} \quad \varepsilon\text{ps} > 0.02845 \\
& \text{fps}
\end{aligned}
$$

Note: Prestressing strand stress calculation based on stress-strain relationship presented in Section 3.2.2 (re-presented in Figure A-1)

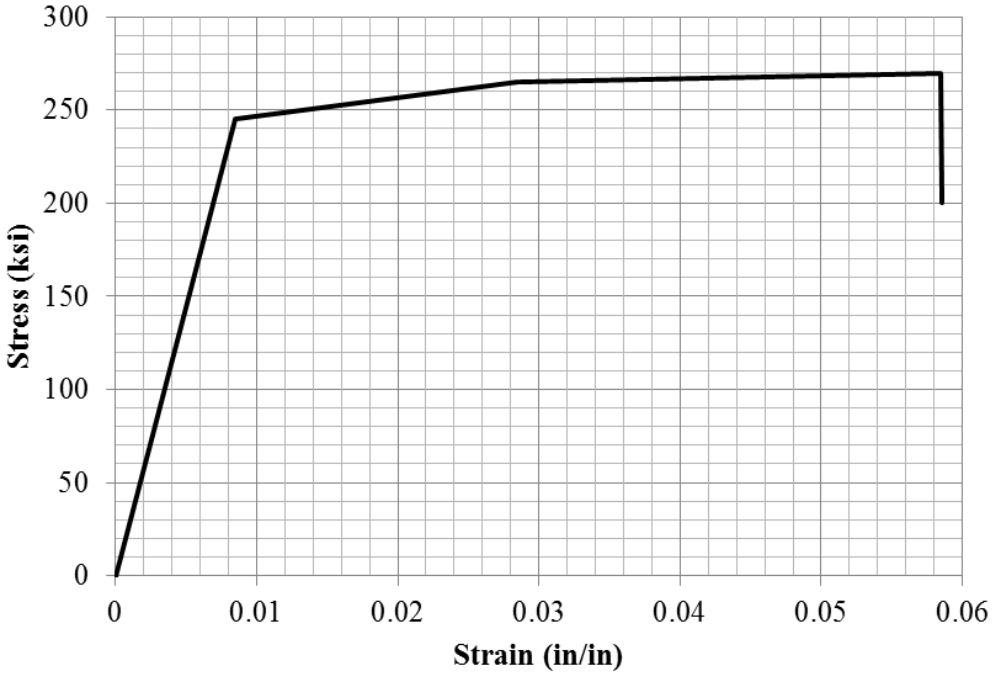

Figure A-1: Stress-Strain Relationship of Prestressing Strand Used in FE Analyses (adapted from PCI 2004)

A.2 Tie Connector Design Strength Calculation

$TieStr := 280\ lb/in \qquad TieL_{prov} := 12 \cdot 2\ ft$

$$TieL_{req} := \frac{2 \cdot T}{\frac{TieStr}{1000} \cdot 12}$$

$TieL_{req} = 27.2\ ft \qquad TieL_{prov} = 24\ ft \qquad TieOverStrength := \frac{TieL_{prov}}{TieL_{req}} = 0.88$

$$T_{design} := \frac{TieL_{prov}}{2} \cdot \frac{TieStr}{1000} \cdot 12 \qquad T_{design} = 40.3\ kips$$

Assuming moment arm is the same:

$$M := T_{design} \cdot \left(dp - \frac{a}{2} \right) = 255.3\ kip\text{-}in \qquad p := \frac{M \cdot 8 \cdot 1000}{b \cdot L^2} = 4.43\ psi$$

Note: This calculation shows that in terms of transferring shear between the concrete wythes at the flexural design strength of the panel, the tie system was under-designed by a factor of 0.88. The length of shear ties provided had the capacity to transfer 40.3 kips in shear, which corresponds to a flexural strength of 4.43 psi. However, as seen in Chapters 3 and 4, the prestressed sandwich panel still met the design strength of 5.0 psi, and the prestressed solid panel surpassed the design strength, reaching 6.0 psi. One factor contributing to this over-performance is the presence of compression steel in both panels. The calculation for the panel design strength ignores the contribution of the compression steel to the flexural strength. Depending on the strain distribution in the cross section, the compression steel can have a significant effect on the flexural strength without increasing the demand on the shear ties, since the strands are located in the top wythe.

A.3 Shear Tie Strength Parameter Calculations

Strength*1.5

$TieStr := 1.5 \cdot 280\ lb/in \qquad TieL_{prov} := 12 \cdot 2\ ft$

$$T_{design} := \frac{TieL_{prov}}{2} \cdot \frac{TieStr}{1000} \cdot 12 \qquad T_{design} = 60.5\ kips$$

Assuming moment arm is the same:

$$M := T_{design} \cdot \left(dp - \frac{a}{2} \right) = 383\ kip\text{-}in \qquad p := \frac{M \cdot 8 \cdot 1000}{b \cdot L^2} = 6.65 psi$$

Strength*2.0

$TieStr := 2.0 \cdot 280\ lb/in \qquad TieL_{prov} := 12 \cdot 2\ ft$

$$T_{design} := \frac{TieL_{prov}}{2} \cdot \frac{TieStr}{1000} \cdot 12 \qquad T_{design} = 80.6\ kips$$

Assuming moment arm is the same:

$$M := T_{design} \cdot \left(dp - \frac{a}{2} \right) = 510.6\ kip\text{-}in \qquad p := \frac{M \cdot 8 \cdot 1000}{b \cdot L^2} = 8.86 psi$$